INFORMATION TO USERS

This manuscript has been reproduced from the microfilm master. UMI films the text directly from the original or copy submitted. Thus, some thesis and dissertation copies are in typewriter face, while others may be from any type of computer printer.

The quality of this reproduction is dependent upon the quality of the copy submitted. Broken or indistinct print, colored or poor quality illustrations and photographs, print bleedthrough, substandard margins, and improper alignment can adversely affect reproduction.

In the unlikely event that the author did not send UMI a complete manuscript and there are missing pages, these will be noted. Also, if unauthorized copyright material had to be removed, a note will indicate the deletion.

Oversize materials (e.g., maps, drawings, charts) are reproduced by sectioning the original, beginning at the upper left-hand corner and continuing from left to right in equal sections with small overlaps.

Photographs included in the original manuscript have been reproduced xerographically in this copy. Higher quality 6" x 9" black and white photographic prints are available for any photographs or illustrations appearing in this copy for an additional charge. Contact UMI directly to order.

Bell & Howell Information and Learning
300 North Zeeb Road, Ann Arbor, MI 48106-1346 USA

UMI®
800-521-0600

UNIVERSITY OF OKLAHOMA

GRADUATE COLLEGE

SYNTHESIS AND CARBON-13 NMR STUDIES OF LIQUID CRYSTALS

A Dissertation

SUBMITTED TO THE GRADUATE FACULTY

in partial fulfillment of the requirements for the

degree of

Doctor of Philosophy

By

Hong Sun
Norman, Oklahoma
2000

SYNTHESIS AND CARBON-13 NMR STUDIES

OF LIQUID CRYSTALS

A Dissertation APPROVED FOR THE

DEPARTMENT OF CHEMISTRY AND BIOCHEMISTRY

BY

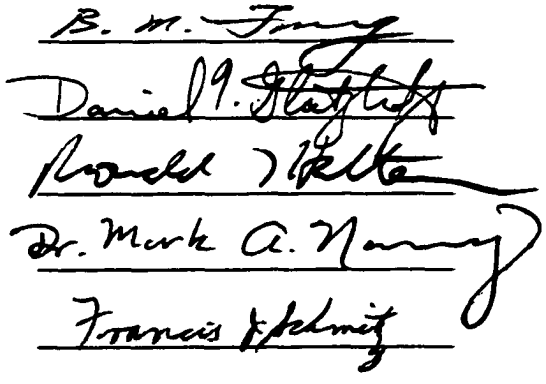

ACKNOWLEDGEMENT

I want to express my great appreciation to my mentor, Dr. Bing M. Fung, for the opportunity to work in his lab. His patient guidance led me through this journey and his diligence also inspires everyone working in his group. I can never thank him enough for his concern with my career and my future. The experience in his lab will be a treasure that will benefit me for the rest of my life.

I would also like to thank Dr. Schmitz, Dr. Glatzhofer, Dr. Halterman and Dr. Nanny for serving in my committee.

I feel deeply indebted to my wife, Qiaoyan Wang, for her support and taking care of things around me, so that this dissertation can be written.

I am very grateful to the following people I met in Dr. Fung's group: Dr. Youlu Yu, Dr. Wing Shun Cheung, Dr. Chibing Tan, Dr. Doug Masterson, Dr. Anatoly Khitrin, Dr. Cecile Canlet, Dr. Venster Reddy, Dr. Gyoujin Cho, Mr. Simon Marburger and Ms. Almut Rapp.

I thank Dr. Lin Cheng for sharing me with his experience of operations of tin dichloride reduction reactions. I thank Dr. Frederick Roussel for his assistance of building the optical path for birefringence and rise time measurement. I thank Dr. White and Mr. Edouard Bonnet for letting me use and help me modify their Quick Basic program and I enjoy the inspiring discussion with them. I thank John Black for building and maintaining the circuit used in the data acquisition part.

I appreciate the initial accommodation by Dr. Zhili Wang, Dr. Ying Mao and Dr. Roch, which made this journey an enjoyable one from the very first day. I

thank Russell Franks for the cheerful moments in his house during Super Bowls XXXII and XXXIII.

Finally, I would like to thank the Chemistry Department, National Science Foundation and Air Force Office of Science Research for the financial support that makes this research possible.

TABLE OF CONTENTS

List of Tables.....ix

List of Figures.....xi

List of Schemes.....xviii

Abstract.....xx

I. Introduction

1.1. The fourth state of matter.....1

1.2. Types of liquid crystals.....3

1.3. Classification of liquid crystal phases.....7

1.4. Liquid crystal displays.....13

1.5. Past, present and future of liquid crystal research.....19

1.6. References.....22

II. NMR Study of 4'-Cyaophenyl 4-*n*-heptylbenzoate (7CPB) and a Mixture with Its Chain-perfluorinated Analog

2.1. Introduction.....26

2.2. The PELF/OMAS technique.....32

2.3. Orientational ordering information from PELF/OMAS technique.....37

2.4. Orientational ordering information from 1D ^{13}C NMR method.....38

2.5. Experimental.....41

2.6. Results and discussion.....45

2.7. Conclusions.....70

2.8. References.....71

III. Synthesis and characterization of Diazo Liquid Crystals for Potential IR Applications

3.1. Introduction.....76

3.2. Physical properties of liquid crystals.....76

3.3. Structure-property relations of liquid crystals.....88

3.4. Preliminary results of liquid crystals for IR application.....97

3.5. Experimental.....101

3.6. Results and discussion.....126

3.7. Conclusions.....141

3.8. References.....143

IV. Appendices

A.1. Least-squares fitting of the two phenyl rings in 7CPB.....146

A.2. Linear correlation between order parameters and chemical shift anisotropy.....147

A.3. Haller fitting of aromatic carbons in 7CPB.....149

A.4. Attempted synthesis.....159

A.5. The data acquisition part.....163

A.6. Data for birefringence measurement.....167

A.7. UV-vis absorption spectra for synthesized liquid crystals.....169

A.8. NMR spectra for synthesized liquid crystals.....178

A.9. Rise time.....186

LIST OF TABLES

2.1. Comparison of measured and calculated chemical shifts of aromatic carbons and a summary of scalar coupling constants for all carbons of 7CPB.....47

2.2. Semi-empirical parameters for the aromatic carbons of 7CPB.....62

2.3. Semi-empirical parameters for the aromatic carbons of 7CPB.....63

2.4. S_0 and F obtained by fitting the calculated order parameters to the Haller equation.....66

2.5. Order parameters of the rings and aliphatic C-H bonds of 7CPB in the mixture at two temperatures.....70

3.1. Phase transition temperatures of the liquid crystals substituted with different groups on the central ring.....128

3.2. Phase transition temperatures of liquid crystals **VI** with fluorination at different positions.....130

3.3. Phase transition temperatures of three cyano liquid crystals **VII** and their nitro analogs **VI**.....131

3.4. λ_{max} values of liquid crystals **VI** in DMSO.....132

3.5. λ_{max} and logε values of liquid crystals **VI** in acetonitrile.....134

3.6. Dielectric anisotropy of 10% liquid crystal in E7.....137

3.7. Elastic constant ratio and threshold voltage of 10 wt% LC mixtures.....138

3.8. Birefringence of liquid crystal mixtures at two wavelengths.....139

3.9. Rise time for 10 wt% liquid crystal mixtures in E7.....141

A.1.1. Least-squares fitting for Ring 1 (phenyl ring with the heptyl chain) of 7CPB....146

A.1.2. Least-squares fitting for Ring 2 (phenyl ring with cyano group) of 7CPB....146

A.2.1. Data for the correlation of order parameters and chemical shift anisotropy for Ring 1....147

A.2.2. Data for the correlation of order parameters and chemical shift anisotropy for Ring 2....147

A.2.3. Data for the correlation of order parameters and chemical shift anisotropy for aliphatic carbons....148

A.3.1. S_0, F and T* from the first Haller fitting of aromatic carbons of Ring 1 of 7CPB....153

A.3.2. S_0, F and T* from the first Haller fitting of aromatic carbons of Ring 2 of 7CPB....153

A.3.3. S_0, F from the second Haller fitting of aromatic carbons of Ring 1 of 7CPB....158

A.3.4. S_0, F from the second Haller fitting of aromatic carbons of Ring 2 of 7CPB....158

LIST OF FIGURES

1.1. Typical calamitic liquid crystal....4

1.2. A typical discotic liquid crystal....5

1.3. Two lyotropic liquid crystals: (a) a soap, and (b) a phospholipid....6

1.4. Structures formed by amphiphilic molecules in a polar solvent....6

1.5. Lyotropic liquid crystal phases: (a) cubic phase; (b) hexagonal phase....6

1.6. Schematic representation of molecule arrangement of nematic phase....8

1.7. Schematic representation of molecule arrangement of S_A phase....9

1.8. Schematic representation of molecule arrangement of S_C phase....9

1.9. Structure of the cholesteric phase (N*)....11

1.10. Structure of the S_C* phase and **P** denotes the spontaneous polarization direction....12

1.11. Schematic drawing of LCD using guest-host mode. On the right hand of the picture are the pictures are the absorption curve corresponding to the "ON" and "OFF" state, respectively (adopted from Ref. 9)....14

1.12. Schematic drawing of LCD using twisted nematic mode (normal white mode)....15

1.13. Uniform state generated in a thin FLC cell. **Ps** denotes the spontaneous polarization (adopted from Ref. 4)....18

1.14. Schematic drawing of LCD using FLC birefringence mode (adopted from Ref. 4)....19

2.1. Schematic diagram of the 2D proton-encoded local field spectroscopy. CP = cross polarization. The last two $\pi/2$ pulses of the S spin act as a "z-filter"....36

2.2. Proton-coupled and decoupled ^{13}C NMR spectra of 7CPB in $CDCl_3$....46

2.3. ^{13}C NMR spectra at 100.58 MHz for (a) 7CPB in the isotropic phase; (b) 7CPB in the nematic phase (at 43 °C); (c) 7PFCPB in the isotropic phase; (d) 7PFCPB in the smectic A phase (at 128 °C)....49

2.4. Chemical shift change of aromatic carbon atoms of 7CPB with the change of temperature....50

2.5. Chemical shift change of aliphatic carbon atoms of 7CPB with the change of temperature....51

2.6. ^{13}C NMR spectra of 7CPB at $T/T_{NI} = 0.945$ with the sample spinning at a rate of about 1.0 kHz along an axis forming an angle 47.58° with respect to B_0, presented with traces in the w1 dimension in a 2D PELF experiment....53

2.7. Correlation between chemical shift anisotropy ($\Delta\delta$) and order parameters for C1 of 7CPB....55

2.8. Correlation between chemical shift anisotropy ($\Delta\delta$) and order parameters for C2 of 7CPB....55

2.9. Correlation between chemical shift anisotropy ($\Delta\delta$) and order parameters for C3 of 7CPB....56

2.10. Correlation between chemical shift anisotropy (Δδ) and order parameters for C4 of 7CPB....56

2.11. Correlation between chemical shift anisotropy (Δδ) and order parameters for C1' of 7CPB....57

2.12. Correlation between chemical shift anisotropy (Δδ) and order parameters for C2' of 7CPB....57

2.13. Correlation between chemical shift anisotropy (Δδ) and order parameters for C3' of 7CPB....58

2.14. Correlation between chemical shift anisotropy (Δδ) and order parameters for C4' of 7CPB....58

2.15. Correlation between chemical shift anisotropy (Δδ) and order parameters for Cα of 7CPB....59

2.16. Correlation between chemical shift anisotropy (Δδ) and order parameters for Cβ of 7CPB....59

2.17. Correlation between chemical shift anisotropy (Δδ) and order parameters for Cγ of 7CPB....60

2.18. Correlation between chemical shift anisotropy (Δδ) and order parameters for Cδ of 7CPB....60

2.19. Correlation between chemical shift anisotropy (Δδ) and order parameters for Cε of 7CPB....61

2.20. Correlation between chemical shift anisotropy (Δδ) and order parameters for Cζ of 7CPB....61

2.21. Correlation between chemical shift anisotropy ($\Delta\delta$) and order parameters for Cω of 7CPB....62

2.22. Plot of order parameters of the aromatic carbons of 7CPB against T/T^*....64

2.23. Plot of order parameters of the aliphatic carbons of 7CPB against T/T^*....65

2.24. ^{13}C NMR spectra for a mixture of 7PFCPB and 7CPB at: (a) 137 °C, (b) 114 °C, (c) 104 °C, (d) 78 °C, (e) 48 °C....68

3.1. Schematic representation of the polarizability for birefringent materials....81

3.2. Voltage-dependent transmittance of a 7.72-mm-thick, parallel-aligned E-7 LC cell at 633 nm and two polarizer positions....85

3.3. Three possible deformations of a liquid crystal....86

3.4. General structure of liquid crystals....90

3.5. Unusual liquid crystals without ring systems....91

3.6. Commonly used ring systems....92

3.7. Common linking groups....93

3.8. Two liquid crystal dyes synthesized in this laboratory....98

3.9. Wave-length-dependent birefringence of E7 (filled circles), 10% **I** ($R = C_6H_{13}$) in E7 (open circles), and 20% **I** ($R = C_6H_{13}$) in E7 (filled squares)....98

3.10. Some 4-ring nematic liquid crystals synthesized in this laboratory....99

3.11. Setup for birefringence measurement....126

A.3.1. First fitting of temperature dependence of order parameter of C1 in 7CPB.....149
A.3.2. First fitting of temperature dependence of order parameter of C2 in 7CPB.....149
A.3.3. First fitting of temperature dependence of order parameter of C3 in 7CPB.....150
A.3.4. First fitting of temperature dependence of order parameter of C4 in 7CPB.....150
A.3.5. First fitting of temperature dependence of order parameter of C1' in 7CPB.....151
A.3.6. First fitting of temperature dependence of order parameter of C2' in 7CPB.....151
A.3.7. First fitting of temperature dependence of order parameter of C3' in 7CPB.....152
A.3.8. First fitting of temperature dependence of order parameter of C4' in 7CPB.....152
A.3.9. Second fitting of temperature dependence of order parameter of C1 in 7CPB.....154
A.3.10. Second fitting of temperature dependence of order parameter of C2 in 7CPB.....154
A.3.11. Second fitting of temperature dependence of order parameter of C3 in 7CPB.....155

A.3.12. Second fitting of temperature dependence of order parameter of C4 in 7CPB.....155

A.3.13. Second fitting of temperature dependence of order parameter of C1' in 7CPB.....156

A.3.14. Second fitting of temperature dependence of order parameter of C2' in 7CPB.....156

A.3.15. Second fitting of temperature dependence of order parameter of C3' in 7CPB.....157

A.3.16. Second fitting of temperature dependence of order parameter of C4' in 7CPB.....157

A.7.1. The UV-vis spectrum of **16a** (n = 5) in DMSO (λ_{max} = 443 nm).....169

A.7.2. The UV-vis spectrum of **16c** (n = 5) in DMSO (λ_{max} = 406 nm).....169

A.7.3. The UV-vis spectrum of **16d** (n = 5) in DMSO (λ_{max} = 418 nm).....170

A.7.4. The UV-vis spectrum of **16b** (n = 5) in DMSO (λ_{max} = 435 nm).....170

A.7.5. The UV-vis spectrum of **12** (n = 5) in DMSO (λ_{max} = 493 nm).....171

A.7.6. The UV-vis spectrum of **19** (n = 5) in DMSO (λ_{max} = 483 nm).....171

A.7.7. The UV-vis spectrum of * (n = 5) in DMSO (λ_{max} = 482 nm).....172

A.7.8. The UV-vis spectrum of **29** (n = 5) in DMSO (λ_{max} = 493 nm).....172

A.7.9. The UV-vis spectrum of **30** (n = 5) in DMSO (λ_{max} = 448 nm).....173

A.7.10. The UV-vis spectrum of 13.0 μm **16a** (n = 5) in CH_3CN (λ_{max} = 456 nm and A = 0.296).....173

A.7.11. The UV-vis spectrum of 27.8 μm **12** (n = 5) in CH_3CN (λ_{max} = 455 nm and A = 0.718).....174

A.7.12. The UV-vis spectrum of 24.1 μm **19** (n = 5) in CH_3CN (λ_{max} = 465 nm and A = 0.956).....174

A.7.13. The UV-vis spectrum of 30.0 μm * (n = 5) in CH_3CN (λ_{max} = 453 nm and A = 0.878).....175

A.7.14. The UV-vis spectrum of 35.4 μm **16c** (n = 5) in CH_3CN (λ_{max} = 413 nm and A = 0.692).....175

A.7.15. The UV-vis spectrum of 19.3 μm **16d** (n = 5) in CH_3CN (λ_{max} = 406 nm and A = 0.234).....176

A.7.16. The UV-vis spectrum of 35.1 μm **16a** (n = 5) in CH_3CN (λ_{max} = 392 nm and A = 0.911).....176

A.7.17. The UV-vis spectrum of 25.1 μm **29** (n = 5) in CH_3CN (λ_{max} = 474 nm and A = 0.653).....177

A.7.18. The UV-vis spectrum of 38.4 μm **30** (n = 5) in CH_3CN (λ_{max} = 434 nm and A = 0.891).....177

A.8.1. ^1H and ^{13}C NMR spectra of **12** (n = 8) in $CDCl_3$.....178

A.8.2. ^1H and ^{13}C NMR spectra of **16a** (n = 7) in $CDCl_3$.....179

A.8.3. ^1H and ^{13}C NMR spectra of **16b** (n = 8) in $CDCl_3$.....180

A.8.4. ^1H and ^{13}C NMR spectra of **16c** (n = 7) in $CDCl_3$.....181

A.8.5. ^1H and ^{13}C NMR spectra of **16d** (n = 8) in $CDCl_3$.....182

A.8.6. ^1H and ^{13}C NMR spectra of **19** (n = 5) in $CDCl_3$.....183

A.8.7. ^1H and ^{13}C NMR spectra of **29** (n = 8) in $CDCl_3$.....184

A.8.8. ^1H and ^{13}C NMR spectra of **30** (n = 8) in $CDCl_3$.....185

LIST OF SCHEMES

2.1. Synthesis of 4'-Cyanophenyl 4-*n*-perfluoroheptylbenzoate.....42

3.1. Synthesis of 3-bromo-6-nitrotoluene, **5**.....101

3.2. Synthesis of 2-methyl-4-(4'-*n*-octylpiperazinyl)-1-(4''-nitrophenylazo)benzene, **12**.....102

3.3. Synthesis of liquid crystals **16a**, **16b**, **16c** and **16d**.....109

3.4. Synthesis of 2-chloro-1-(4'-nitrophenylazo)-4-(4''-octylpiperazinylphenyl)benzene, **19**.....113

3.5. Synthesis of 4-[3'-fluoro-4'-(4''-*n*-octylpiperazinylphenylazo)]benzonitrile, **22**.....115

3.6. Synthesis of 4-[3'-fluoro-4'-(4''-*n*-octylpiperazinylphenylazo)]benzonitrile, **23**.....117

3.7. Synthesis of 2-fluoro-4-nitrosonitrobenzene, **28**.....118

3.8. Synthesis of 1-(3'-fluoro-4'-nitrophenylazo)-4-(4''-*n*-octylpiperazinylphenyl)benzene, **29**.....119

3.9. Synthesis of 3-fluoro-1-(3'-fluoro-4'-nitrophenylazo)-4-(4''-*n*-octylpiperazinylphenyl)benzene, **30**.....123

A.4.1. Originally proposed synthetic route.....159

A.4.2. Dialkylation of *m*-acetylaminoaniline.....159

A.4.3. Direct formation of arylpiperazine.....160

A.4.4. Coupling of arylhalide and alkylpiperazine.....160

A.4.5. Chromium mediated aromatic nucleophilic substitution.....161

A.4.6. Diazo coupling 2-(4-*n*-hexylpiperazinyl)-

chlorobenzene.....161

ABSTRACT

The orientation of different segments of 4'-cyanophenyl 4-heptylbenzoate (7CPB) has been investigated using ^{13}C NMR. The method of proton encoded local field (PELF) spectroscopy was used in combination with off-magic-angle spinning (OMAS) of the sample. High-resolution 2D spectra were obtained and the order parameters were calculated from the spectra. Linear relationships between the obtained order parameters and anisotropic chemical shifts determined by 1D ^{13}C NMR were established and semi-empirical parameters were obtained. A 1:2 mixture of 7CPB and its chain-perfluorinated analog (7PFCPB) shows interesting phase behavior with changing of temperature. The mixture was studied by the use of ^{13}C NMR and polarizing optical microscopy. The order parameters of 7CPB in the smectic A phase of the mixture were calculated using the semi-empirical parameters obtained by the 2D NMR method.

Eight series of liquid crystals containing an electron-donating group at one end of a conjugated system and an electron-withdrawing group at the other end have been synthesized. The electron-donating group is 4-*n*-alkylpiperazinyl group, the electron-withdrawing group is nitro group and the conjugated system is diphenyldiazene with zero, one or two substituents on the phenyl rings. The substituents are -F, -Cl, and $-CH_3$. Two series of compounds with cyano group as electron-withdrawing group were also synthesized. Most of the compounds synthesized are nematogenic and exhibit rather broad liquid crystalline ranges. The effects of the lateral substituents on the optical absorption and phase

transition temperatures are correlated with their nature and position of substitution. Birefringence, dielectric anisotropy, elastic constant ratio and rise time of the liquid crystals were carried out using 10 wt% LC mixtures in E7. It has been found that lateral substituents have subtle effects on the properties. The presence of lateral substituents depresses melting points and clearing points of the liquid crystals. All the liquid crystals synthesized in this work have relatively large values of birefringence, although the dielectric anisotropy values were not as high as desired. The incorporation of a fluorine atom onto the position neighboring the nitro group enhances the conjugation of the push-pull system and liquid crystals with better physical properties were obtained.

Chapter I. Introduction

1. 1. The fourth state of matter

It is well-known that many substances can exist in more than one state of matter. Solids, liquids, and gases are the most common states of matter. These three common states are different from each other because the molecules in each state possess different degrees of order.

The solid state consists of a more or less rigid arrangement of molecules. Each molecule has no transitional degree of freedom. Not only are the molecules constrained to occupy a specific position, they are also oriented in a specific way. In other words, the molecules in solids (except plastic solids) do not rotate freely. They do have vibrational motions, but on average they constantly remain a highly ordered arrangement. Strong attractive forces are present in solids, which makes the solid state energetically stable and needs large external forces to disrupt the structure. Strictly speaking, this description of solids is only applied to crystals. There are some materials which have definite shapes and are not very easy to deform, but their molecules lack regular arrangement. In other words, they are amorphous.

Liquids are quite different from solids in that the molecules neither occupy a specific average position nor remain oriented in a particular way. The molecules are free to diffuse around in a random fashion, which was substantiated by the phenomenon of Brownian motion. Attractive forces obviously still exist in liquids but the random transitional and rotational motions of the molecules do not allow

the interactions between molecules to add up. However, this interaction is strong enough to hold molecules close to each other. The evidence for this is that it is very difficult to compress liquids and in fact liquids have been used in hydraulic systems.

In the gaseous state, attractive forces are even weaker. As a result, gas molecules can move around more chaotically and spread throughout the container regardless of its volume.

When heated from a low temperature, most substances will undergo phase transitions at certain temperatures: melting (from solids to liquids), evaporation (from liquids to gases) or sublimation (from solids to gases directly).

In 1888, Friedrich Reinitzer, an Austrian botanist, synthesized an ester from cholesterol, and found that this ester had two melting points. At 145.5 °C it melted from a solid to a cloudy fluid and at 178.5 °C it turned into a clear liquid. He also observed some unusual color change upon cooling. Then he wrote to Otto Lemann, a German physics professor, who was studying the crystallization properties of various substances. He built a cross polarizing microscope with a hot stage which made it possible to precisely control the temperature of the sample. He studied Reinitzer's sample and found that the cloudy fluid was similar to some crystalline samples, so he called it "soft crystal" and later "crystalline fluid". As he became more convinced that the opaque phase was a uniform phase of matter sharing properties of both liquids and solids, he began to call them liquid crystals.[1, 2]

As mentioned before, molecules in a solid are constrained to occupy only certain positions. In other words, they possess positional order. In addition, the molecules in these specific positions also possess orientational order and they are also arranged in the ways they orient themselves with respect to each other. When a solid melts to a liquid, both type of order are lost completely and the molecules move and tumble randomly. However, when a solid turns to a liquid crystalline phase, some of the orientational order remains.[3] Normally liquid crystals are turbid because there exist many differently oriented domains which scatter light differently.

The discovery of liquid crystals, together with plasma, completed the picture of states of the matter.

1. 2. Types of liquid crystals

In this section, a general picture of liquid crystals will be given by consideration of their most important features.

A number of different types of molecules can form liquid crystalline phases. What they have in common is that they are anisotropic. Either their shape is such that one molecular axis is very different from the other two or in some cases different parts of the molecules have very different solubility properties. In either case, the interactions between these anisotropic molecules promote orientational and sometimes partial positional order in an otherwise liquid phase.[2]

Liquid crystals can be classified by their shapes.[2,4] The most common type of molecules that form liquid crystal phases are rod-like molecules (i.e., one

molecular axis is much longer than the other two). Such compounds are called calamitic (derived from the Greek word "calamos" for rod) liquid crystals and many different phases are possible. It is important that the molecule be fairly rigid for at least some portion of its length, since it must maintain an elongated shape in order to produce some interactions that favor alignment. The general structures of these liquid crystals are two or more rings, either linked directly or via short linking groups, and hydrocarbon chains at one or both ends. There are numerous variations of this general feature, as will be discussed in depth in Chapter 3. A typical example, 5CB (4-cyano-4'-pentylbiphenyl), is given below in Figure 1.1.

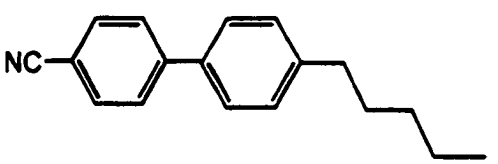

Figure 1.1. Typical calamitic liquid crystal.

Disk-like molecules, for which one molecular axis is much shorter the other two, also form liquid crystal phases. These compounds are called discotic liquid crystals, and the rigidity of the center of the molecule is essential. The core of a typical discotic liquid crystal molecule is usually based on benzene, triphenylene, cyclohexane, or truxene, with six or eight side chains. Figure 1.2 is an example of a discotic liquid crystal.

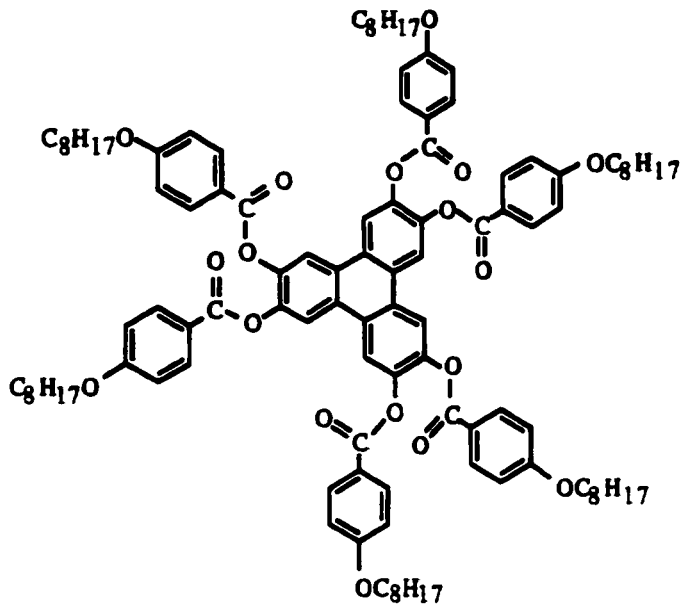

Figure 1.2. A typical discotic liquid crystal.

Compounds that can change from a solid to a liquid crystal upon heating are called thermotropic liquid crystals. On the other hand, when some special amphiphilic substance is dissolved in a certain solvent, in a certain concentration range, the system can exhibit liquid crystalline properties. Such liquid crystals are called lyotropic liquid crystals. Good examples are surfactants and various phospholipids. Figure 1.3 shows the structures of a surfactant and a phospholipid. At low concentrations, these amphiphilic substances tend to form micelles or vesicles.[2] The structures of a micelle and a vesicle formed in polar solvents are shown in Figure 1.4. At higher concentrations, these smaller units can further aggregate to form liquid crystals (Figure 1.5).

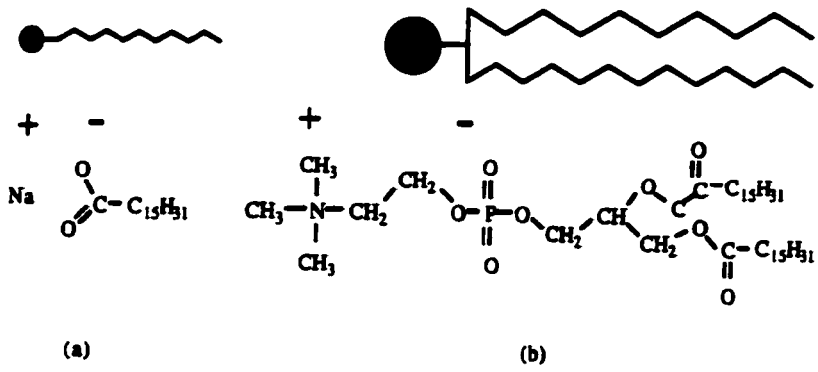

Figure 1.3. Two lyotropic liquid crystals: (a) a soap, and (b) a phospholipid.

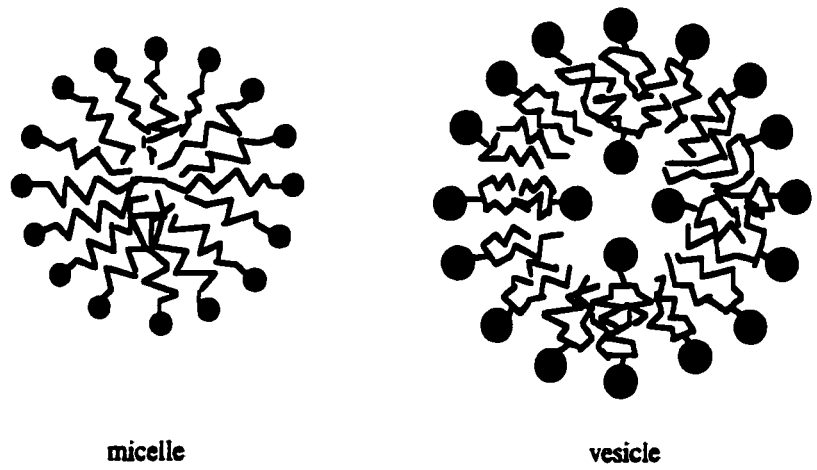

Figure 1.4. Structures formed by amphiphilic molecules in a polar solvent.

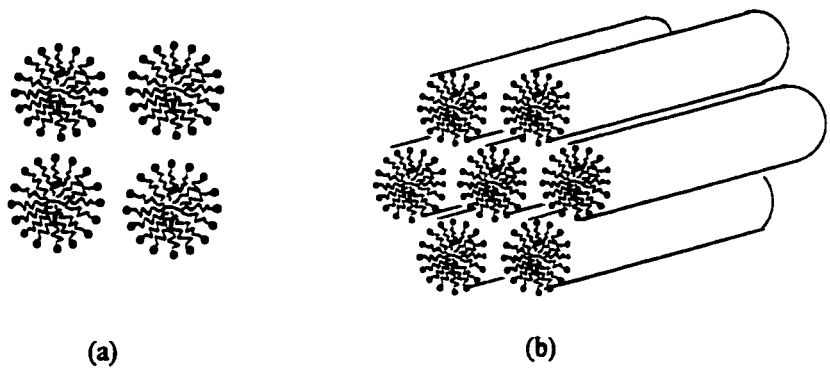

Figure 1.5. Lyotropic liquid crystal phases: (a) cubic phase; (b) hexagonal phase.

Polymers with rigid structural units can also form liquid crystalline phases.[3] A main chain polymer can be viewed as calamitic liquid crystal molecular segments separated by flexible hydrocarbon chains. In a side chain polymer, the rigid sections are attached to the flexible polymer chain by short flexible hydrocarbon chains. Polymer liquid crystals are often related to super strong materials. Kevlar, an excellent example of this, is made from extrusion of a lyotropic liquid crystal solution of aramide[5] through a spinneret. The resultant fiber possesses extreme strength and can be utilized to fabricate bulletproof vests and other materials.[6]

1. 3. Classification of liquid crystal phases

Since most liquid crystals are calamitic and only this kind of liquid crystal has been used in practical applications, only calamitic liquid crystal phases will be discussed in this part.

The phase classification of liquid crystals can be made by using three criteria: the structure determination (mainly by X-ray, supported by neutron scattering, NMR, IR and Raman spectroscopy), texture (defects of molecular arrangement, which can be observed using a cross-polarizing microscope) and miscibility investigation.[4]

In simple terms, liquid crystal phases consist of nematic (derived from the Greek word for thread) and smectic (derived from the Greek word for soap) phases.

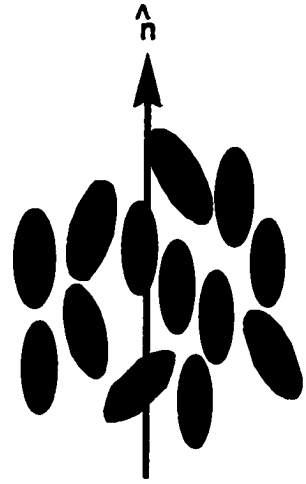

Figure 1.6. Schematic representation of molecule arrangement of nematic phase.

The nematic phase is probably the simplest liquid crystal phase. In this phase, the molecules maintain a preferred orientational direction as they diffuse throughout the sample (Figure 1.6). There is no positional order in the bulk of the molecules. The average of the alignment is characterized by one symmetric axis called the director. The director can be oriented by an external field, such as electric field, magnetic field and mechanical field. The existence of this phase can be confirmed using X-ray diffraction, and it can also be observed using a cross-polarizing microscope. Typical textures for nematic liquid crystals are nematic marbled and nematic schlieren textures.[7]

Smectic phases are more ordered phases than the nematic phases.[8] Smectic states always have layered structures. When the director of each layer is perpendicular to the plane of the layer, the phase is characterized as Smectic A (Figure 1.7), while in the Smectic C phase the director is tilted from the normal of the plane (Figure 1.8). Molecules in smectic A and C phases are randomly ordered within the layers, and therefore these phase types are also called smectic

phases "without order". The molecules can rotate around their long axes with only small hindrance. Because the alkyl chains are not completely stretched, the layer thickness d is usually smaller than the length of molecules L for the most extended conformers.

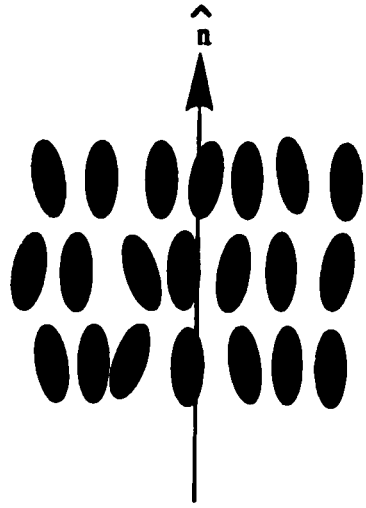

Figure 1.7. Schematic representation of molecule arrangement of S_A phase.

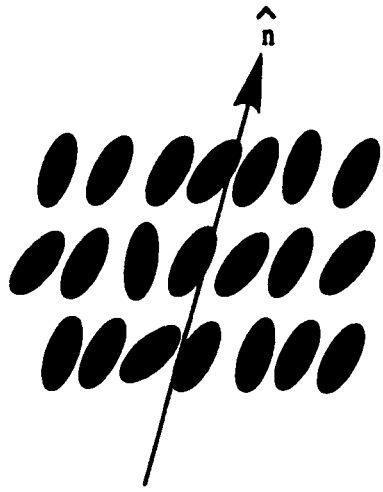

Figure 1.8. Schematic representation of molecule arrangement of S_C phase.

The smectic B, F and I phases are more highly ordered. Inside the layers, the molecules are ordered on a two-dimensional lattice (smectic phases "with

order"), however, the layers do not have long-range correlation. Still more ordered smectic phases are L, J, G, E, K, and H, which possess three dimensional long range order and therefore are also called "crystal smectics". In most of the smectic phase "with order", the layer thickness d is in good agreement with the length of the molecules L for the most extended conformations, and of course in tilted phases,

$$d = L \cos\theta$$

where, θ is the tilt angle. However, rotation along the axis of the molecules is so strongly hindered that only a 180° flip of the molecules is possible. It should be mentioned that the labeling of smectic phases has nothing to do with the microscopic properties of the phases, but instead they were designated in chronological order of their discovery.[9]

Under a cross-polarizing microscope, there are also special textures for smectic A and C, e.g. cone shape fan texture for the smectic A phase, and S_C schlieren texture for the smectic C phase. It is very difficult to tell more ordered smectic phases from each other microscopically. In some compounds phase transition between two or more very similar structures can have such enthalpies as low as 3 $J \cdot mol^{-1}$, so discrimination between them will demand the use of very sophisticated techniques.

A complete sequence of phase transitions between different phases is shown below. Since there is not a single compound that exhibits all these phases, this sequence can be achieved only by comparing the known sequences of many different liquid crystals. The existence of this sequence is a valuable tool for

phase classification investigation using miscibility criteria.[10] The miscibility method is uniquely possible in the liquid crystalline state since complete miscibility is found for phases with equal or closely related structures, even when their size difference exceeds 100%.

Solid crystal-H-K-E-G-J-F-B(crystal)-I-B(hexagonal)-C-A-N-blue-isotropic

The above calamitic liquid crystals are all non-chiral. However, chiral compounds with structures related to those non-chiral liquid crystals are also able to form mesophases and different properties are expected. For example, all chiral LC phases possess optical activity and can selectively reflect light.

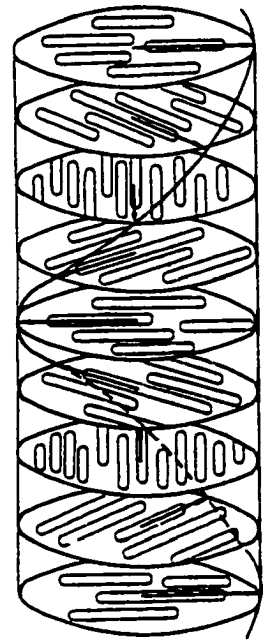

Figure 1.9. Structure of the cholesteric phase (N*).

The chiral nematic phase (N^*) is also called the cholesteric phase. It contains nematic layers in which the director is shifted by a constant angle from

one layer to the next. This twist or helical structure (Figure 1.9) has several special optical properties useful in practical applications. Chiral nematic liquid crystals can be used in electrooptic displays and thermographic devices.

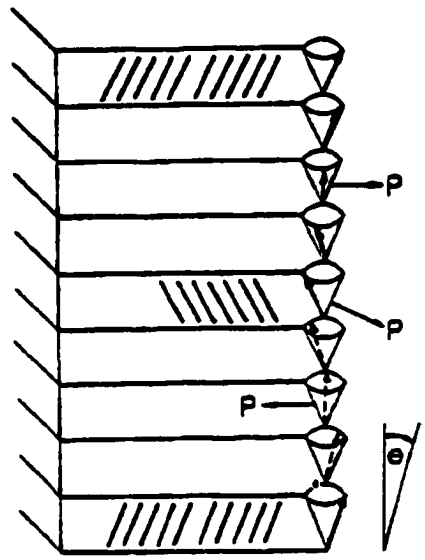

Figure 1.10. Structure of the S_C^* phase and **P** denotes the spontaneous polarization direction.

All smectic phases with tilted structures derived from chiral compounds exhibit ferroelectric properties: they can exhibit spontaneous polarization and piezoelectric properties.[11] Figure 1.10 shows the structure of the chiral smectic C (S_C^*) phase. The ferroelectric liquid crystals (FLCs) have been very important for fast switching electrooptical displays which will be discussed later this chapter. Higher order chiral smectic phases can also be used in ferroelectric displays, at least in principle, but the current study of these phases is far from the point where practical applications are possible. All ferroelectric liquid crystals can selectively reflect circularly polarized light.

1. 4. Liquid crystal displays (LCDs)

Many liquid crystal displays have been introduced since the discovery of the phenomenon of dynamic scattering[12] of liquid crystals. Nowadays, guest-host (GH) mode, twisted nematic (TN), super-twisted nematic (STN), ferroelectric (FLC)[13,14] and active matrix (AM) LCDs[15] all have found their applications. The thorough understanding of the basic principles of all kinds of liquid crystal displays provides useful information to guide future modification of the devices and design and synthesis of new liquid crystal materials.

1. 4. 1. GH mode[16-18]

The GH mode LCD was first proposed in 1966 by Heilmeier and co-workers.[16-18] This mode takes advantage of the anisotropic dyes doped in the liquid crystals. For example, if a dichroic dye is rod-like, the molecules tend to arrange parallel to the liquid crystal molecules and therefore, when the liquid crystal molecules change their orientation in response to the applied external electric field, the orientation direction of the dye molecules will also change. Thus, different colors of different pixels will be observed by varying the applied electric field. Polarizers can also be used to improve the contrast ratio of this kind of device.[9]

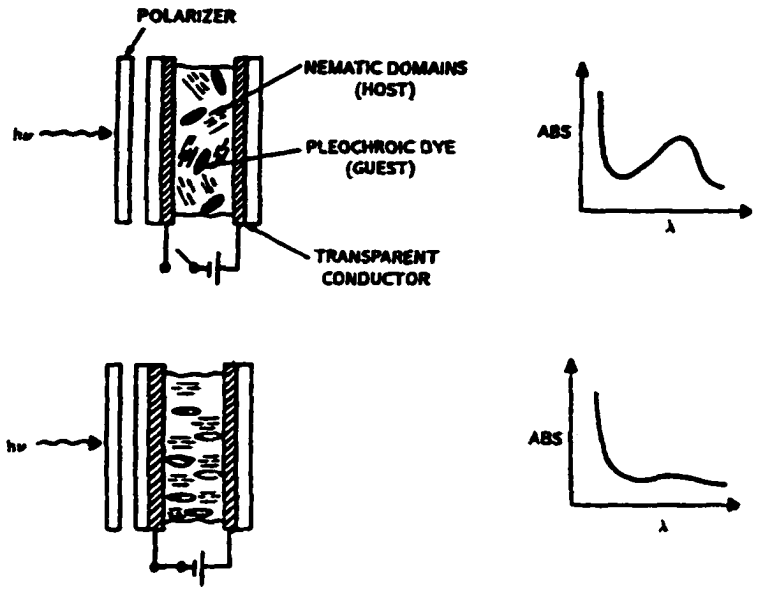

Figure 1.11. Schematic drawing of an LCD using the guest-host mode. On the right hand of the picture are the absorption curves corresponding to the "ON" and "OFF" states, respectively (adopted from Ref. 9).

The performance of GH LCD depends greatly on dye parameters (such as solubility, stability, absorption, etc.) and host liquid crystal mixture properties (such as viscosity, temperature, birefringence, stability, etc.) and the dye's compatibility with the host.

1. 4. 2. TN mode[19]

The TN mode LCD, invented by Schadt and Helfrich,[20] can be used to fabricate LCDs with low operating voltage, low energy consumption, and long life. It is the most widely used LCD mode, and represents the first successful application of liquid crystals. It has been used in wristwatches, calculators and electronic devices for many years.

In this mode, a thin film of liquid crystal (or liquid crystal mixture) with positive dielectric anisotropy, $\Delta\varepsilon > 0$) is sandwiched between two pieces of substrates, the insides of which are transparent ITO (indium-tin oxide) electrodes covered with polyimide films. The polyimide films are rubbed along special directions, so the film can serve to align the vicinal molecules in certain directions. The alignment directions of the two substrates are perpendicular to each other, and as a result, the director of the molecules undergo a smooth 90° twist within the cell (hence the name "twisted" nematic LCD). Outside of the LC cell, two polarizers are used and arranged in such a way that each polarized direction is parallel to the alignment direction of the polymer film of corresponding substrate.

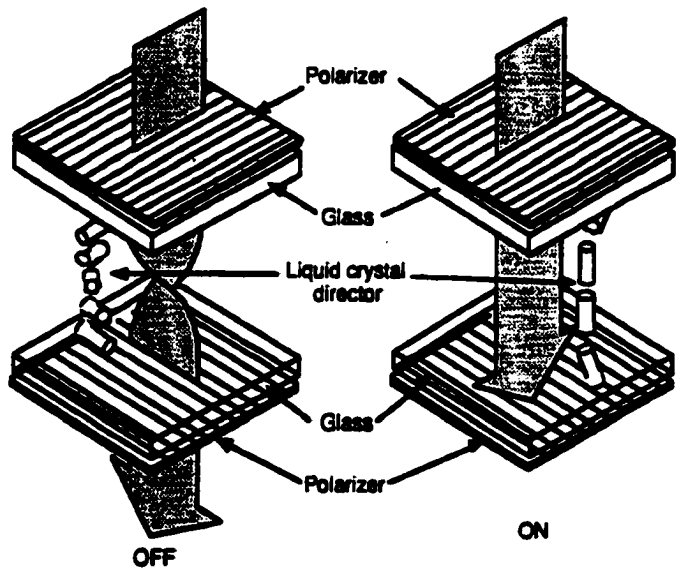

Figure 1.12. Schematic drawing of LCD using twisted nematic mode (normal white mode).[19]

When a beam of light passes through the first polarizer, the non-polarized light now becomes polarized in the same plane as the local orientation of the LC molecules. The twisted arrangement of the LC molecules within the cell then acts as an optical wave guide and rotates the plane of polarization by 90 degrees so that the light which reaches the second polarizer can pass through it. In this state the cell is transparent and this arrangement is called normal white mode.

However, when a voltage is applied to the electrodes, the liquid crystal molecules are forced to align with the resulting electric field and the optical wave guiding property of the cell is lost. The cell is dark, as it would be without the LC present. When the electric field is turned off, the molecules relax back to their twisted state and the cell becomes transparent again. This relaxation step is controlled by the interaction between the alignment film and vicinal LC molecules and the viscosity of the liquid crystal.

To increase the stability of the twisted configuration, some liquid crystals with certain chirality are used as dopant to induce the desired twisting (i.e. clockwise, not anti-clockwise, or vice versa). To obtain a satisfactory contrast ratio, the following requirement (Mauguin condition) must be satisfied:[21]

$$d\,\Delta n >> \lambda/2$$

where d is the thickness of the cell and Δn is the birefringence of the chosen liquid crystal mixture and λ is the wavelength at which the LCD is operated.

1. 4. 3. STN mode[19]

LCDs require high steepness of the electro-optical response to obtain a high quality display. It was found that the twisted configuration of LC cells used in the TN mode can accomplish this provided that the twisting angle is increased to larger than 180°. The STN mode is derived from the TN mode. Liquid crystals used in the STN mode are cholesteric liquid crystals. Another important cell parameter is the pretilt angle (the angle formed by the director of molecules and the substrate). For TN mode, this angle is normally 3° for a rubbed polyimide (PI) alignment film, but a higher twisting angle needs higher pretilt angles such as 20°, which generally is not obtainable from polyimide films. Consequently, other techniques will have to be applied to manufacture alignment films that can provide larger pretilt angle.

STN LCDs require precise control of the flatness of the LC cells, and usually, the accuracy of the cell thickness is below ±0.1~0.2 μm, which limits the availability of large screen STN displays. Currently, high quality STN-LCDs are widely used in lap-top computers and flat panel TV sets.

1. 4. 4. FLC mode[13,14]

FLC displays have advantages such as high storage ability and high response speed and will be a good candidate for large screen, flat, high definition television sets, which was thought to be almost impossible for current STN LCDs.

Due to symmetry considerations, when a molecule is chiral, a spontaneous polarization **Ps** exists and the direction of this vector is tangent to the circle intersection of the cone with the layer plane in S_C^*. Thus a macroscopic sample of

S_C^* is not ferroelectric due to the zero value of the averaged spontaneous polarization along one pitch of the sample.

To achieve macroscopic alignment of the dipoles, a special technique must be used to arrange the molecules in such a way that this helix is not generated in the sample. Very thin LC cells are used, in order that the boundary conditions imposed by the alignment layer would be strong enough to suppress the helix. Thus the smectic layers are perpendicular to the substrates and the state is characterized by a uniform orientation of **Ps** (Figure 1.13).

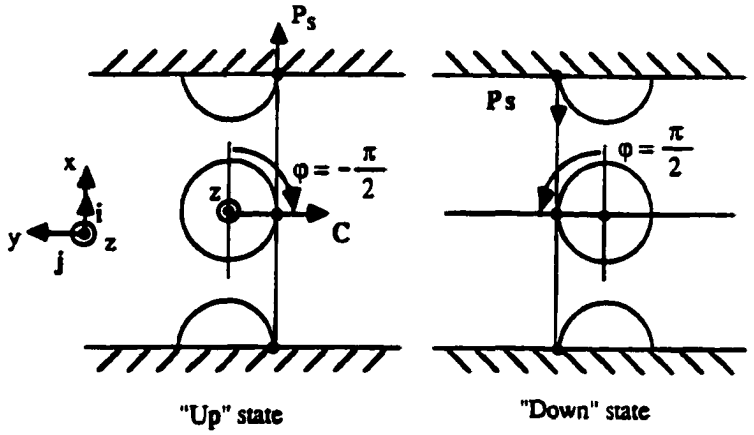

Figure 1.13. Uniform state generated in a thin FLC cell. **Ps** denotes the spontaneous polarization (adopted from Ref. 4).

When uniform states have been successfully generated in the cell, it is possible to switch the orientation of the molecules with the aid of electric field. Then this device can be operated using the same principle as in the TN mode (birefringence type) or GH mode. Figure 1.14 is a schematic representation of the birefringence mode display. The crossed polarizers are arranged with one

polarizer parallel to one possible molecular orientation of one stable state, so one state is non-transmissive, while the other one allows light to cross the cell.

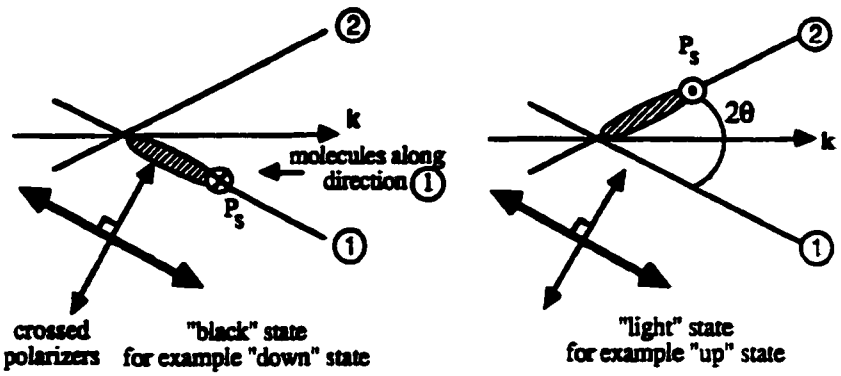

Figure 1.14. Schematic drawing of LCD using FLC birefringence mode (adopted from Ref. 4).

1. 5. Past, present and future of liquid crystal research

After the discovery of liquid crystals, liquid crystal research underwent very slow progress for several decades.[2] In the early stages, studies focused on understanding the basic properties of various liquid crystals and establishing proper methods to study liquid crystals. Shortly after 1960, interest in liquid crystals increased greatly in the United States, Great Britain and the Soviet Union due to the scientific importance of these materials. During the 1970s and 1980s, desires to investigate the relation between structure and properties of liquid crystals and their practical applications led to the rapid flourish of liquid crystal research.

Currently, liquid crystal research has expanded worldwide and various liquid crystal displays have been invented; most of them have found exciting applications. LCDs have many advantages such as small size, low operating

energy, low power consumption, low irradiation and high resolution, which result in new applications previously impossible for traditional CRT displays. For example, portable TV sets with 2.5" LCD screens have been commercially available for some time. Further improvement of the viewing angle and the lowering of prices will lead to wider applications of LCDs.

Obviously, liquid crystal research is multi-disciplinary, requiring concepts and techniques from chemistry and physics at the very least and in some cases also demanding ideas from mathematics, biology and some types of engineering. Nowadays, it is still of interest to find new liquid crystals with low viscosity, low melting point, broad liquid crystal range and good properties for special applications as well. Works to improve the properties, especially the viewing angle,[22-24] contrast ratio[25] and driving speed[26] of LCDs are very popular topics in LCD researches. At the same time, now ideas are being proposed to make LCDs using new materials, such as vitrified liquid crystals,[27,28] polymer composites,[29-31] etc., or LCDs based on new principles, such as bistable cholesteric displays[32] and spatial modulators.[33-35] New alignment techniques are being studied to improve pretilt angle[36-38] and to replace traditional PI alignment films which need to be further rubbed and consequently increase the failure rate of manufacturing substrates and increase the price of LCDs.[39-41]

Liquid crystal displays are the most promising candidates to replace presently dominant CRT displays in the near future. With the development of other techniques such as microelectronics to further improve the capacity and density of the memory elements, it may not be too surprising to see LCDs replace

books printed on paper in the future. Electronic displays combining the high quality of CRT images with the convenience of a flat panel will be a trend of future displays. Because LCDs have the previously mentioned advantages and very good compatibility with electronic elements, new displays to replace LCDs in near future must possess comparable or even higher merits and overcome the weakness of LCDs. Although there have been some reports proposing manufacturing flat panel displays with new materials,[42,43] LCDs will still be expected to dominate the market of displays in the near future and probably expand their applications to many other fields due to the fast development of LCD techniques.

1.6. References

1. Kelker, H., *Mol. Cryst. Liq. Cryst.*, **1988**, *165*, 1.
2. Collings, P. J. and Hird, M., *Introduction to Liquid Crystals, Chemistry and Physics* (Taylor & Francis), **1997**, p 14.
3. Collings, P. J., *Liquid Crystals, Nature's Delicate Phase of Matter* (Princeton University Press), **1990**, p 8.
4. Demus, D., *Liquid Crystals, Applications and Uses* (World Scientific), edited by Bahadur, B., **1990**, *Vol. 1*, p 3.
5. Aoki, H., White, J. L. and Fellers, H. F., *J. Appl. Polym. Sci.*, **1979**, *23 (8)*, 2293.
6. Stevens, M. P., *Polymer Chemistry* (Oxford University Press), Second Edition, **1990**, p 97.
7. Demus D. and Ritcher, L., *Textures of Liquid Crystals* (Deutscher Werl. f. Grundstoffindustrie), Second Edition, **1978**.
8. Gray, G. W. and Goodby, J. W., *Smectic Liquid Crystals* (Glasgow: Leonard Hill), **1984**.
9. Khoo, I.-C and Wu, S.-T., *Optics and Nonlinear Optics of Liquid Crystals* (World Scientific), **1993**, p 4.
10. Demus, D., Diele, S., Grande, S. and Sackman, H., *Advances in Liquid Crystals* (Academic Press), **1983**, *Vol. 6*, p 1.
11. Skarp, K. and Handschy, M. A., *Mol. Cryst. Liq. Cryst.*, **1986**, *165*, 439.
12. Heilmeier, G. H., Zanoni, L. A. and Barton, L. A., *Proc. IEEE*, **1968**, *56*, 1162.

13. Clark, N. A. and Lagerwall, S. T., *Appl. Phys. Lett.*, **1980**, *36*, 899.

14. Harada, T., Taguchi, M., Iwasa, K. and Kai, M., *Proc. SID*, **1985**, *16*, 131.

15. Luo, F. C. *Liquid Crystals, Applications and Uses* (World Scientific), edited by Bahadur, B., **1990**, *Vol. 1*, p 397.

16. Heilmeier, G. H., Zanoni, L. A., *Appl. Phys. Lett.*, **1966**, *13*, 91.

17. Heilmeier, G. H., Castellano, J. A. and Zanoni, L. A., *Mol. Cryst. Liq. Cryst.*, **1969**, *8*, 293.

18. Bahadur, B., *Liquid Crystals: Applications and Uses* (World Scientific), edited by Bahadur, B., **1990**, *Vol. 3*, 65.

19. Scheffer, T. and Nehring, J., *Liquid Crystals: Applications and Uses* (World Scientific), edited by Bahadur, B., **1990**, *Vol. 3*, 232.

20. Schadt, M. and Helfrich, W., *Appl. Phys. Lett.*, **1971**, *18*, 127.

21. Mauguin, C., *Bull. Soc. Franc. Mineral.*, **1911**, *34*, 71.

22. Yuan, H. and Palffy-Muhoray, P., *Mol. Cryst. Liq. Cryst. Sci. Technol. Sect. A*, **1999**, *331*, 2141.

23. Gong, S., Kanicki, J., Xu, G. and Zhong, J. Z. Z., *Jpn. J. Appl. Phys., Part 1*, **1999**, *38*, 4110.

24. Seki, H., Uwano, T. and Uchida, T., *Mol. Cryst. Liq. Cryst. Sci. Technol. Sect. A*, **1999**, *331*, 2275.

25. Kobayashi, S. and Furue, H., *Proc. SPIE-Int. Soc. Opt. Eng.*, **1998**, *3421*, 2.

26. Seo, D. and Lee, J., *Jpn. J. Appl. Phys., Part 1*, **1999**, *38*, L1432.

27. Chen, S. H., Shi, H., Conger, B. M., Katsis, D. and Mastrangelo, J. C., *Mater. Res. Soc. Sym. Proc.*, **1996**, *425*, 3.

28. Katsis, D., Chen, H. M., Mastrangelo, J. C., Chen, S. H. and Blanton, T. N., *Chem. Mater.*, **1999**, *11*, 1590.

29. Maschke, U., Gloaguen, J. -M., Tugis, J. -D. and Cogueret, X., *Mol. Cryst. Liq. Cryst. Sci. Technol., Sec. A*, **1996**, *282*, 407.

30. Zharkova, G. M., Samsonova, L V., Streltzov, S. A., Khochaturyan, V. M., Kutulya, L. A. and Vashchenko, V. V., *Proc. SPIE-Int. Soc. Opt. Eng.*, **1998**, *3488*, 97.

31. Blacker, R. S., Lewis, K. L., Mason, I. and Webb, K., *Mater. Res. Soc. Symp. Proc.*, **1998**, *488*, 441.

32. Taheri, B., West, J. L. and Yang, D. K., *Proc. SPIE-Int. Soc. Opt. Eng.*, **1998**, *3297*, 115.

33. Wu, S. T., *Appl. Phys. Lett.*, **1990**, *57*, 986.

34. Takizawa, K., Fujii, T., Kikuchi, H., Fujikake, H., Kawakita, M., Hirano, Y. and Sato, F., *Appl. Opt.*, **1999**, *38*, 5646.

35. Haase, W., Ganzke, D. and Pozhidaev, E. P., *Mater. Res. Soc. Symp. Proc.*, **1999**, *559*, 15.

36. Drushlyak, A. C., Dobrolyubova, E. I., Dorozhkina, G. G., Novoseletskii, N. V. and Umanskii, B. A., *Mol. Cryst. Liq. Cryst. Sci. Technol., Sect. A*, **1999**, *329*, 1137.

37. Cui, L., Jin, W., Liu, Y., Xie, P., Zhang, R., Zhu, C. and Wang, C., *Mol. Cryst. Liq. Cryst. Sci. Technol., Sect. A*, **1999**, *333*, 135.

38. Seo, D., *J. Appl. Phys.*, **1999**, *86*, 3594.

39. Schadt, M., Schmit, K., Kozinkov, V. and Chigrinov, V., *Jpn, J. Appl. Phys., Part 1*, **1992**, *31*, 2155.

40. Gibbons, M., McGinnis, B. P., Shannon, P. J. and Sun, S. -T., *Proc. SPIE-Int. Soc. Opt. Eng.*, **1999**, *3635*, 32.

41. Seo, D. and Lee, C., *Mol. Cryst. Liq. Cryst. Sci. Technol., Sect. A*, **1999**, *329*, 867.

42. Wang, Q., Li, W., Jabbour, G. E., Cui, J., Marks, T. J., Kippelen, B. and Peyghambarian, N., *Polym. Prepr.*, **1999**, *40*, 1248.

43. Choi, W. B., Chung, D. S., Kang, J. H., Kim, H. Y., Jin, Y. W., Han, I. T., Lee, Y. H., Jung, J. E., Lee, N. S., Park, G. S. and Kim, J. M., *Appl. Phys. Lett.*, **1999**, *75*, 3129.

Chapter II. NMR Study of 4'-Cyanophenyl 4-*n*-heptylbenzoate (7CPB) and A Mixture with Its Chain-perfluorinated Analog*

2.1. Introduction

2.1.1. Fluorinated liquid crystals and liquid crystal mixtures

Fluorinated liquid crystals have received much attention[1-3] for the fact that fluorine substitution can increase the impedance and decrease the viscosity of liquid crystalline compounds substantially, making them advantageous in fabricating high performance TFT (thin-film transistor) display devices. The presence of fluorine atoms can also change the polarity and phase behavior of molecules. It has been shown that the replacement of a hydrocarbon chain in a liquid crystal by a perfluorinated or semi-perfluorinated chain highly favors the smectic A or smectic C phase.[4-6] The poor miscibility of hydrocarbon and fluorocarbon segments causes different parts in segmentally fluorinated alkanes to organize themselves in layered structures or microdomains of different compositions.[7] The same case can be found in the crystalline state, where the molecular packing is controlled by steric structure and intermolecular interactions.[8] Therefore, the phase behavior of mixtures of liquid crystals with hydrocarbon and fluorocarbon chains, respectively, should be different from that of normal hydrocarbon liquid crystal mixtures. However, it is surprising that there are not many studies of hydrocarbon/fluorocarbon liquid crystal mixtures.

* Some of the material in this chapter is presented in a paper entitled "Orientational ordering of a nematic liquid crystal and its mixture with its chain-perfluorinated analog" by Hong Sun and B. M. Fung, *Liquid Crystals*, in press.

2.1.2. Order parameters

As mentioned in Chapter I, there is no positional order in the bulk of liquid crystals, while they do exhibit some orientational order. This behavior is described quantitatively by order parameters.

In liquid crystal phases, the molecules have a preference of orientation, denoted as the director and it can be represented as a unit vector. The director can also be viewed as the average of molecular orientation. One way we can visualize taking an average in the orientation is to take a snapshot of a representative group of molecules considered as rigid rods at a certain time. Each molecule in the picture is oriented at some angle with respect to the director. The angles can be measured and used to calculate the average angle as a measure of the amount of orientational order. All the angles are between 0° and 90°, so the average should also be between 0° and 90°. The higher the orientational order, the closer the average angle would be to zero. Because this arrangement is in three dimensions, the most useful formulation is to find the average of the second Legendre polynomial,[9,10] $\frac{1}{2}(3\cos^2\theta-1)$, in a polar coordinate system:

$$S = \langle P_2(\cos\theta)\rangle = \langle \frac{3}{2}\cos^2\theta - \frac{1}{2}\rangle = \int_0^{\pi} f(\theta)\,(\frac{3}{2}\cos^2\theta - \frac{1}{2})\sin\theta\, d\theta \int_0^{2\pi} d\phi$$

where θ is the angle formed by the molecules and the director, ϕ is the azimuthal angle formed by molecules and some arbitrary axis within a plane perpendicular to the director, and $f(\theta)$ is the angular distribution function of orientational order of molecules. $f(\theta)$ can be defined by either taking a snapshot of a certain group of

molecules at any time and noting the number of molecules that form an angle of θ or by following a single molecule, noting at specified times the angle θ between the molecular axis and the director. Statistically, these two definitions are the same if it is assumed that all molecules undergo the same type of random motion. Since all directions perpendicular to the director are equivalent in the most simple liquid crystal phase, the orientation does not depend on the azimuthal angle ϕ. It should be noticed that this distribution function is not normalized.

In general, numerous orientations can make an angle of 90° to the director, but only one arrangement corresponds to 0°. Therefore, in an isotropic phase there will be many more molecules making an angle of 90° with the director compared to 0°. If we average the measurement of angles of random arrangement, the value should be $\theta = \cos^{-1}(1/\sqrt{3}) = 54.73°$. Therefore, no orientational order means an average angle of 54.73° and a smaller average angle indicates the existence of orientational order.

To further understand how the order parameter S represents the amount of orientational order, let us calculate the value of S if the molecules are perfectly oriented, that is if $\theta = 0$ for all molecules. Now, the distribution function $f(\theta)$ becomes 1, when $\theta = 0$; while $f(\theta) = 0$ at any other angle θ. Now the integration can not be done, but the average is easy to perform and the averaged term is constant 1. Let us now consider another extreme case and the molecules are arranged in an absolutely disordered way, that is, the molecules point in all directions. In this case, the distribution function is a constant (independent of θ, assume it to be a, an arbitrary constant), so

$$S = \frac{\int_0^{\pi} f(\theta)(\frac{3}{2}\cos^2\theta - \frac{1}{2})\sin\theta d\theta \int_0^{2\pi} d\phi}{\int_0^{\pi} f(\theta)\sin\theta d\theta \int_0^{2\pi} d\phi} = \frac{\int_1^{-1} -a(\frac{3}{2}x^2 - \frac{1}{2})dx \int_0^{2\pi} d\phi}{\int_1^{-1} -adx \int_0^{2\pi} d\phi} = 0$$

where, $x = \cos\theta$. Thus S is zero if there is no orientational order. In the calculation, the denominator is used to normalize the distribution function. From the above discussion, it can be found that the value of S is between 0 for absolute disorder to 1 for perfect order and it quantifies the orientational order of the liquid crystal phase.

For cases in between, if the distribution function can be found, it is rather easy to calculate the corresponding order parameter S. It should be kept in mind that the above definition of the order parameters is used for "sticks" (or uniaxial phase of cylindrical rods), and for molecules with more complex structure, more order parameters are needed to describe the orientational order. For example, in a biaxial phase, two order parameters are needed:[11]

$$S_{zz} = \frac{1}{2}\langle 3\cos^2\theta - 1\rangle$$

$$S_{xx}\text{-}S_{yy} = \frac{3}{2}\langle \sin^2\theta\cos 2\phi\rangle$$

where, the z axis points to the director and the x and y axes are within the plane perpendicular to the director. S_{xx}-S_{yy} is an order parameter related to the "flatness" of the molecules. More general definitions can be found in Ref. 11.

To a first approximation S is a function of temperature. A closed analytical dependence of S on T is not available since it is strongly dependent on

the type of molecules considered. A useful empirical relation between S and T will be discussed in Section **2.6.**

As a result of ordering, liquid crystals exhibit anisotropy in many of their properties, which can be related to the order parameter,[12] such as,

$$\Delta\varepsilon = \varepsilon_{//} - \varepsilon_{\perp}$$

$$= (NhF/\varepsilon_0)[\alpha_l - \alpha_t - F(\mu^2/2k_BT)(1-3\cos^2\beta)]S$$

$$\Delta n \sim \rho^{1/2} S$$

$$\Delta\chi = \chi_{//} - \chi_{\perp} = (\chi_l - \chi_t) S$$

where $\Delta\varepsilon$, Δn and $\Delta\chi$ are dielectric anisotropy, birefringence, and magnetic susceptibility anisotropy, respectively. N is the number of particles, F and h are constants of proportionality called the reaction field factor and cavity factor. α_l and α_t are the two major components of polarizability tensor α, where the subscripts *l* and *t* stand for contributions from longitudinal and perpendicular to the molecular axis. μ is the moment of molecule, β is the angle between μ and the direction of α_l, and ρ is the mass density. On the other hand, order parameter can be used to estimate the anisotropic properties of the liquid crystal system provided that the relations between the properties and order parameters are known.

2.1.3. Methods to measure order parameters

The order parameter S can be measured in a number of ways, such as dielectric relaxation,[12] infrared spectroscopy,[13] X-ray diffraction[14] and nuclear magnetic resonance (NMR). Usually a macroscopic property of the liquid crystal

phase is measured, which then can be used to determine S if the molecular parameters that produce the macroscopic property are known.

Of all the methods mentioned above, NMR probably gives the most detailed information at the molecular level since it probes each nucleus via its distinct signal and it can therefore determine the ordering and motion of individual parts of liquid crystal molecules. For this reason, NMR has been used extensively to investigate the orientational ordering of liquid crystals. Proton NMR is suitable for the study of small solute molecules in liquid crystalline solutions, but it does not offer detailed information for pure liquid crystalline phases as the peaks are usually not well resolved.[15-19] On the other hand, by measuring quadrupolar splittings and relaxation, ^{2}H NMR has been applied successfully to study the orientational ordering and motions of liquid crystals.[20-26] However, it is not trivial work to synthesize liquid crystals with unfunctionalized sites deuterated, which limits the application of ^{2}H NMR as a consequence.

A 2D ^{13}C NMR technique was developed in this laboratory to measure the orientational ordering of nematic and smectic A liquid crystals in 1986.[27-42] This method involves a combination of SLF (separated local field spectroscopy)[43-46] and VAS (variable angle spinning), which is also called OMAS (off-magic-angle-spinning),[47] and has proven very effective. A recent improvement of this technique increased the resolution of the 2D spectra,[48-51] and it is now called PELF (proton-encoded local field) spectroscopy.[52] The combination of PELF with OMAS was used in this study, so the principle of this method is briefly discussed in the following.

2.2. The PELF/OMAS technique

The NMR spectra of liquid crystals and solids are often complicated by the existence of extensive dipolar interactions. Without any decoupling mechanism, the dipolar interactions are usually strong and cause complex splitting patterns, resulting in the formation of broad peaks. In a spin system containing protons and carbon-13, the ^{13}C NMR spectrum can be simplified with the application of a homonuclear (proton-proton) decoupling, and carbon-proton dipolar coupling constants can be measured from the simplified spectrum. From these dipolar coupling constants, the orientational ordering of the liquid crystals can be determined.

In the past, many decoupling pulse sequences have been developed to remove the homonuclear dipolar couplings. It was found in this laboratory that the BLEW-48 sequence[53] is the most effective one in eliminating homonuclear couplings with moderate decoupling power. It is also least sensitive to the offset of the decoupler from the center of proton resonance. The success of PELF/OMAS and SLF/VAS relies on the application of BLEW-48 sequence, which is represented as

$$1\ \bar{1}\ \bar{1}\ 1\ \ 1'\ \bar{1}'\ \ \bar{1}'\ 1'$$

Where $1 = X\,Y\,\bar{X}\,\bar{X}\,\bar{Y}\,\bar{X}$

$\bar{1} = X\,Y\,X\,X\,\bar{Y}\,\bar{X}$

$1' = X\,\bar{Y}\,\bar{X}\,\bar{X}\,Y\,\bar{X}$

$\bar{1}' = X\,\bar{Y}\,X\,X\,Y\,\bar{X}$

and X is a 90° pulse on the x axis, Y is a 90° pulse on the y axis, $\overline{X}$ is a 90° pulse on the -x axis, and $\overline{Y}$ is a 90° pulse on the -y axis.

Even with the removal of proton-proton dipolar couplings by the BLEW-48 sequence, the proton-carbon dipolar couplings are still retained. Therefore, the ^{13}C NMR spectra of liquid crystal samples are complicated with splittings by scalar couplings and H-C dipolar couplings, which are not resolvable in the coupled spectra. Each splitting for carbons is related to the H-C dipolar coupling and scalar coupling by the following equation

$$\Delta\nu = f(2D + J) \tag{2.1}$$

where f is a factor determined by the BLEW-48 decoupling sequence. Its theoretical value is 0.420[53] and experimental value is 0.414.[52] D is dipolar coupling constant and J is the scalar coupling constant.

To distinguish the splittings for individual ^{13}C peaks with different chemical shifts, the 2D separated local field[43-46] technique can then be applied. Normally, in this kind of 2D technique, a broadband decoupling sequence is applied to obtain normal proton-decoupled ^{13}C spectrum in the ω_2 dimension. Because the proton spectra of liquid crystals have wide spectral windows, the decoupler power applied must be considerably larger than that for liquid samples. Excessive decoupler power, on the other hand, leads to rf heating, which is an extremely undesirable effect because the orientational ordering of liquid crystals is very sensitive to temperature.[41] To alleviate this problem, the OMAS (off-magic-angle-spinning) technique can be utilized. For solids, MAS (magic angle spinning) is usually used to reduce the linewidths of the peaks, but all information

on anisotropic interactions is lost. Fortunately, liquid crystals give rather sharp ^{13}C peaks under the condition of OMAS. OMAS scales down the anisotropic chemical shifts and dipolar couplings, which are the most important information for the study of orientational ordering of liquid crystals. The reduction of dipolar couplings makes it possible to use milder conditions for both homonuclear and heteronuclear decoupling.

In the OMAS technique, a liquid crystal sample is spun rapidly at an angle θ with respect to the magnetic field of the NMR spectrometer. Now, the magnetic torque exerted on the liquid crystal sample is overcome by the viscous torque and as a result, for $\theta < 54.73°$, a liquid crystal with positive magnetic susceptibility $\Delta\chi > 0$ would have its nematic director aligned along the spinning axis instead of magnetic field; a liquid crystal with $\Delta\chi < 0$ would have its nematic director aligned perpendicular to the spinning axis. For $\theta > 54.73°$, the situations are the opposite.

For the parallel alignment, now the anisotropic coupling is reduced by a factor $(3\cos^2\theta\text{-}1)/2$ and Eq. 2.1 is changed to

$$\Delta\nu = f[(3\cos^2\theta - 1)\, D + J] \qquad (2.2)$$

because the anisotropy in the scalar coupling is negligible.

In the separation of C-H dipolar couplings according to the ^{13}C chemical shifts, the SLF technique probes the anisotropic C-H dipolar local fields at the carbon sites. Because dipolar coupling is basically through space and because of the much higher number density of the ^{1}H nuclei, each ^{13}C nucleus is coupled to several protons, which are either directly bonded or not bonded to it (long-range

coupling). Due to the successive splittings, the SLF spectrum of a carbon coupled to N protons exhibits up to 2^N lines, even when homonuclear dipolar interaction among the protons is removed. Since most of the long-range couplings overlap with each other and cannot be resolved, the peaks in the SLF spectra are usually quite broad.

An improvement was made by Pines and co-workers on this 2D method to detect the dipolar-coupling local field on the proton sites.[48-51] The idea is that with the effective removal of the proton-proton dipolar coupling by a homonuclear decoupling sequence (they used MERV-8), each proton is only coupled to one ^{13}C site due to the low natural abundance of ^{13}C and this dipolar coupling information can be encoded in the proton magnetization and then be transferred from the abundant spin (proton) to the rare spin (carbon) local field by cross polarization. When the signals for each carbon are observed, each kind of dipolar-coupled proton will only give a doublet. The line number for each carbon is now reduced to up to 2N and thus the spectrum is much simplified. This method is now called PELF (proton encoded local field) spectroscopy.[52]

In this modified method, during the acquisition period, a very effective heteronuclear decoupling sequence SPINAL-64[54] (*S*mall *P*hase *IN*cremental *AL*ternation with 64 steps) is applied, which was developed in this laboratory and was found that for liquid crystal samples it is superior to many other broadband decoupling sequences, such as, MLEV,[55-58] WALTZ,[59,60] and GAPP.[61,62] The sequence is represented as:

$$Q\,\bar{Q}\,\bar{Q}\,Q\;\;\bar{Q}\,\bar{Q}\,Q\,Q$$

where Q = 165(10°) 165(-10°) 165(15°) 165(-15°) 165(20°) 165(-20°) 165(15°) 165(-15°)

$\overline{Q}$ = 165(-10°) 165(10°) 165(-15°) 165(15°) 165(-20°) 165(20°) 165 (-15°) 165 (15°).

The pulse sequence of the PELF/OMAS method is shown below in Figure 2.1.[52] During evolution period, BLEW-48 decoupling is used to remove proton-proton dipolar coupling as explained above, and then the encoded proton-carbon dipolar coupling information is transferred to carbons by cross polarization, so that in the ω_1 dimension, one-bond couplings and some two-bond couplings can be observed. During acquisition period, the SPINAL-64 broadband decoupling sequence is applied to obtain normal proton-decoupled ^{13}C spectrum in the ω_2 dimension.

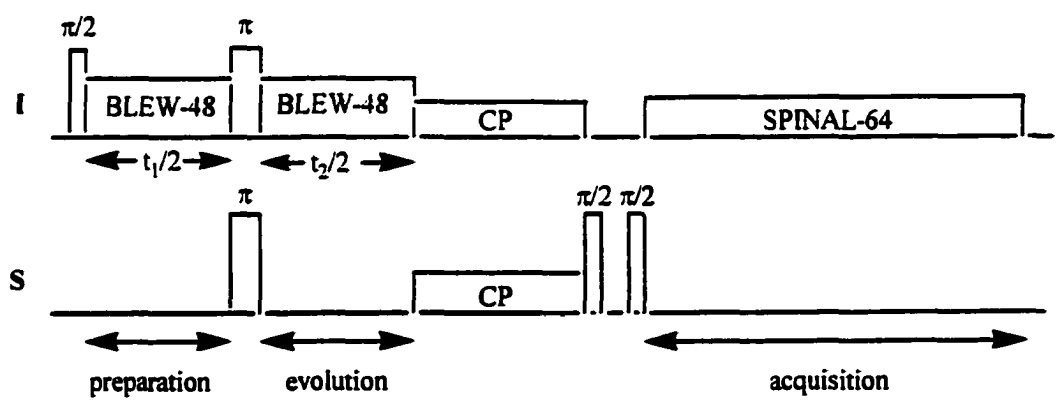

Figure 2.1. Schematic diagram of the 2D proton-encoded local field spectroscopy. CP = cross polarization. The last two π/2 pulses of the S spin act as a "z-filter".

2.3. Orientational ordering information from PELF/OMAS technique

In the liquid crystalline phase, each benzene ring has an effective C_{2v} symmetry because it undergoes rapid flips between two equilibrium positions. Therefore, two order parameters, S_{zz} and S_{xx}-S_{yy}, are sufficient to describe the orientational ordering of each ring. These order parameters can be related to the dipolar coupling constant of each C-H pair in the ring by[63]

$$D_{ij} = -\frac{\gamma_i \gamma_j h}{8\pi^2 r_{ij}^3}[(3\cos^2\theta_{ijz} - 1)S_{zz} + (\cos^2\theta_{ijx} - \cos^2\theta_{ijy})(S_{xx} - S_{yy})] \qquad (2.3)$$

where r_{ij} is the internuclear distance and $\theta_{ij\alpha}$ is the angle between ring and the molecular axis α. The twofold axis of the phenyl ring is taken as the *z* axis, and the axis perpendicular to the plane of the phenyl ring is taken as the *y* axis. Normally, the values, r_{CC} = 0.140 nm, r_{CH} = 0.108 nm are used in the calculation, so the order parameters and the bond angle can be determined from least-squares fitting of a set of D values to Eq. 2.3.

The aliphatic chain, on the other hand, has a large number of segmental motions, and it is difficult to define the order parameters for the whole chain. A simplified treatment can be made to define a C-H bond order parameter for each aliphatic segment, considering the C-H bond as having an approximate axial symmetry. Taking r_{CH} = 0.110 nm for CH_2 and CH_3 groups, the order parameter of the C-H bond is related to the corresponding C-H dipolar coupling constant by[41]

$$D = -\frac{\gamma_C \gamma_H h}{4\pi^2 r_{CH}^3} S_{CH} = -4.047 \times 10^{-5} D_{CH} \qquad (2.4)$$

2.4. Orientational ordering information from 1D ^{13}C NMR method

Although the 2D PELF/OMAS method (and the earlier 2D VAS/SLF version) has proven to be very successful to determine order parameters of liquid crystals, it requires special hardware and software and needs stringent control of experiment conditions, which limits its application. In addition, prolonged spectrometer time and extensive data processing can not be avoided for these 2D methods. Therefore, it is preferable to determine order parameters by using 1D ^{13}C NMR. For macroscopically oriented liquid crystal samples, the major advantage is the simplicity of the spectra with the application of suitable broadband decoupling pulse sequence. The existence of chemical shift anisotropy normally makes the chemical shifts of different carbons vary from those for liquid samples. Anisotropic chemical shift is related to isotropic chemical shift by the following equation[41]

$$\begin{aligned}\delta_{obs} &= \delta_{iso} + \delta_{ani} \\ &= \delta_{iso} + \frac{2}{3}S_{zz}[\sigma_{zz} - \frac{1}{2}(\sigma_{xx} + \sigma_{yy})] + \frac{1}{3}(S_{xx} - S_{yy})(\sigma_{xx} - \sigma_{yy}) \\ &+ \frac{2}{3}S_{xy}\sigma_{xy} + \frac{2}{3}S_{xz}\sigma_{xz} + \frac{2}{3}S_{yz}\sigma_{yz} \qquad (2.5)\end{aligned}$$

where the S_{ij}'s are components of the order matrix, and the σ_{ij}'s are components of chemical shift tensor, both being in the same axis system.

Obviously, from the equation, one cannot get order parameters without knowing the chemical shift tensors. However, it needs single crystal samples to obtain chemical shift tensors and for polycrystalline samples, complicated axis

transformation is a must. Fortunately, for systems with higher symmetry, for example, phenyl rings of C_{2v} symmetry, Eq. 2.5 can be simplified to

$$\delta_{obs} - \delta_{iso} = \frac{2}{3} S_{zz}[\sigma_{zz} - \frac{1}{2}(\sigma_{xx} + \sigma_{yy})] + \frac{1}{3}(S_{xx} - S_{yy})(\sigma_{xx} - \sigma_{yy}) \qquad (2.6)$$

It was found that experimental values of S_{xx}-S_{yy} are almost always less than 10% of those of S_{zz} and do not show systematic variation with the change in temperature. Therefore, by replacing the last term with an empirical constant *b*, Eq. 2.6 can be further simplified to

$$\Delta\delta = \delta_{obs} - \delta_{iso} \approx \frac{2}{3} S_{zz}[\delta_{zz} - \frac{1}{2}(\delta_{xx} + \delta_{yy})] + b \qquad (2.7)$$

Letting $a = \frac{2}{3}[\delta_{zz} - \frac{1}{2}(\delta_{xx} + \delta_{yy})]$, Eq. 2.7 can be rewritten as[38,42]

$$\Delta\delta = a\,S + b \qquad (2.8)$$

where S is previous S_{zz} and the subscript z is dropped. This requires that the major axis of chemical shift tensor coincide with the z axis of the phenyl ring. Although this is approximately true for the carbon atoms lying on the symmetry axis of the phenyl ring, it is not necessarily so for the rest carbon atoms; for aliphatic carbon atoms, the above approximation is not fulfilled. Nevertheless, the semi-empirical relationship has been found to work surprisingly well for both aromatic and aliphatic carbon atoms in many types of liquid crystal samples.[42]

The method to determine order parameters by using ^{13}C chemical shift data is described in the following. First, the PELF/OMAS technique is used to study the liquid crystal sample at several different temperatures within the liquid crystal range. The order parameters are then calculated by the dipolar coupling constants obtained in this method, using Eqs. 2.3 (least-squares fitting method

needed, of course) and 2.4. The anisotropic chemical shifts of the same compound are then determined from 1D spectra at the same temperatures. Then the order parameters and anisotropic chemical shifts are correlated by Eq. 2.8 to obtain the empirical constants *a* and *b*, from which order parameters at other temperatures can be calculated from chemical shift values.

This method has the following advantages. First, the chemical shifts can be obtained from 1D experiments, which requires much less spectrometer time, making it possible to investigate changes of the order parameter with temperatures in smaller temperature steps. Second, the chemical shift data can be determined more precisely than the dipolar coupling constants, and their systematic changes with temperature are less subjected to random experimental uncertainties. Many interesting studies can be carried out with this method, such as, effect of various solutes on the orientational ordering of liquid crystal solvents, the phase behavior of liquid crystal mixtures, order of phase transitions of liquid crystals and the temperature dependence of the position of the major axis of the mesogenic core, etc.

The goal of this research was first to obtain the empirical relationship between order parameters and ^{13}C chemical shift anisotropy of a liquid crystal 7CPB (4'-cyanophenyl 4-*n*-heptylbenzoate) and to study the change of the order parameter with temperature over the whole nematic range. The empirical constants obtained in this study can also be utilized in the orientational ordering study by those that have no access to the PELF/OMAS technique. Fitting the

temperature dependence of the order parameter into the Haller equation could provide information about the segmental movement of the molecules at a limit of perfect ordering. Such information for the aliphatic chain has not been investigated thus far. Due to the importance of the study of phase behavior of hydrocarbon and fluorocarbon mixtures, the second part of this work deals with the phase behavior of a mixture of 7CPB and its chain-perfluorinated analog 7PFCPB (4'-cyanophenyl 4-*n*-perfluoroheptylbenzoate). The mixture was studied by 1D ^{13}C NMR method, and the ordering of the 7CPB component was then evaluated to obtain useful information about the system.

2.5. Experimental

2.5.1. Synthesis of 4'-cyanophenyl 4-*n*-heptylbenzoate (7CPB)

4'-Cyanophenyl 4-*n*-heptylbenzoate was synthesized by following a general procedure:[40,64] To a solution of 4-cyanophenol (1.1 g, 9.2 mmol) in pyridine (30 mL) was slowly added a solution of 4-*n*-heptylbenzoyl chloride (2.0 g, 8.4 mmol) in 1, 4-dioxane (15 mL), and the mixture was then refluxed for 5-6 hours. After cooling, the reaction mixture was poured into a 1:1 mixture of ice and concentrated hydrochloric acid (50 mL). Chloroform (30 mL) was added to dissolve the white precipitate and the aqueous part was further extracted with chloroform (30 mL x 3). The organic portions were combined, washed with H_2O (30 mL x 2), 20% NaOH (20 mL x 2), H_2O (30 mL x 3) successively and then dried over Na_2SO_4. After the removal of the solvent, the solid was further purified by multiple recrystallizations from a mixture of ethanol and water.

Yield, 1.5 g (56%); white crystals, mp 40-42 °C; 400-MHz ^{1}H NMR ($CDCl_3$) 8.98 (d, J = 7.8 Hz, 2H), 7.74 (d, J = 8.3 Hz, 2H), 7.32-7.37 (m, 4H), 2.71 (t, J = 7.8 Hz, 2H), 1.66 (m, 2H), 1.28-1.34 (br, 8H), 0.89 (t, J = 6.1 Hz, 3H); 100-MHz ^{13}C NMR ($CDCl_3$) 165.5, 155.5, 151.2, 134.8, 131.5, 129.9, 127.1, 124.0, 119.4, 110.8, 37.2, 32.8 (CH_2), 32.2, 30.3, 30.2, 23.7, 15.2.

2.5.2. Synthesis of 4'-cyanophenyl 4-*n*-perfluoroheptylbenzoate (7PFCPB)

The synthesis of 4'-cyanophenyl 4-*n*-perfloroheptylbenzoate (7PFCPB) is shown below in Scheme 2.1.

Scheme 2.1

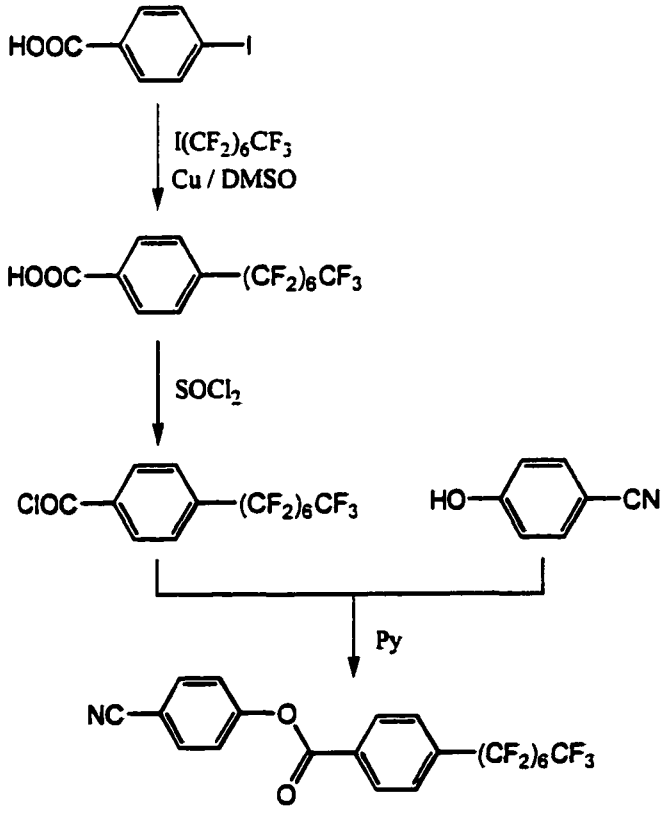

2.5.2.1. 4-*n*-Perfluoroheptylbenzoic acid[65]

A 3-necked round bottom flask equipped with thermometer, condenser and nitrogen inlet, was charged with $CF_3(CF_2)_6I$ (15.5 g, 31.3 mmol), 4-iodobenzoic acid (7.8 g, 31.3 mmol), freshly activated copper bronze (10.0 g, 157.5 mmol)[66] and freshly distilled dimethyl sulfoxide (50 mL). The reaction system was purged with N_2 first and then heated at 110 °C under N_2 with stirring overnight. After cooling to room temperature, ether (300 mL) was added. A blue precipitate was formed which was then filtered off. The liquid part was treated with water (200 mL), and the resultant blue precipitate was separated and combined with the previous solid portion. The solid was treated with hydrochloric acid and then extracted with ether (50 mL x 4). All extracts were combined, washed with water till neutral and then dried over Na_2SO_4. A solid (a mixture of 4-iodo-benzoic acid and 4-*n*-perfluoroheptylbenzoic acid, 10.1 g) was obtained after the distillation of the solvent.

2.5.2.2. 4'-Cyanophenyl 4-*n*-perfluoroheptylbenzoate

The 4-*n*-perfluoroheptylbenzoic acid mixture (4.5 g, ~ 9.2 mmol) obtained from the last step was dissolved in hot toluene (70 mL). Thionyl chloride (1.5 mL) was added dropwise to the above solution and the reaction mixture was refluxed for 5 hours. Toluene and excess thionyl chloride was removed using a rotary evaporator. The residual solid was washed with toluene and dried under reduced pressure. The residual yellow solid was dissolved in 1, 4-dioxane (30 mL) and added dropwise to a solution of 4-cyanophenol (1.29 g, 10.8 mmol) in

pyridine (30 mL). The mixture was then heated at 100 °C for 15 hours. The work-up procedure of this reaction was similar to that of 4'-cyanophenyl 4-*n*-heptylbenzoate (7CPB), except that this compound needed further silica gel column chromatographic separation (ethyl ether). White crystals were obtained. Yield, 2.5 g (29%); 400-MHz ^{1}H NMR ($CDCl_3$) 8.34 (d, J = 8.3 Hz, 2H), 7.78 (d, J = 8.3 Hz, 2H), 7.77 (d, J = 8.3 Hz, 2H), 7.39 (d, J = 8.3 Hz, 2H); 100-MHz ^{13}C NMR (bulk) 162.8, 154.2, 134.4, 133.3, 130.1, 127.0, 122.2, 117.3, 110.6, 108.0-132.0 (CF_2's and CF_3).

2.5.3. Phase transition measurements

The phase transitions of the two compounds were measured using a Perkin Elmer DSC7 differential scanning calorimeter. The liquid crystalline phases were checked under cross polarizing microscope (Olympus BH-2).

2.5.4. ^{13}C NMR

^{13}C NMR experiments using the 2D PELF/OMAS technique were performed on 4'-cyanophenyl 4-*n*-heptylbenzoate with the use of a Varian UNITY/INOVA 400 NMR spectrometer equipped with a variable-angle spinning probe. The PELF pulse was used with proton-carbon cross-polarization and the BLEW-48 decoupling sequence. Temperature calibration was made by observing the temperature-dependent chemical shift change of ethylene glycol. In this experiment, the sample was spun at an angle θ with respect to the magnetic field B_0, which was 47.58° and calibrated by measuring the ^{2}H splitting of a sample of

$CDCl_3$ dissolved in a liquid-crystalline solvent ZLI-1291 with and without sample spinning.

The chemical shift determination of pure 4'-cyanophenyl 4-*n*-heptylbenzoate (7CPB) and a mixture of 7CPB and its fluorocarbon analog 7PFCPB was conducted on the same spectrometer. An indirect detection probe manufactured by Narolac Corporation, Mastinez, CA, was used. The sample was first heated above its clearing point and the chemical shift of the terminal methyl was set to be 14.05 ppm with respect to tetramethylsilane (TMS), so that the data were self-consistent. The chemical shift measurement was then made with decreasing temperature at 1 °C intervals. To prevent rf overheating, a 1.6% decoupler duty cycle was used with a total cycling time of 3.558 s and a $\gamma B_2/2\pi$ value of 9.06 kHz. The calibration of temperature was made using ethylene glycol.

2.6. Results and discussion

4'-Cyanophenyl 4-*n*-heptylbenzoate (7CPB) melts at 40.3 °C to form a nematic phase, which then turns isotropic at 52.7 °C. These are slightly different from literature values.[40] Its chain-fluorinated analog 7PFCPB melts at 107.5 °C to form a smectic A phase, which becomes isotropic at 136.4 °C.

The peak assignments of aromatic carbons of the ^{13}C NMR spectrum in the isotropic phase were made with the aid of the group contribution method. In this method, the chemical shift value of unsubstituted benzene, 128.0 ppm is used as base value, and substituents cause the chemical shift changes of *ortho*-, *meta*-,

para- and directly bonded carbon atoms differently. The changes are known as increment values, which are tabulated in many books, such as Ref. 67. Then the chemical shift of each aromatic carbon can be calculated by adding up all increment values induced by all substituents on the phenyl ring. For the aliphatic carbons, the assignments were based on comparison with corresponding cyanobiphenyls. The proton coupled ^{13}C NMR spectrum of this compound was taken to find out the scalar coupling constants, J's, for the later calculation of dipolar coupling constants (Eq. 2.2). All results are summarized in Table 2.1.

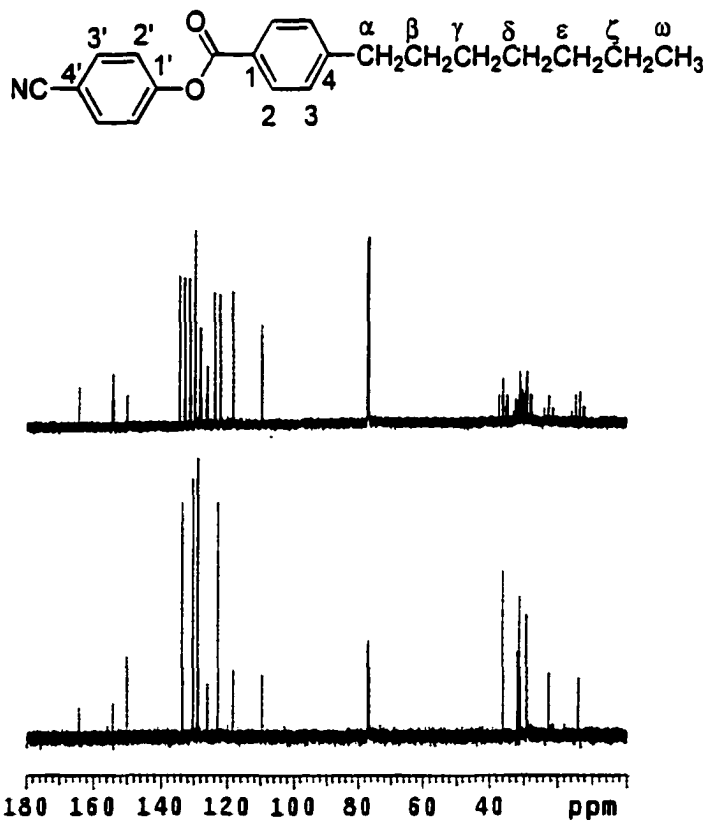

Figure 2.2. Proton-coupled and decoupled ^{13}C NMR spectra of 7CPB in $CDCl_3$.

Table 2.1. Comparison of measured and calculated chemical shifts of aromatic carbons and a summary of scalar coupling constants for all carbons of 7CPB.

Carbon	Calculated δ	Actual δ	*J* values / Hz			Splitting patterns
			^1J	^2J	^3J	
1'	154.7	154.3		10.1	4.1	tt
2'	121.6	122.9	166.2	5.0		dd
3'	132.0	133.7	166.6	6.9		dd
4'	109.1	109.6		9.2		t
1	127.2	126.0		7.8		t
2	129.1	130.4	158.1	6.0		dd
3	128.0	128.8	152.4	5.1		dd
4	146.8	150.1				br
-CN		118.3		5.3		t
-COO-		164.4				s
α		36.1	126.6			t
β		31.1	125.4			t
γ		29.1	129.5			t
δ		29.2	125.4			t
ε		31.7	125.4			t
ζ		22.6	126.3			t
ω		14.1	125.7			q

The proton decoupled ^{13}C NMR spectra of 7CPB and 7PFCPB in their isotropic and liquid crystalline phases are shown in Figure 2.3. As usual, the aromatic peaks shift down field when the compounds are cooled from the isotropic phase to the liquid crystalline phase. The aliphatic peaks of 7CPB shift slightly up field correspondingly (Figure 2.3, b), but the aliphatic peaks for 7PFCPB are too broad to be observed due to extensive ^{13}C-^{19}F coupling (Figure 2.3, c and d). Even though the aromatic carbons have no directly bonded fluorine atoms, the ^{13}C-^{19}F dipolar couplings in the smectic A phase are large enough to cause severe broadening of the aromatic carbon peaks (Figure 2.3, d).

The chemical shift change over the whole liquid crystalline range of 7CPB is shown below in Figures 2.4 and 2.5. To prevent overcrowding, the aromatic and aliphatic carbons are plotted separately. The change in chemical shifts is due to incomplete averaging of the chemical shift tensors in the liquid crystalline phase. However, unless all the components of the tensors in the axis system of the ordering matrix are known, it is not possible to calculate the order parameters from the chemical shifts. A more direct way to obtain the order parameters is to measure the C-H dipolar coupling constants using the 2D PELF/OMAS method, as described above.

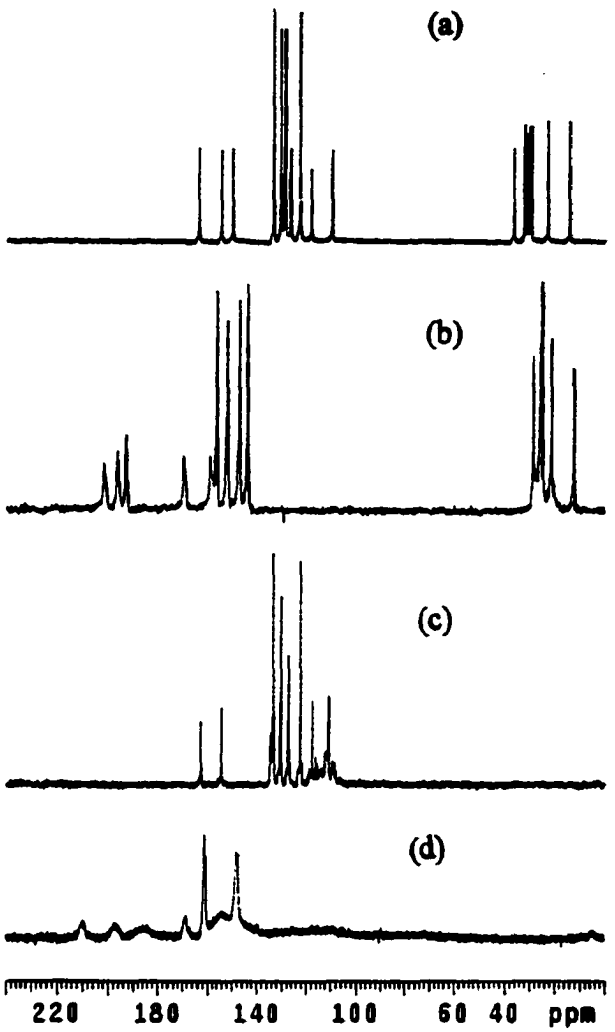

Figure 2.3. ^{13}C NMR spectra at 100.58 MHz for (a) 7CPB in the isotropic phase; (b) 7CPB in the nematic phase (at 43 °C); (c) 7PFCPB in the isotropic phase; (d) 7PFCPB in the smectic A phase (at 128 °C).

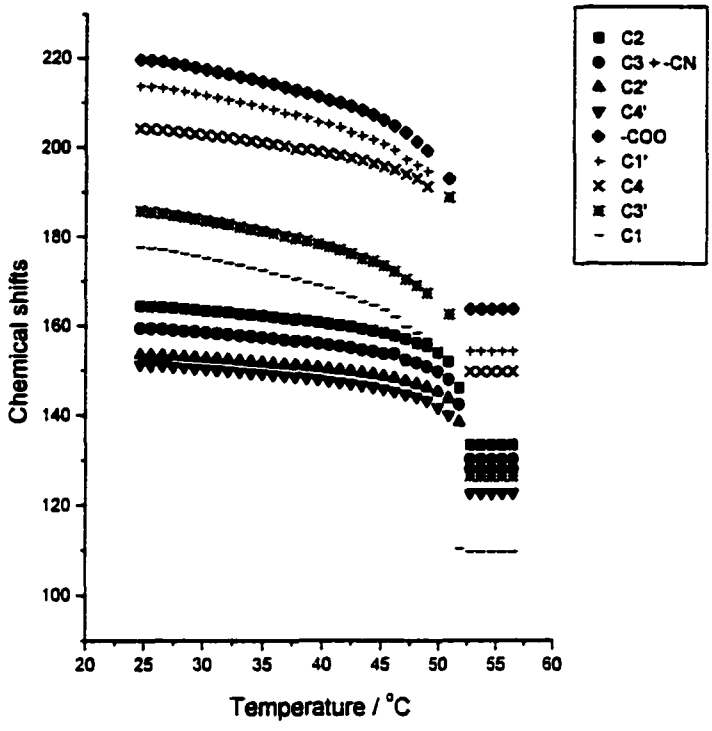

Figure 2.4. Chemical shift change of aromatic carbon atoms of 7CPB with the change of temperature.

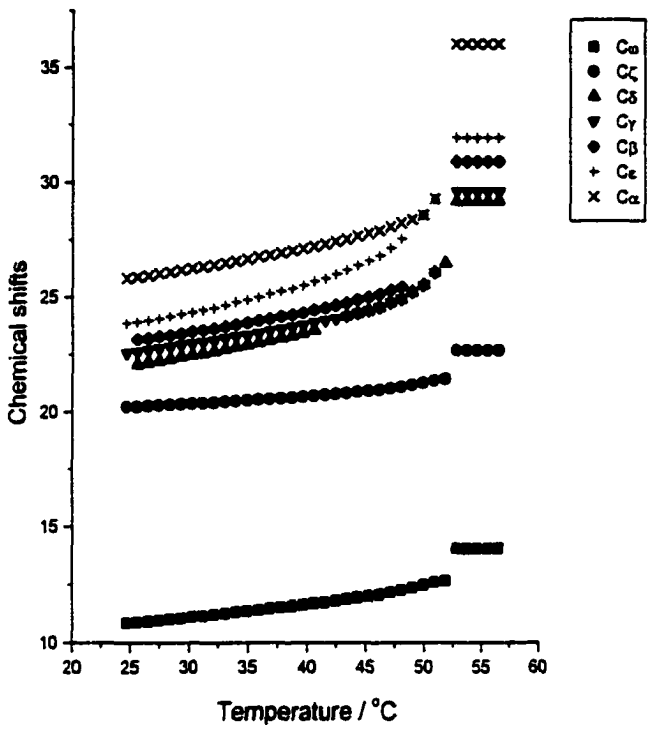

Figure 2.5. Chemical shift change of aliphatic carbon atoms of 7CPB with the change of temperature.

In this experiment, to reduce the dipolar couplings and obtain sharp ^{13}C peaks, the sample was spun rapidly (~1 kHz) at an angle θ with respect to the magnetic field B_0, which was chosen to be 47.58°. In the evolution period, the BLEW-48 decoupling sequence is used to remove proton-proton dipolar coupling so that first-order C-H couplings can be observed in the ω_1 dimension. In the detection period, the SPINAL-64 broadband decoupling sequence was used to obtain normal proton decoupled ^{13}C spectrum in the ω_2 dimension.

The 2D PELF/VAS spectra of 4'-cyanophenyl 4-*n*-heptylbenzoate at temperature $T/T_{NI} = 0.945$ are shown in Figure 2.6. In the spectra, in the ω_1 dimension one-bond C-H coupling and some 2-bond coupling can be observed. Each type of proton gives a doublet, and the central peaks are due to overlapping of many unresolved long range couplings. The quality of spectra in Figure 2.6 is better than that obtained by the SLF/VAS method, in which 2-bond couplings can only be obtained by deconvolution of the overlapping peaks.[27,28]

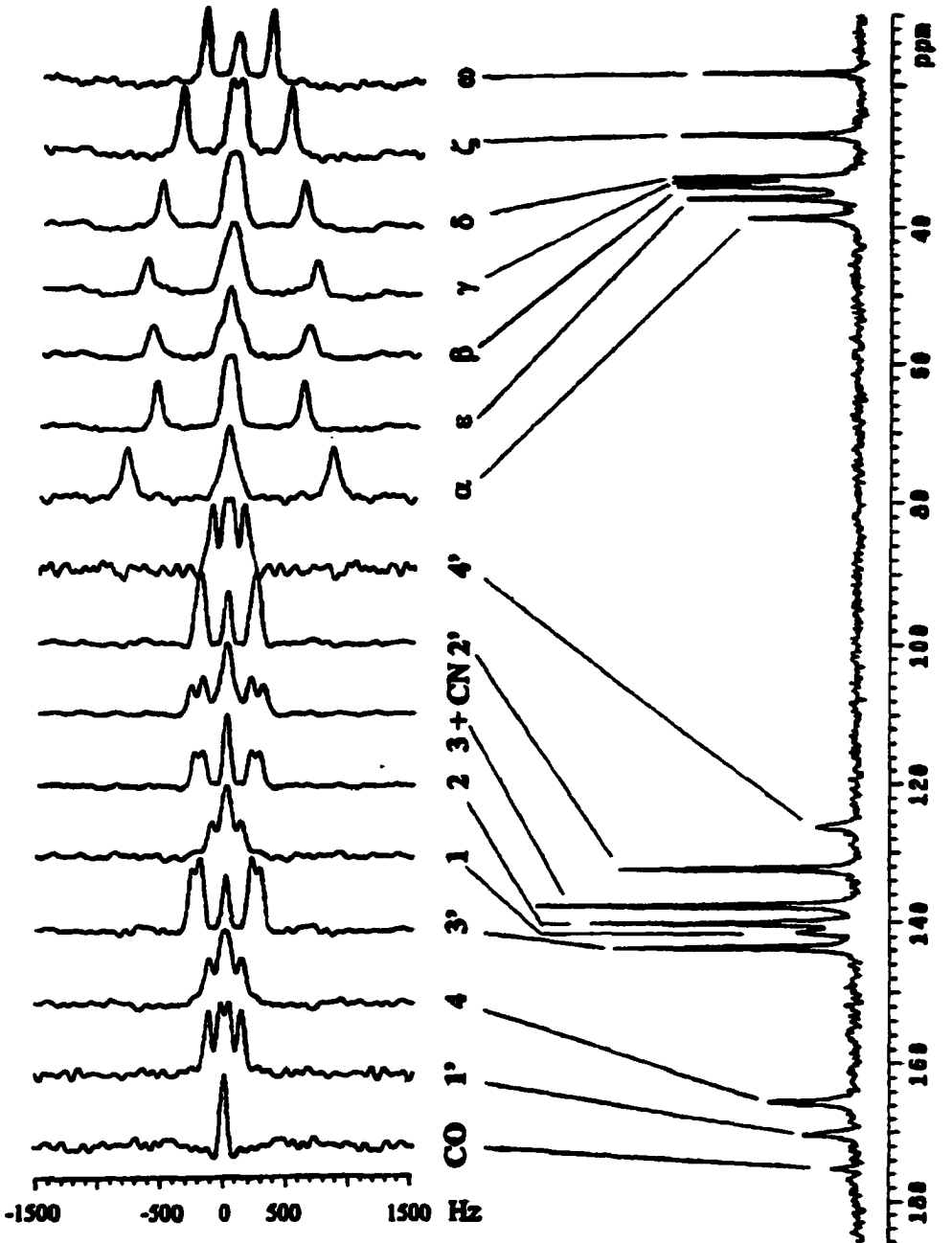

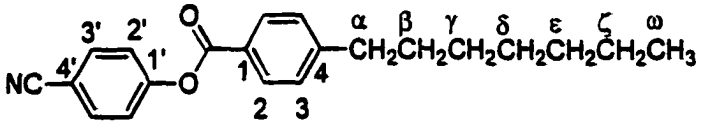

Fig. 2.6. ^{13}C NMR spectra of 7CPB at $T/T_{NI} = 0.945$ with the sample spinning at a rate of about 1.0 kHz along an axis forming an angle 47.58° with respect to B_0, presented together with traces in the ω_1 dimension in a 2D PELF experiment.

The method to calculate order parameters from the C-H splittings has been described in detail previously,[27-42] and will not be repeated here. Related data can be found in Appendix A.1. For the phenyl ring carrying an aliphatic chain, the average values of the calculated angles are: $\angle$ H2-C2-C3 = 120.3 ± 0.4° and $\angle$ H3-C3-C2 = 119.8 ± 0.4°; for the phenyl ring bearing cyano group, the angles are: $\angle$ H2'-C2'-C3' = 120.8 ± 0.3° and $\angle$ H3'-C3'-C2' = 120.1 ± 0.3°. These data are comparable to the previous results obtained with the SLF/VAS method.[40]

To calculate the order parameters obtained from the 2D data with the ^{13}C chemical shifts (δ's), the semi-empirical equation

$$\Delta\delta = a\,S + b \tag{2.8}$$

can be used. For the phenyl rings, S refers to the order parameter of the two-fold axis of the ring; for the aliphatic carbons, S refers to the order parameters of the C-H axis.

In the present study, the PELF/OMAS technique was used to obtain the order parameters of 7CPB at four different temperatures. The values of Δδ for each carbon nucleus at these temperatures were then plotted against the order parameters to calculate the values of *a* and *b*. The plots are shown in following figures.

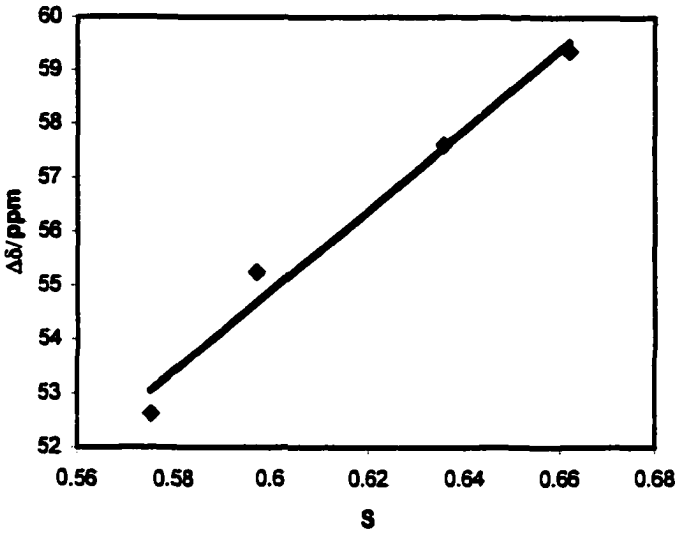

Figure 2.7. Correlation between chemical shift anisotropy (Δδ) and order parameters for C1 of 7CPB.

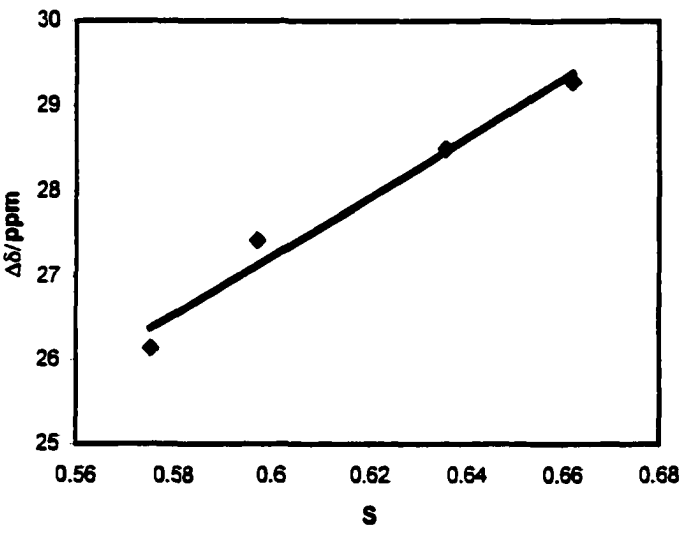

Figure 2.8. Correlation between chemical shift anisotropy (Δδ) and order parameters for C2 of 7CPB.

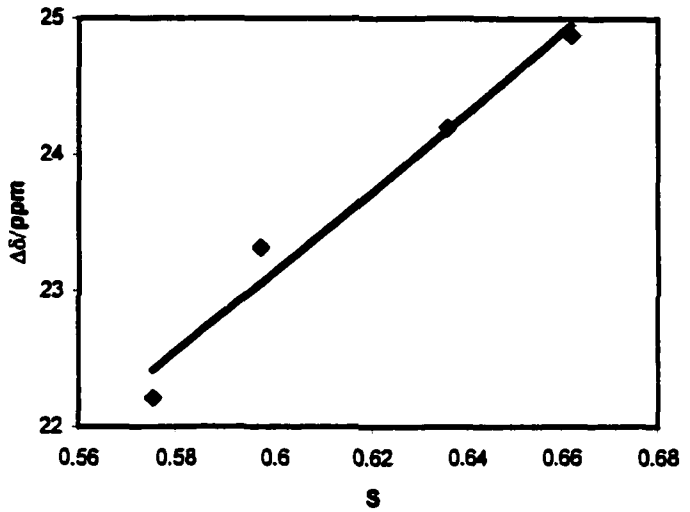

Figure 2.9. Correlation between chemical shift anisotropy (Δδ) and order parameters for C3 of 7CPB.

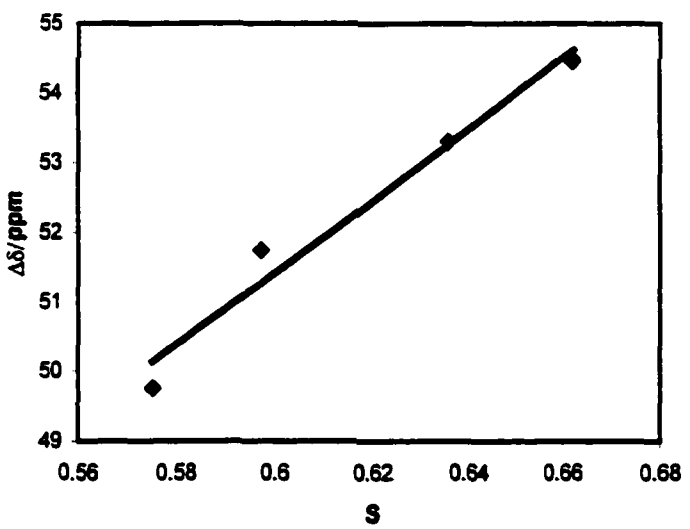

Figure 2.10. Correlation between chemical shift anisotropy (Δδ) and order parameters for C4 of 7CPB.

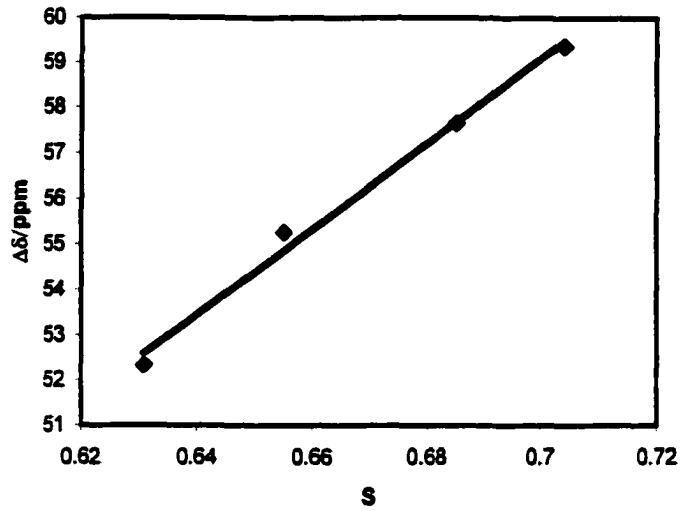

Figure 2.11. Correlation between chemical shift anisotropy (Δδ) and order parameters for C1' of 7CPB.

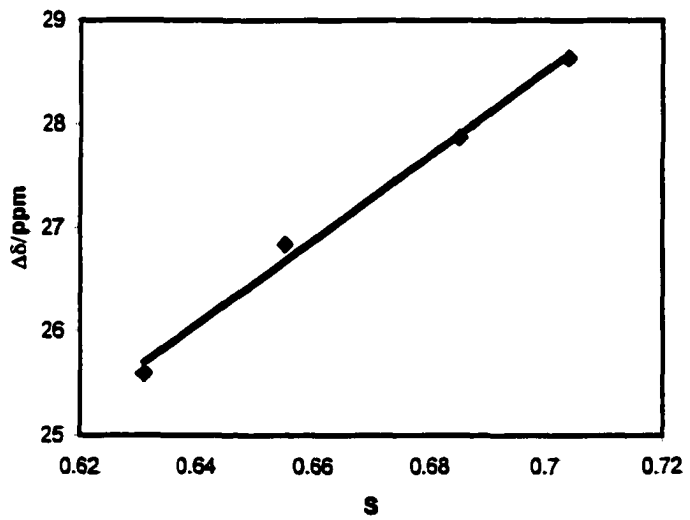

Figure 2.12. Correlation between chemical shift anisotropy (Δδ) and order parameters for C2' of 7CPB.

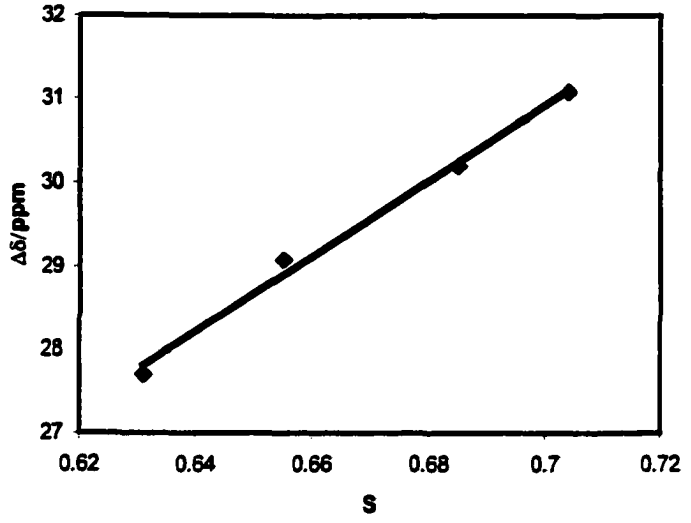

Figure 2.13. Correlation between chemical shift anisotropy (Δδ) and order parameters for C3' of 7CPB.

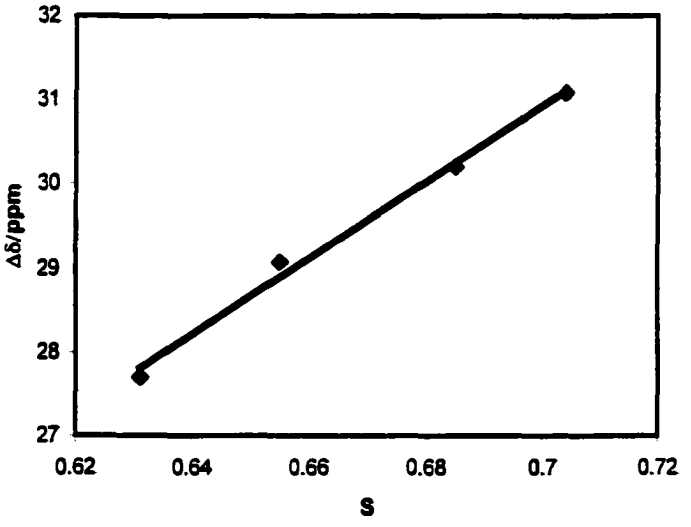

Figure 2.14. Correlation between chemical shift anisotropy (Δδ) and order parameters for C4' of 7CPB.

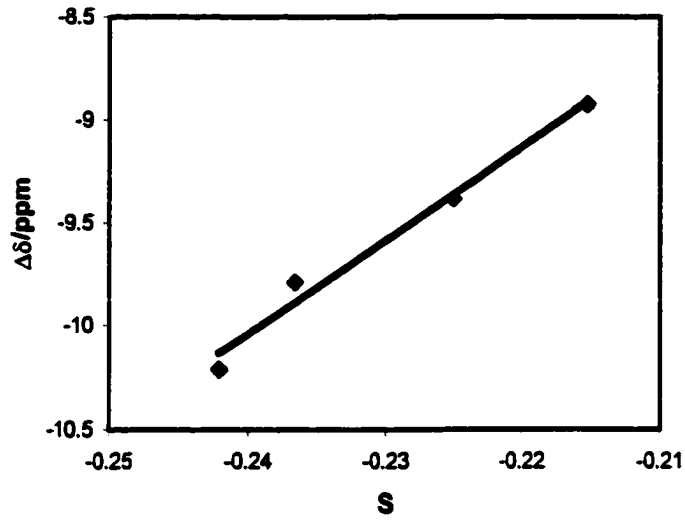

Figure 2.15. Correlation between chemical shift anisotropy (Δδ) and order parameters for Cα of 7CPB.

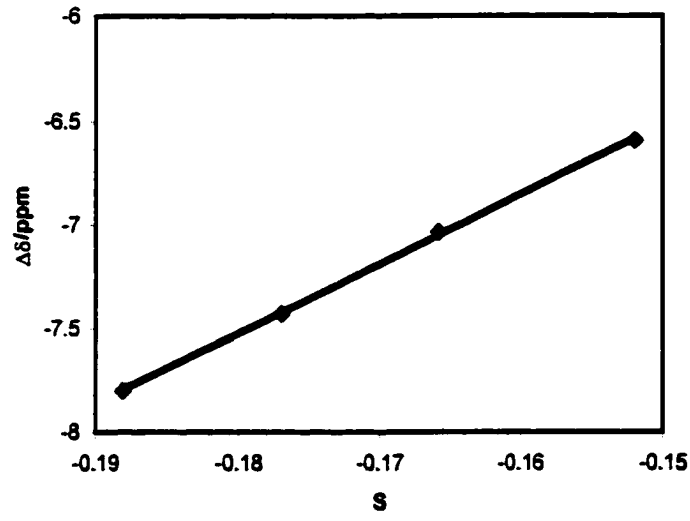

Figure 2.16. Correlation between chemical shift anisotropy (Δδ) and order parameters for Cβ of 7CPB.

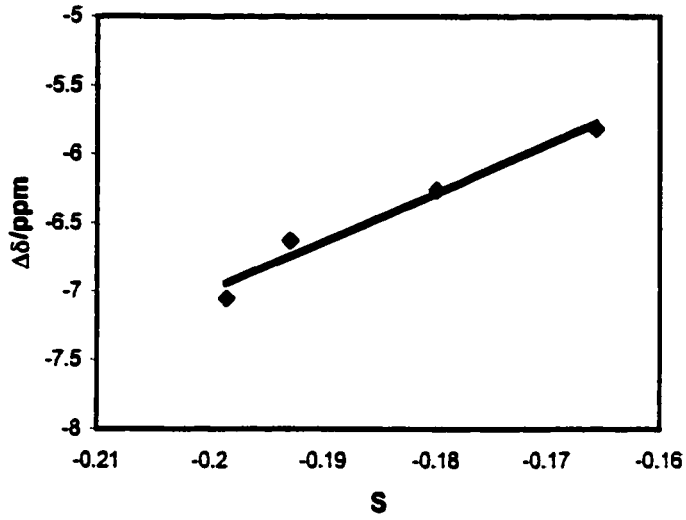

Figure 2.17. Correlation between chemical shift anisotropy (Δδ) and order parameters for Cγ of 7CPB.

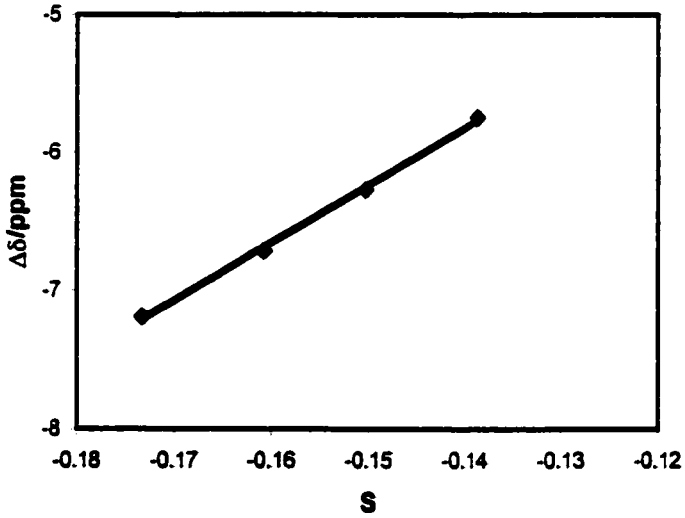

Figure 2.18. Correlation between chemical shift anisotropy (Δδ) and order parameters for Cδ of 7CPB.

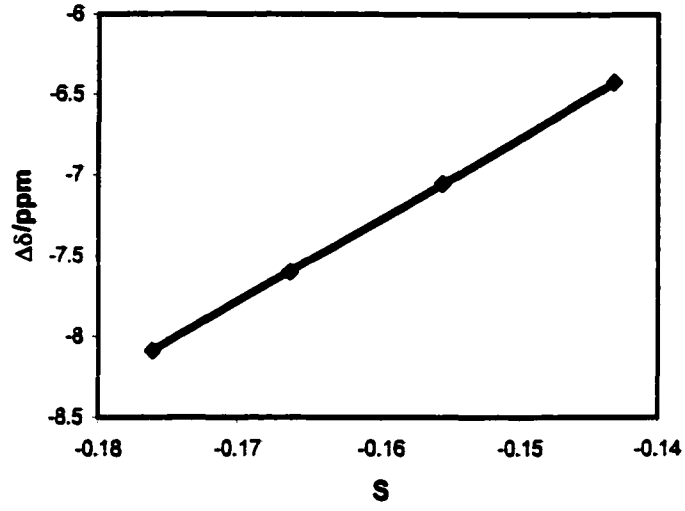

Figure 2.19. Correlation between chemical shift anisotropy (Δδ) and order parameters for Cε of 7CPB.

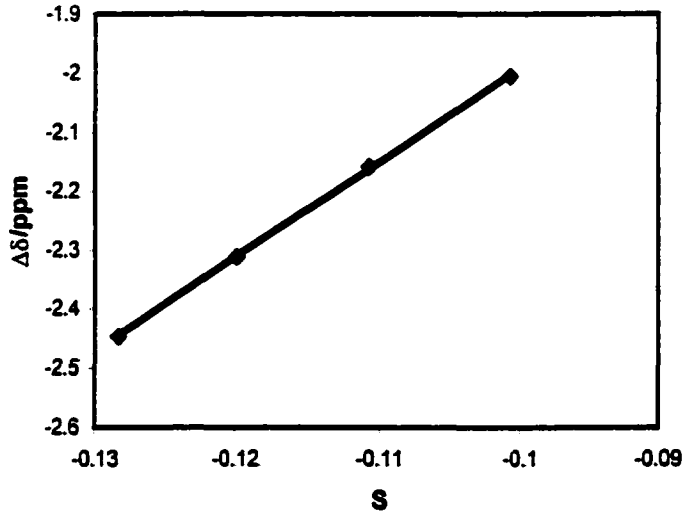

Figure 2.20. Correlation between chemical shift anisotropy (Δδ) and order parameters for Cζ of 7CPB.

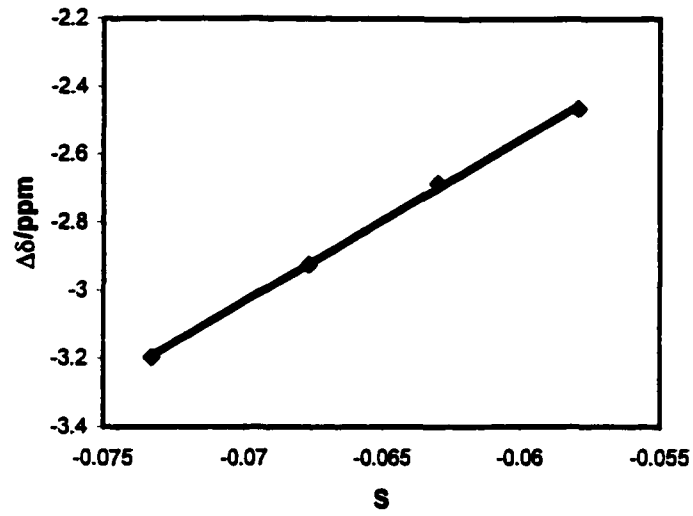

Figure 2.21. Correlation between chemical shift anisotropy ($\Delta\delta$) and order parameters for Cω of 7CPB.

The results, together with the correlation coefficients, are given in Tables 2.2 and 2.3. The high values of the correlation coefficients show that the data obey the linear relation expressed in Eq. 2.8 very well.

Table 2.2. Semi-empirical parameters for the aromatic carbons of 7CPB.

C	1	2	3	4	1'	2'	3'	4'
a	74.7	34.6	29.3	51.7	94.3	40.8	45.1	106.9
b	10.1	6.44	5.56	20.4	-6.91	-0.02	-0.68	-7.10
Correlation coefficient	0.989	0.986	0.985	0.984	0.996	0.996	0.996	0.996

Table 2.3. Semi-empirical parameters for the aliphatic carbons of 7CPB.

C	α	β	γ	δ	ε	ζ	ω
a	42.9	31.6	33.5	38.6	46.7	14.8	48.3
b	0.22	-1.89	-0.32	-0.54	0.12	-0.55	0.32
Correlation coefficient	0.994	0.998	0.989	0.998	1.000	1.000	0.996

Once the values of *a* and *b* are determined, they can be used to calculate the order parameters from the chemical shift values, which can be measured more conveniently as a function of temperature using 1D data. The data for the aromatic and aliphatic carbons are presented in Figures 2.21 and 2.22, respectively. The validity of this calculation was further examined by fitting the calculated values to the Haller equation[68-70]

$$S(T) = S_0 (1-T/T^*)^F \qquad (2.9)$$

where S_0 and F are empirical constants and T^* is a temperature at which the order parameter becomes zero. The best fitting curves are represented as dashed lines in Figures 2.22 and 2.23. The detailed procedure to obtain the best fitting curve for the aromatic carbons is given in Appendix A.3. T^* was initially treated as a variable parameter for fitting each curve; then, the average value of 324.7 K was used as a fixed parameter for all final fittings. Data for carbon atoms on the same ring are positioned on the same line. A good agreement between the experimental data and S by the theoretical calculation can be found in the plots.

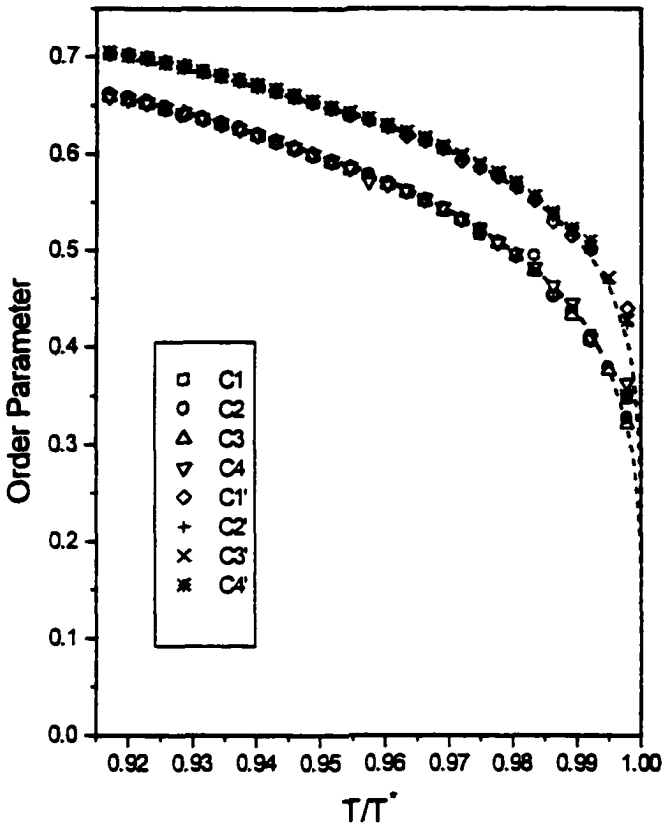

Figure 2.22. Plot of order parameters of the aromatic carbons of 7CPB against T/T^*.

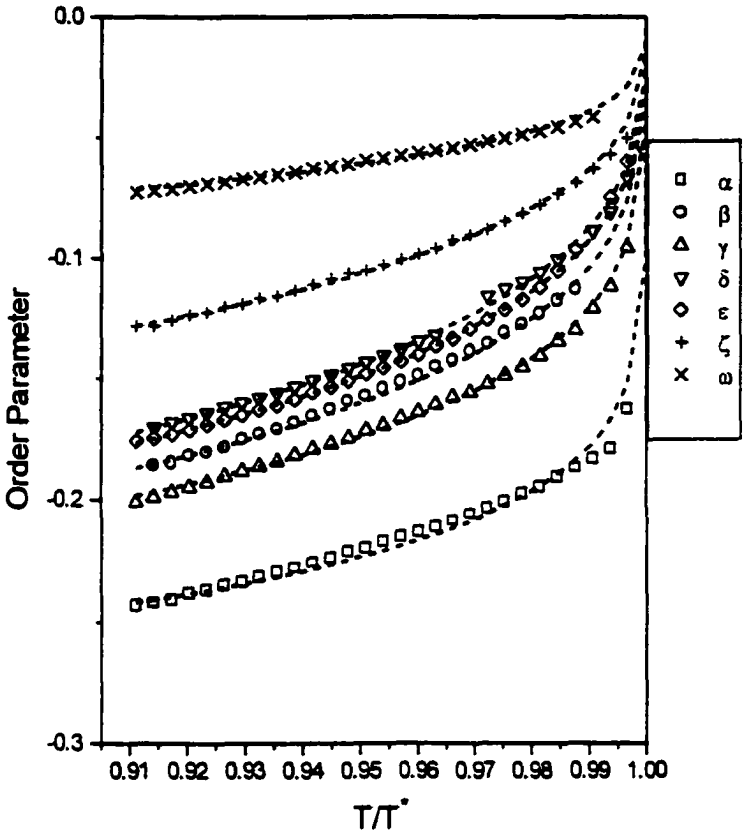

Figure 2.23. Plot of order parameters of the aliphatic carbons of 7CPB against T/T^*.

Table 2.4. S_0 and F obtained by fitting the calculated order parameter to the Haller equation.

C	Ring 1	Ring 2	α	β	γ	δ	ε	ζ	ω
S_0	1.09	1.02	-0.340	-0.360	-0.344	-0.366	-0.361	-0.282	-0.139
F	0.20	0.15	0.14	0.27	0.23	0.31	0.30	0.33	0.28

The S_0 and F values for the best fitting are listed in Table 2.4, where Ring 1 refers to the phenyl ring containing the heptyl chain. It has been suggested that the numerical values of S_0 for the phenyl ring should be close to unity.[68] Although a variety of experimental techniques utilized in the determinations of order parameters indicated that this is not always true,[69] the values of S_0 for both phenyl rings in 7CPB are actually quite close to unity. For a perfectly aligned all-*trans* conformation of the aliphatic chain, S_0 for each C-H bond should be close to -0.333 [i.e. $(3\cos^2 109°28' - 1)/2$]. The values listed in Table 2.4 for the first five carbon atoms agree with this estimation reasonably well. However, an obvious odd-even alternation trend can be observed in the table, indicating that the bond angles are not strictly 109°28'. The two most outer carbon atoms (i.e. ζ and ω) have S_0 values substantially less negative than the ideal value. This means that, in the theoretical state of perfect nematic ordering for the liquid crystalline core, the chain end would still undergo considerable motions. The value F is an indication of how fast a molecular segment approaches this perfect state with the lowering of temperature. The data in Table 2.4 show that in general F increases gradually from the core to the chain. This is quite reasonable because in the nematic phase

the motions of the core are more limited than those of the chain, and the "freezing" of chain motions with the lowering of temperature is more pronounced.

Because of the lack of resolution in the ^{13}C spectrum of 7PFCPB in the smectic A phase (Figure 2.3, d), the order parameters could not be obtained with good accuracy. Nevertheless, a study of the ^{13}C spectra of mixture of 7PFCPB and 7CPB offers useful information on the phase behavior of these systems.

Fig. 2.24 shows the ^{13}C spectra of a mixture of 7PFCPB and 7CPB (mole ratio 2:1) at five different temperatures. At 137 °C, which is higher than the clearing points of both compounds, the spectrum (Figure 2.24, a) is the sum of two isotropic spectra (Figure 2.3, a and c). When the temperature is lowered, the spectrum consists of both isotropic and anisotropic peaks for both compounds (Figure 2.24, b). As the temperature is further lowered, the intensities of the isotropic peaks decrease (Figure 2.24, c). However, upon a further decrease of temperature, the intensities of the isotropic peaks increase substantially (Figure 2.24, d); in the meantime, the anisotropic peaks become very broad. Finally, at 48 °C, the isotropic peaks disappear completely, while the anisotropic peaks sharpen again, but appear as partial powder pattern rather than single peaks.

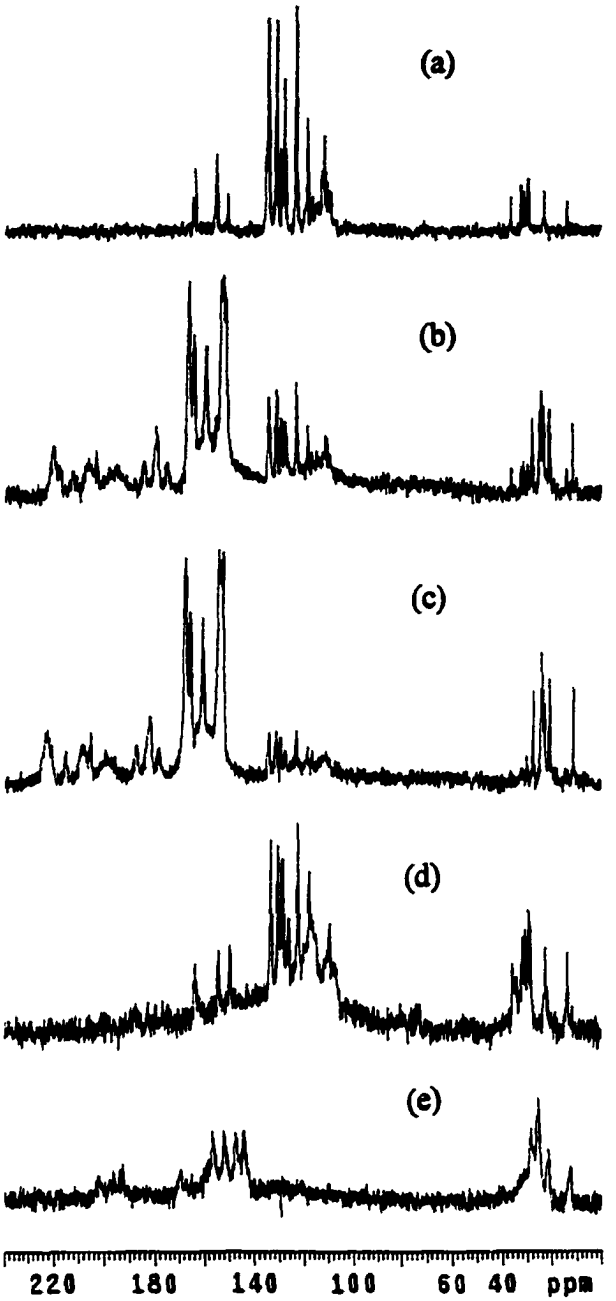

Figure 2.24. ^{13}C NMR spectra for a mixture of 7PFCPB and 7CPB at: (a) 137 °C, (b) 114 °C, (c) 104 °C, (d) 78 °C, (e) 48 °C.

This interesting sequence of spectral changes can be explained in the following. As the mixture is cooled from the isotropic phase, part of the sample turns into a smectic A phase. The smectic A phase seems to be well aligned in the magnetic field, so that the linewidths (Figure 2.24, b and c) are comparable to those in the nematic phase (Figure 2.3, b). The two phases coexist for a fairly large temperature range (from *ca.* 133 °C to 80 °C), with the amount of isotropic phase diminishing. Further lowering of temperature reduces the solubility of 7PFCPB in 7CPB because the fluorocarbon chain is not compatible with the hydrocarbon chain. Then, the system, which has been mostly smectic A with only a small amount of isotropic phase, turns into a mixture of isotropic and a higher order smectic phase. Judging from the characteristic of the spectrum (Figure 2.24, d), the isotropic phase contains mostly 7CPB, with a small amount of dissolved 7PFCPB to keep it in the isotropic state. The director of the smectic phase does not have a unique orientation in the magnetic field, and the ^{13}C peaks are broad. Finally, at still lower temperatures, the isotropic portion freezes, and the smectic phase has better ordering to show partial powder patterns (Figure 2.24, e). These explanations were substantiated by observations under the polarizing microscope, which showed the smectic A phase started to appear at ~133 °C and turned into a higher smectic phase at ~80 °C.

In the smectic A phase, the order parameters of the rings and aliphatic C-H bonds in 7CPB can be calculated from Eq. 2.8 by using the data listed in Tables 2.2 and 2.3. The results obtained at two temperatures are listed in Table 2.5,

where Ring 2 refers to the phenyl ring carrying the cyano group. As expected, the liquid crystal becomes more ordered with the decrease of temperature.

Table 2.5. Order parameters of the rings and aliphatic C-H bonds of 7CPB in the mixture at two temperatures.

	Ring 1	Ring 2	α	β	γ	δ	ε	ζ	ω
114 °C	0.65	0.70	-0.19	-0.15	-0.13	-0.13	-0.15	-0.068	-0.057
104 °C	0.69	0.72	-0.20	-0.18	-0.14	-0.14	-0.16	-0.075	-0.061

2.7. Conclusions

In conclusion, the orientational ordering of 4'-cyanophenyl 4-*n*-heptylbenzoate (7CPB) has been studied by using 2D PELF/OMAS method, which provides higher resolution than previous SLF/VAS method and long range dipolar coupling can be directly visualized. Linear relations between chemical shifts and order parameters were established, and semi-empirical parameters were obtained to facilitate the study on the order behavior of 7CPB over the entire nematic range by using 1D anisotropic ^{13}C chemical shift measurements. A 1:2 mixture of 7CPB with its chain-perfluorinated analog has very interesting phase behavior with the change of temperature. The order parameters of 7CPB in the smectic A phase of the mixture were calculated from the ^{13}C chemical shifts.

2.8. References

1. Gray, G. W., Hird, M. and Toyne, K. J., *Mol. Cryst. Liq. Cryst.*, **1991**, *204*, 91.

2. Geelhaar, T., *Liq. Cryst.*, **1998**, *24*, 91.

3. Hird, M. and Toyne, K. J., *Mol. Cryst. Liq. Cryst. Sci. Technol., Sect. A*, **1998**, *323*, 1.

4. Nguyen, H. T., Sigaud, G., Achard, M. F. and Hardouin, F., *Liq. Cryst.*, **1991**, *10*, 389.

5. Arehart, S. V. and Pugh, C., *J. Am. Chem. Soc.*, **1997**, *119*, 3027.

6. Liu, H. and Nohira, H., *Liq. Cryst.*, **1998**, *24*, 719.

7. Höpken, J., Pugh, C., Richtering, W. and Möller, M., *Makromol. Chem.*, **1988**, *189*, 911.

8. Rabolt, J. F., Russell, T. P. and Twieg, R. J., *Macromolecules*, **1984**, *17*, 2786.

9. Collings, P., *Liquid Crystals: Nature's Delicate Phase of Matter* (Princeton University Press), **1990**, p 10.

10. Collings, P. and Hird, M., *Introduction to Liquid Crystals: Chemistry and Physics* (Taylor & Francis), **1997**, p 1.

11. Vertogen, G. and de Jeu, W. H., *Thermotropic Liquid Crystals, Fundamentals* (Springer-Verlag), **1988**, p.167.

12. Pohl, L. and Merck, E., in *Liquid Crystals, Applications and Uses* (World Scientific), **1990**, *Vol. 1*, p.139.

13. Saupe, A., *Mol. Cryst. Liq. Cryst.*, **1972**, *16*, 87.

14. Doucet, J., in *The Molecular Physics of Liquid Crystals* (Academic press, New York), **1979**.

15. Emsley, J. W., Luckhurst, G. R., Gray, G. W. and Mosley, A., *Mol. Phys.*, **1978**, *35*, 1499.

16. Stinton, S. W. and Pines, A., *Chem. Phys. Lett.*, **1980**, *76*, 263.

17. Emsley, J. W., Luckhurst, G. R. and Stockley, C. P., *Mol. Phys.*, **1981**, *44*, 565.

18. Avent, A. G., Emsley, J. W. and Turner, D. L., *J. Mag. Reson.*, **1983**, *52*, 57.

19. Stinton, S. W., Zax, D. B., Murdoch, J. B. and Pines, A., *Mol. Phys.*, **1984**, *53*, 333.

20. Emsley, J. W., Lindon, J. C., and Luckhurst, G. R., *Mol. Phys.*, **1975**, *30*, 1913.

21. Boden, N., Clark, L. D., Bushby, R. J., Emsley, J. W., Luckhurst, G. R. and Stockley, C. P., *Mol. Phys.*, **1981**, *42*, 565.

22. Bechmann, P. A., Emsley, J. W., Luckhurst, G. R. and Turner, D. L., *Mol. Phys.*, **1984**, *52*, 499.

23. Counsell, C. J. R., Emsley, J. W., Heaton, N. J. and Luckhurst, G. R., *Mol. Phys.*, **1985**, *54*, 847.

24. Emsley, J. W., Luchhurst, G. R., Parsons, P. J. and Timimi, B. A., *Mol. Phys.*, **1985**, *56*, 767.

25. Beckmann, P. A., Emsley, J. W., Luckhurst, G. R. and Turner, D. L., *Mol. Phys.*, **1986**, *59*, 97.

26. Counsell, C. J. R., Emsley, J. W., Luckhurst, G. R. and Sachdev, H. S., *Mol. Phys.*, **1988**, *63*, 33.

27. Fung, B. M. and Afzel, J., *J. Am. Chem. Soc.*, **1986**, *108*, 1107.

28. Fung, B. M., Afzal, J., Foss, T. L. and Chau, M.-H., *J. Chem. Phys.*, **1986**, *85*, 4808.

29. Fung, B. M., Poon, C.-D., Gangoda, M., Enwall, E. L., Diep, T. A. D. and Bui, C. V., *Mol. Cryst. Liq. Cryst.*, **1986**, *141*, 267.

30. Forster, P. and Fung, B. M., *J. Chem. Soc. Faraday Trans. II*, **1988**, *84*, 1083.

31. Poon, C.-D., Wooldridge, C. M. and Fung, B. M., *Mol. Cryst. Liq. Cryst.*, **1988**, *157*, 303.

32. Frech, C. B., Fung, B. M. and Schadt, M., *Liq. Cryst.*, **1988**, *3*, 713.

33. Frech, C. B., Fung, B. M. and Schadt, M., *Proc. SPIE*, **1989**, *1080*, 215.

34. Poon, C.-D. and Fung, B. M., *Liq. Cryst.*, **1989**, *5*, 1159.

35. Poon, C.-D. and Fung, B. M., *J. Chem. Phys.*, **1989**, *91*, 7392.

36. Ritcher, W., Fung, B. M. and Schadt, M., *Liq. Cryst.*, **1990**, *8*, 63.

37. Ritcher, W., Reimer, D., Fung, B. M., Tweig, R. J. and Betterton, K., *Liq. Cryst.*, **1990**, *8*, 687.

38. Guo, W. and Fung, B. M., *J. Chem. Phys.*, **1991**, *95*, 3917.

39. Guo, W. and Fung, B. M., *Liq. Cryst.*, **1991**, *9*, 117.

40. Balakrishnan, N. S., Bayle, J. P., Ho., M.-S., Pham, S. C. and Fung, B. M., *Liq. Cryst.*, **1993**, *14*, 591.

41. Fung, B. M., in *Encyclopedia of Nuclear Magnetic Resonance*, edited by D. M. Grant and R. K. Harris (Chichester: Wiley), **1996**, p 2744.

42. Tong, T.-H., Bayle, J. P. and Fung, B. M., *Liq. Cryst.*, **1997**, *22*, 165.

43. Waugh, J. S., *Proc. Natl. Acad. Sci. U. S. A.*, **1976**, *73*, 1394.

44. Hester, R. K., Ackerman, J. L., Neff, B. L., Waugh, J. S. and Sherfinski, J. S., *Phys. Rev. Lett.*, **1976**, *36*, 1081.

45. Waugh, J. S. and Opella, S., *J. Chem. Phys.*, **1977**, *66*, 4916.

46. Rybaczewski, E. F., Neff, B. L., Waugh, J. S. and Sherfinski, J. S., *J. Chem. Phys.*, **1977**, *67*, 1231.

47. Courtieu, J., Bayle, J. P. and Fung, B. M., *Prog. NMR Spec.*, **1994**, *26*, 141.

48. Schmidt-Rohr, K., Nanz, D., Emsley, L. and Pines, A., *J. Phys. Chem.*, **1994**, *98*, 6668.

49. Hong, M., Schmidt-Rohr, K. and Pines, A., *J. Am. Chem. Soc.*, **1995**, *117*, 3310.

50. Hong, M., Pines, A. and Caldarelli, S., *J. Phys. Chem.*, **1996**, *100*, 14815.

51. Caldarelli, S., Hong, M., Emsley, L. and Pines, A., *J. Phys. Chem.*, **1996**, *100*, 18696.

52. Fung, B. M., Ermolaev, K. and Yu, Y., *J. Magn. Reson.*, **1999**, *138*, 28.

53. Burum, D. P., Linder, N. and Ernst, R. R., *J. Magn. Reson.*, **1981**, *44*, 173.

54. Fung, B. M., Khitrin, A. K. and Ermolaev, K., *J. Magn. Reson.*, **2000**, *142*, 97.

55. Levitt, M. H. and Freeman, R., *J. Magn. Reson.*, **1981**, *43*, 502.

56. Levitt, M., Freeman, R. and Frenkiel, T., *J. Magn. Reson.*, **1982**, *47*, 328.

57. Levitt, M., Freeman, R. and Frenkiel, T., *J. Magn. Reson.*, **1982**, *50*, 157.

58. Levitt, M., Freeman, R. and Frenkiel, T., in *Advances in Magnetic Resonance* (Academic Press, New York), edited by J. S. Waugh, **1983**, *Vol. 11*, p 47.

59. Shaka, A. J., Keeler, L., Frenkiel, T. and Freeman, R., *J. Magn. Reson.*, **1983**, *52*, 335.

60. Shaka, A. J., Keeler, J. and Freeman, R., *J. Magn. Reson.*, **1983**, *53*, 313.

61. Shaka, A. J., Barker, P. B. and Freeman, R., *J. Magn. Reson.*, **1985**, *64*, 547.

62. Shaka, A. J. and Keeler, J., *Prog. NMR Spec.*, **1987**, *19*, 47.

63. Emsley, J. W. (ed.), *Nuclear Magnetic Resonance of Liquid Crystals* (D. Reidel), **1985**.

64. Kelly, S. M., *Helv. Chim. Acta.*, **1984**, *67*, 1573.

65. McLoughlin, V. C. R. and Thrower, J., *Tetrahedron*, **1969**, *25*, 5921.

66. Furniss, B. S., Hannford, A. J., Smith, P. W. G. and Tatchell, A. R., *Vogel's Textbook of Practical Organic Chemistry* (Longman), **1989**, p 426.

67. Crews, P., Podriguez, J. and Jaspars, M., *Organic Structure Analysis* (Oxford University Press), **1997**, p 100.

68. Haller, I., *Prog. Solid St. Chem.*, **1975**, *10*, 103.

69. Gasparoux, H., Lalanne, J. R. and Martin, B., *Mol. Cryst. Liq. Cryst.*, **1979**, *51*, 221.

70. Vello, A. M. and Diogo, A. C., *Liq. Cryst.*, **1989**, *5*, 349.

Chapter III. Synthesis and Characterization of Diazo Liquid Crystals for Potential IR Applications*

3.1. Introduction

Currently, liquid crystal displays (LCDs) are mainly designed for application in the visible region. However, some special operations require electro-optic devices specially designed to function in the IR region for electronic sensing and communication. Although electro-mechanical IR modulators have been proven to be successful,[1] LCDs operated in the near- and mid-IR ranges are a more desirable technological option because they have such advantages as small size and weight, low operating voltage, and low power consumption. Commercial liquid crystals were used to fabricate IR LCDs,[2-6] but they suffer from such problems as insufficient birefringence (Δn) and high optical loss because these liquid crystals are designed to be used in the visible range. Therefore, liquid crystals specially designed for use in IR range and with high dielectric anisotropy and birefringence need to be synthesized to overcome these problems.

3.2. Physical properties of liquid crystals

The presence of long-range orientational ordering is a fundamental characteristic of liquid crystals. Many interesting properties and important

* Part of the material in this chapter is presented in a paper entitled "Diazo liquid crystals for potential infrared applications" by Hong Sun, Wing Shun Cheung and B. M. Fung, submitted for publication.

applications of liquid crystals result from their anisotropic orientational ordering. A study of the macroscopic properties of liquid crystals is essential not only for the evaluation of various theories but also for practical application consideration.

Dielectric anisotropy, birefringence and elastic constants are among the most important physical properties of liquid crystals, which will be discussed in detail in the following sections. Viscosity is also crucial for application, but since most of the liquid crystals for display devices are liquid crystal mixtures, this property is mainly tunable. Measurement of the viscosity of liquid crystals was not performed in this research and no discussion is made.

3.2.1. Dielectric permittivity

Dielectric permittivity ε is a physical quantity related to the susceptibility to external electric field.[7] Unfortunately, there is no good definition of this quantity. In general, ε is related to capacitance C by the following equation

$$C = \frac{\varepsilon A}{d} \tag{3.1}$$

where A is the overlapped area of the two plates of a capacitor, d is the distance between the two layers, and the quantity ε is the permittivity of the material between the plates. For vacuum, the free-space value of ε_0 is 8.85×10^{-12} F/m. Air has only a slightly different value. The permittivity ε of a material is expressed in terms of the permittivity of free space as

$$\varepsilon = \varepsilon_r \varepsilon_0 \tag{3.2}$$

where ε_r is the relative permittivity and is often called the dielectric constant.

As in all covalent molecules, the bonds in liquid crystals are formed by overlapping electron clouds. Atoms with high electronegativity have stronger attractions for shared electrons, so a covalent bond formed between two atoms having different electronegativity has an unbalanced charge distribution, resulting in a permanent dipole. The dipole moment of a molecule is the vector sum of the dipole moments of individual molecular segments. If a molecule has a permanent dipole moment, it exists with or without an applied electric field, but its contribution to ε is frequency dependent since the external electric field will inevitably change the alignment of the molecules.

Induced dipoles are created by the applied electric field which causes a distortion of the electron clouds, resulting in a redistribution of electrons shared by atoms with similar electronegativity. The contribution of this component to ε is not frequency dependent since the formation and alignment of these dipoles does not require molecular motion.

Both permanent and induced dipoles account for the different dielectric permittivity of different materials.[8]

By applying an electric field along the long axis of the liquid crystals, the permittivity observed is $\varepsilon_{//}$, while the application of an electric field perpendicular to this axis, $\varepsilon_{\perp}$ is measured. The dielectric anisotropy $\Delta\varepsilon$ is defined as

$$\Delta\varepsilon = \varepsilon_{//} - \varepsilon_{\perp} \tag{3.3}$$

$\Delta\varepsilon$ is of fundamental importance in the switching performance of a material. For instance, in a twisted nematic display, $\Delta\varepsilon$ is required to be high enough to enable fast switching at low voltage. Values for $\Delta\varepsilon$ of technically useful materials range

from -6 to +50. Materials with negative $\Delta\varepsilon$ can be used in a device called electrically controlled birefringence (ECB) display.[9] In fact, the ratio $\Delta\varepsilon/\varepsilon_{\perp}$ is important and is required to be minimized for the steep electrooptic response necessary for the highly multiplex nematic mixtures used in complex display.[9]

In electrostatics, the measurement of dielectric constant is almost always accomplished by the application of capacitors by using Equation 3.1. In LC measurement, this requires precise measurement of parasite capacitance (C_p, due to the rest of the circuit) and thickness (d) of LC cells. Since the accuracy of this measurement is extremely important for the practical application of liquid crystal materials, normally the measurement of $\varepsilon_{//}$, $\varepsilon_{\perp}$, and $\Delta\varepsilon$ is performed on the same liquid crystal sample cell. In this method, the thickness of the cell is first measured on the empty LC cell after obtaining the C_p value, and d can be calculated by

$$d = \varepsilon_0 A/(C_{empty} - C_p) \tag{3.4}$$

This equation can be derived from Eq. 3.1 pretty easily. Now, standard LC cells are commercially available and in order to prevent the potential error induced by the bubbles formed in the procedure of filling cells, the transparent electrodes are normally arranged in the center of the cells and liquid crystal materials should cover the whole surface of the two electrodes. The measurement is taken on the electrode area instead of the whole area of the cell. Since the electrodes are formed by lithography, the areas are precisely known.

Without or with a low external electric field, at least one surface layer of LC molecules is aligned parallel to the surface of the cells, but just like liquid

crystals put into a glassy flask, the liquid crystal is opaque because there exist some microdomains in the bulk of the liquid crystal which have different orientation and anisotropic properties (e.g. they reflect light differently). To make sure the $\varepsilon_{\perp}$ is the actual dielectric constant for the perpendicular arrangement, a certain technique (i.e., alignment) must be applied to make the needed uniform orientation of the bulk liquid crystals. The electrodes of the standard cells are coated with alignment polyimide (PI) films, which were rubbed along the same direction, ensuring parallel alignment (to the surface of the electrodes and substrates, but perpendicular to the external electric field applied for the measurement). By applying a voltage much lower than the threshold voltage, the capacitance of the cell can be measured and $\varepsilon_{\perp}$ can then be calculated from Eq. 3.1. With the application of high enough external electric field, by Fredericks transition, all the molecules are aligned parallel to the electric field. Therefore, the dielectric constant thus obtained should be $\varepsilon_{//}$. Dielectric anisotropy can then be calculated by Eq. 3.3.

3.2.2. Birefringence

Double refraction occurs in optically anisotropic media, that is, media having optical properties dependent on direction. The phenomenon is also referred to as birefringence. The "double" and "bi" in the name of this effect refers to a difference in the refractive indices along the two different directions of propagation that a given incident ray can take in such media, depending on the direction of polarization. UniformLy aligned liquid crystals possess the same

property. Because liquid crystals are uniaxial systems, let us just consider the simplest kind of birefringent medium.

If diffraction effects are neglected, propagation of waves in uniaxial birefringent medium can be described by a generalization of Huygens' principle.[10] The spherical secondary wavelets are replaced by wave surfaces of greater complexity, consisting of a spherical wave (referred to as ordinary ray) plus a wave (referred to as extraordinary ray) that is an ellipsoid of revolution. The ellipsoid is tangent to the sphere at two points that lie on a line though the center of the elliptical waves. The line is called the optic axis (O.A.) and it forms the axis for the ellipsoid of revolution. In liquid crystals, this optic axis is the same as the director of the molecules.

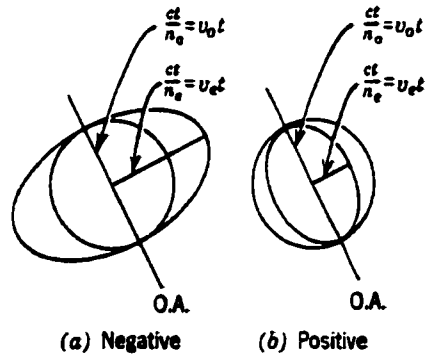

Figure 3.1. Schematic representation of the polarizability for birefringent materials (adopted from Ref. 10).

The spherical wavelet spreads with a velocity $v_o = c/n_o$, and so at time t its radius will be $(c/n_o)t$. The ellipsoidal wavelet spreads with a velocity ranging between c/n_o along the optic axis to a velocity to a velocity $v_e = c/n_e$ in a plane

perpendicular to the optic axis. Here, n_o and n_e refer to the refractive indices for ordinary and extraordinary rays respectively. The ellipsoid can be described by the following equation

$$\frac{(x^2+y^2)}{v_e^2}+\frac{z^2}{v_o^2}=t^2 \tag{3.5}$$

if a coordinate is picked to have its z axis along the optic axis. Obviously this equation can be rewritten as

$$n_e^2(x^2+y^2)+n_o^2z^2=c^2t^2 \tag{3.6}$$

The value of n_e is always greater than that of n_o for all liquid crystals and they are referred to as positive material. The birefringence, or optic anisotropy is defined as $\Delta n = n_e - n_o$. Birefringence can be related to the dielectric anisotropy by the following relation[8]

$$\Delta\varepsilon(\nu)=n_e(\nu)^2-n_o(\nu)^2 \tag{3.7}$$

However, the dielectric anisotropy of interest for LCDs is at very low frequency (ν from 0 to 1 kHz), and is usually much larger than $\Delta\varepsilon(\nu)$ in the visible and IR ranges.

When a beam of light is shone along the optic axis (molecular axis and also director) of the liquid crystal mixture, it will not sense the birefringence and this is the basic principle of LCDs. The magnitude of birefringence of liquid crystal mixtures is important when considering their use in display devices; in fact, it is the optical path difference ($\Delta n \times d$) that is the most important parameter.

When a linearly polarized light impinging on a parallel-aligned cell with the polarization axis perpendicular ($\theta = 90°$) to the LC director, a pure phase

modulation is achieved because the light behaves like an extraordinary ray. On the other hand, if $\theta = 45°$, the polarized light can be viewed as the sum of an extraordinary and an ordinary rays of the same intensity and the phase retardation occurs due to the different propagating speed of the extraordinary and ordinary rays in the LC medium. The phase retardation (δ) can be expressed as[11]

$$\delta(V, T, \lambda) = 2\pi d\Delta n(V, T, \lambda)/\lambda. \tag{3.8}$$

$\Delta n(V, T, \lambda)$ is the effective birefringence of the LC, which is a function of the applied voltage, temperature and the wavelength of the incident light. At $V = 0$, Δn ($= n_e - n_o$) reaches its maximum value, and so does δ.

Wu *et al.* proposed a method to measure the birefringence of LC materials.[11] In their method, the alignment direction of both substrates of the sample cell are parallel to each other. Therefore, LC molecules will orient themselves parallel to each other and at the same time parallel to the alignment direction of the substrates. Then the cell is filled with the LC material to be studied and put between two polarizers (normally, the one closer to the detector is called analyzer and the other one is called polarizer). The angle between the polarization direction of the polarizer and director of the LC molecules is assumed to be θ. When the polarization direction of the analyzer is adjusted to be parallel or perpendicular to that of the polarizer, the normalized transmission of the cell can be expressed as

$$T_{//} = 1 - \sin^2 2\theta \sin^2 \frac{\delta}{2} \tag{3.9}$$

$$T_{\perp} = \sin^2 2\theta \sin^2 \frac{\delta}{2} \tag{3.10}$$

θ is generally set to be 45° and Eqs. 3.9 and 3.10 can be simplified as

$$T_{//} = \cos^2\frac{\delta}{2} \tag{3.11}$$

$$T_{\perp} = \sin^2\frac{\delta}{2} \tag{3.12}$$

where δ is still a function of V, T and λ, as discussed previously. A plot of voltage-dependent transmission is shown below in Figure 3.2.

From Eqs. 3.11 and 3.12

$$\frac{T_{\perp}}{T_{//}} = \tan^2\frac{\delta}{2} \tag{3.13}$$

and it can be deduced that

$$\delta = m\pi + 2\tan^{-1}\sqrt{\frac{T_{\perp}}{T_{//}}} \qquad m = 0, 2, 4 \tag{3.14}$$

$$\delta = (m+1)\pi - 2\tan^{-1}\sqrt{\frac{T_{\perp}}{T_{//}}} \qquad m = 1, 3, 5 \tag{3.15}$$

where the quantity m is the number of maxima determined from a plot such as that shown in Figure 3.2. As mentioned before, when the driving voltage is 0 V, δ and Δn reach their maxima. After the value of δ(V = 0) is calculated from Eq. 3.14 or 3.15, Δn (= $n_e - n_o$) can be calculated using Eq. 3.8. In our measurement, the driving voltage is scanned from way below the threshold voltage to 24 V, the polarization direction of the analyzer is switched to be either parallel or perpendicular to that of the polarizer. Two curves similar to Figure 3.2 corresponding to $T_{\perp}$ and $T_{//}$, respectively, are obtained. The light used in this

measurement should be monochromic, since Δn is also a function of wavelength. A typical calculation is shown in Appendix A.6.

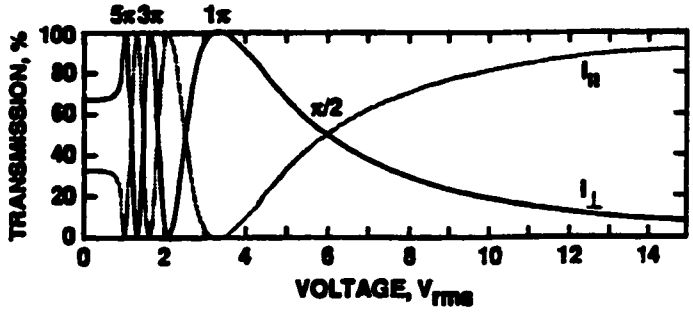

Figure 3.2. Voltage-dependent transmission of a 7.72-μm-thick, parallel-aligned E-7 LC cell at 633nm and two polarizer positions (adopted from Ref. 11).

3.2.3. Elastic constant

The elastic constants of a liquid crystal are restoring torques which become apparent when the system is perturbed from its equilibrium configuration. These restoring forces are very weak in comparison with the restoring forces of solids, e.g. Hook's law. While in displays it is the electric force which induces the initial perturbation, it is the balance between elastic and electric forces which determines the static deformation pattern of a liquid crystal and the dynamic behavior additionally invokes the viscous propertied of the system.

Frank[12] has shown that an arbitrary deformation state can be visualized as the combination of three basic operations: splay, twist and bend, which are described by the corresponding elastic constants K_{11}, K_{22} and K_{33}, respectively, (Figure 3.3). The elastic part of the internal energy of a perturbed liquid crystal is given by the equation[8, 12]

$$F = \frac{1}{2}[K_{11}(\nabla \cdot n)^2 + K_{22}(n \cdot \nabla \times n)^2 + K_{33}(n \cdot \nabla n)^2] \quad (3.16)$$

In order to improve the multiplexability of TN-LCDs, the ratio of bend and splay elastic constants K_{33}/K_{11} of nematic liquid crystal is the most important parameters, that is, small K_{33}/K_{11} gives sharp threshold and hence high multiplexability.

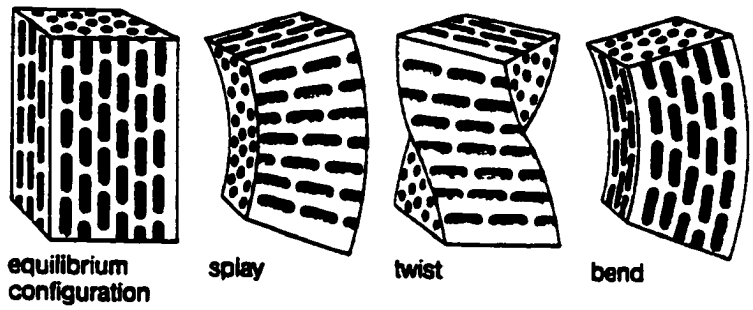

Figure 3.3. Three possible deformations of a liquid crystal.

A method to determine K_{33}/K_{11} from capacitance-voltage curve was reported by Uchita and co-workers.[13] The exact relation between cell capacitance C and applied voltage are obtained by Gruler *et al.* as[13, 14]

$$\frac{V}{V_{th}} = \frac{2}{\pi}(1+\gamma \sin^2\phi_m)^{\frac{1}{2}} \int_0^{\phi_m} \left[\frac{1+K\sin^2\phi}{(1+\gamma\sin^2\phi)(\sin^2\phi_m - \sin^2\phi)}\right]^{\frac{1}{2}} d\phi \quad (3.17)$$

$$\frac{C}{C_\perp} = \frac{\int_0^{\phi_m} \left[\frac{(1+K\sin^2\phi)(1+\gamma\sin^2\phi)}{\sin^2\phi_m - \sin^2\phi}\right]^{\frac{1}{2}} d\phi}{\int_0^{\phi_m} \left[\frac{1+K\sin^2\phi}{(1+\gamma\sin^2\phi)(\sin^2\phi_m - \sin^2\phi)}\right]^{\frac{1}{2}} d\phi} \quad (3.18)$$

where

$$K = \frac{K_{33}}{K_{11}} - 1,$$

$$\gamma = \frac{\Delta\varepsilon}{\varepsilon_\perp} = \frac{\varepsilon_{//}}{\varepsilon_\perp} - 1,$$

ϕ is tilt angle of director of the liquid crystal, and ϕ_m is the tilt angle at the center of the cell. $\frac{K_{33}}{K_{11}}$ can be determined by a numerical curve fitting method using Eqs. 3.17 and 3.18, although the calculation procedure is very complicated. Eq. 3.18 can be transformed to

$$\frac{C}{C_\perp} = (1+\gamma) - \frac{\gamma \int_0^{\phi_m} \left[\frac{1+K\sin^2\phi}{(1+\gamma\sin^2\phi)(\sin^2\phi_m - \sin^2\phi)}\right]^{\frac{1}{2}} \cos^2\phi d\phi}{\int_0^{\phi_m} \left[\frac{1+K\sin^2\phi}{(1+\gamma\sin^2\phi)(\sin^2\phi_m - \sin^2\phi)}\right]^{\frac{1}{2}} d\phi} \qquad (3.19)$$

Eqs. 3.17 and 3.19 give

$$\frac{C-C_\perp}{C_\perp} = \gamma - \frac{2\gamma}{\pi}(1+\gamma\sin^2\phi_m)^{\frac{1}{2}} \frac{V_{th}}{V} \int_0^{\phi_m} \left[\frac{1+K\sin^2\phi}{(1+\gamma\sin^2\phi)(\sin^2\phi_m - \sin^2\phi)}\right]^{\frac{1}{2}} \cos^2\phi d\phi$$

and if let $x = \cos\phi$, it then becomes

$$\frac{C-C_\perp}{C_\perp} = \gamma - \frac{2\gamma}{\pi}(1+\gamma\sin^2\phi_m)^{\frac{1}{2}} \frac{V_{th}}{V} \int_0^{\sin\phi_m} \left[\frac{(1+Kx^2)(1-x^2)}{(1+\gamma x^2)(\sin^2\phi_m - x^2)}\right]^{\frac{1}{2}} dx \qquad (3.20)$$

When the applied voltage is sufficiently high, the approximation $\phi_m = \frac{\pi}{2}$ is valid, and Eq. 3.21 can be simplified as

$$\frac{C-C_\perp}{C_\perp} = \gamma - \frac{2\gamma}{\pi}(1+\gamma)^{\frac{1}{2}} \frac{V_{th}}{V} \int_0^1 \left(\frac{1+Kx^2}{1+\gamma x^2}\right)^{\frac{1}{2}} dx \qquad (3.21)$$

From Eqs. 3.1 and 3.3,

$$\gamma = \frac{\Delta\varepsilon}{\varepsilon_\perp} = \frac{\varepsilon_{//} - \varepsilon_\perp}{\varepsilon_\perp} = \frac{C_{//} - C_\perp}{C_\perp}$$

and therefore, Eq. 3.21 can be rewritten as

$$C_R \equiv \frac{C - C_\perp}{C_{//} - C_\perp} = 1 - \frac{2}{\pi}(1+\gamma)^{\frac{1}{2}} \frac{V_{th}}{V} \int_0^1 \left(\frac{1+K x^2}{1+\gamma x^2}\right)^{\frac{1}{2}} dx \qquad (3.22)$$

Thus, the measurement of $\frac{K_{33}}{K_{11}}$ can be combined with the measurement of dielectric anisotropy. In the dielectric measurement, $C_{//}$, $C_\perp$ and γ can be obtained. Then a scanning of driving voltage is applied and the corresponding capacitance is then recorded. The reduced capacitance C_R is then allowed to plot against $\frac{C - C_\perp}{C_{//} - C_\perp}$ and the slop of this straight line (when $C_R \geq 0.8$) can then be utilized to achieve the value of K and thus of $\frac{K_{33}}{K_{11}} (= K + 1)$.

3.3. Structure-property relations of liquid crystals

An enormous number of organic compounds have been synthesized, but among them only a small portion exhibits any liquid crystal phases. On the other hand, thousands of liquid crystals have been made, and each has its own specific combination of structural moieties which confer a certain phase morphology, phase transition temperatures, and other physical properties. The presence of liquid crystal phases is limited by both steric and polarity factors, that is, liquid crystal phases can only be exhibited by compounds with specific structures. The

combination of structural moieties determines the physical properties of materials which are very important when materials are being considered for specific applications.

Not all liquid crystals are suitable for applications or in fact even designed to do so. Accordingly, much care is required in the design and synthesis of liquid crystal materials in order to generate the desired liquid crystal properties and the necessary general physical properties. Much valuable information of the structure-property relationships[9,15-16] has been provided by fundamental research. Subsequently this knowledge has been applied to the design and synthesis of liquid crystal materials that are used in the rapidly growing range of applications that are of increasing importance to technological advancement.

All scientists working in this field require at least a basic understanding of the structure-property relationships of liquid crystals. This understanding is essential, and it is well recognized that the relationships are extremely interesting aspects of liquid crystal research, although in practice the actual synthesis and evaluation of the materials must be performed.

Of all liquid crystalline phases, the nematic phase is used in many commercially available displays from low information content ones (e.g. watches, calculators, etc) to high information content ones (e.g. portable computers, small screen TV, etc). The nematic liquid crystals are expected to fulfil the future demand for medium-sized displays. In contrast, smectic liquid crystals have found fewer commercially successful applications, although LCD using FLC (S_C^*) has

been commercially successful recently. Thus the following discussion is mainly concerned with the formation and thermal stability of nematic phases.

The structure of calamitic liquid crystals can be illustrated by the following schematic structure, in which A and B are ring systems connected by a linking group Z, M and M' are lateral substituents, R is a terminal chain, and X is the other terminal group. Some general discussion of effect of various groups on the properties of liquid crystals will be given below.

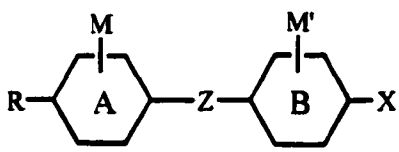

Figure 3.4. General structure of liquid crystals.

3.3.1. Ring system

Most liquid crystals require at least two rings to produce the mesophase. Two of the rare exceptions[9,17] are shown in Figure 3.5. Theoretically, any ring system that allows a linear configuration can be a good candidate for making compounds with mesogenic properties. However, in practice, only some five and six-member rings have been used. The failure is caused either by the difficulty in getting the correct substitution pattern to ensure the wanted linear configuration or by the fact that some ring systems favor crystalline phases too much to form any liquid crystalline phase.

The ring system affects not only the thermal stability of liquid crystals but also dielectric anisotropy, optical birefringence, elastic constants and viscosity.

Large dielectric anisotropy and birefringence can be obtained from aromatic rings, especially highly conjugated ring systems. Normally they also possess large elastic constants, but a problem accompanying this is that these liquid crystals have relatively large viscosity. Alicyclic rings can also be adopted in liquid crystals and the resultant liquid crystals are normally associated with low viscosity, but low dielectric anisotropy and low birefringence as well. In both cases, heterocyclic rings can also be used.[18-19] The hetero atoms on the rings normally broaden the molecules and result in lowered mesogenic stability. The interaction between the hetero atoms can either favor the layered arrangement of the molecules to form smectic phases or the other way around. There exists some subtle balance between the size and the interaction of the atoms in the structure.

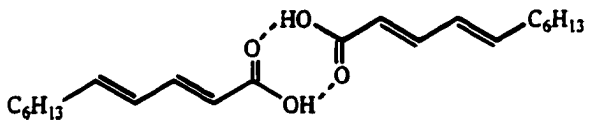

C 32.0 N 62.5 I

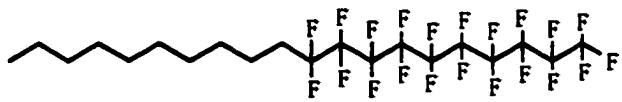

C 46.9 S 63.3 I

Figure 3.5. Unusual liquid crystals without ring systems.[9,17]

Some of the ring systems used in liquid crystals are depicted in Figure 3.6.

3.3.2. Linking group

In liquid crystals, linking groups serve to connect different ring systems. These groups could be a single bond as in 5CB or other groups. Most linking

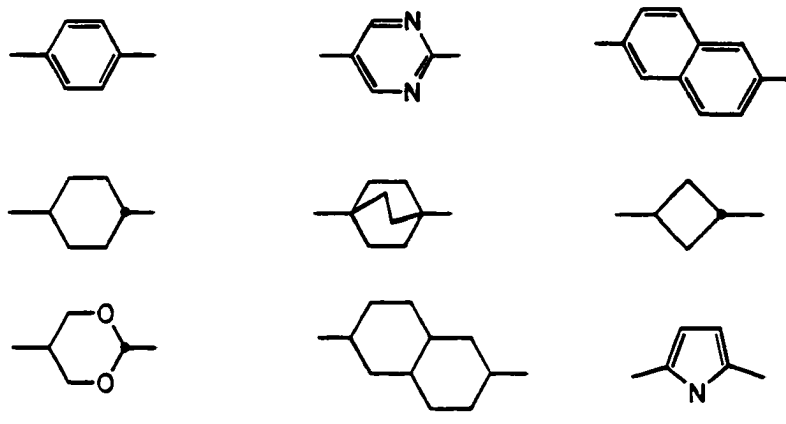

Figure 3.6. Commonly used ring systems.

groups contain two or four binding atoms. because an odd number of binding atoms cause the core to bend and reduce the mesogenic property. Linking groups lengthen the molecules to increase the length-to-breadth ratio of the molecules, thus to favor the mesophase. Linking groups can also change the polarity and polarizability of the whole molecules. thus changing the properties of the molecules. An advantage of unsaturated linking groups is that they can elongate the conjugated system to obtain large dielectric anisotropy and optical birefringence, which are not obtainable in biphenyls since the two phenyl rings are not coplanar due to the steric repulsion between the ortho hydrogen atoms on the different rings. The most common linking groups are listed below in Figure 3.7.

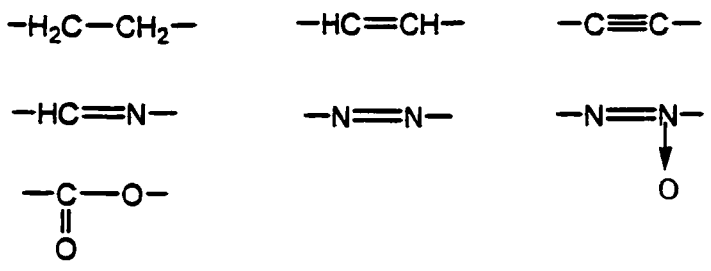

Figure 3.7. Common linking groups.

3.3.3. Terminal moiety

The physical properties of nematic materials are greatly influenced by the choice of terminal unit. Any group that can extend the length without increasing the width of the molecules can be used as a terminal group. Nearly all liquid crystals contain at least one terminal chain, which could be alkyl, alkoxyl or alkenyl chain.[20] Although hydrocarbon terminal chains have low polarizability, they increase the length-to-breadth ratio of molecules. In the mean time, they impart some flexibility into the molecules, and lower the transition temperatures. Therefore, alkyl chains are good promoters of liquid crystal phases.

The effect of chain length on the phase transition properties of liquid crystals is normally irregular and unpredictable. In many cases, the minimum melting points can be obtained in the liquid crystals with pentyl chains. However, often an odd-even effect will be found in the homologous series, that is, the phase transition temperatures of liquid crystals having chain with even number of carbon atoms lie on the same smooth curve, while those with odd carbon numbers on another curve. This phenomenon can be explained by considering that the odd carbon atom alkyl chain having a terminal methyl which extends the molecular

axis, whereas in an even number carbon chain the terminal methyl tends to lie off axis.[15] As the chain length increases, this effect becomes less pronounced and longer chain length favors smectic phases. The length of the chain can also influence the elastic constants of the nematic phase.

Branching the alkyl chains has a significant effect on the liquid crystal phase behavior of a material. Basically, the branching can suppress the orthogonal packing and be used to introduce tilted smectic phases into a system. It lowers the phase transition temperatures of the materials. and this effect is strengthened when the branching is moved towards the core. Another benefit of this effect is that chiral centers can be introduced to the system at the same time, which can then lead to the formation of ferroelectric properties.[21] Surprisingly. the viscosity of materials is also increased by the branching.

Alkoxyl chains can also be incorporated into liquid crystals. The polarity of the oxygen atom often causes an increase of melting point and viscosity. although they may exhibit a trend similar to their alkyl analogs. The nematic stability (N→I transition temperature) also increases.[22] The oxygen atom is generally directly bonded to the aromatic ring, which extends the conjugation and increases the rigidity of the core. Liquid crystals with oxygen connected to aliphatic rings are not well-explored due to the difficulty of synthesis.

Alkenyl chains increase the rigidity of the terminal chain and the whole molecule. However, this affects the phase properties of materials in a subtle manner, i.e. the position of the double bond is crucial in either lowering or increasing the elastic constant ratio and phase transition temperatures.[20]

Besides long chains, other terminal unit can also be chosen to incorporate into the structure of liquid crystals. It was found that the nematic stability decreases in the following sequence:[9,15-16]

$$Ph > NHCOCH_3 > CN > OMe > NO_2 > Cl > Br > NMe_2 > Me > F > H.$$

A polar terminal group such as the carboxyl group can force the molecules to form dimers (by hydrogen bonding) which significantly increases the length of the molecules without increasing the breadth, resulting in better mesogenic properties. The cyano group behaves in a similar manner.[23] The liquid crystal molecules bearing cyano end groups are often arranged in antiparallel fashion but the molecular axes are not in the same line. As a result, the dielectric anisotropy can be reduced. The resultant molecular pair is broader and transient and the extent of the antiparallel ordering is determined by the structure of the molecules, but as yet this cannot be predicted accurately.

The physical properties of the molecules are influenced greatly by the selection of the end group and in most cases high dielectric anisotropy requires the incorporation of cyano group. However, the molecular arrangement is another important factor. The existence of polar terminal groups in liquid crystals will inevitably invoke larger viscosity of the materials.

3.3.4. Lateral substitution

A lateral substituent is one that is attached off the linear axis of the molecule, usually on the side of an aromatic or aliphatic ring. A wide range of different lateral substituents (e.g., F, Cl, CN, NO_2, Me, CF_3) have been adopted

into many different liquid crystal systems in many different environments. Alkyl chains can also serve as lateral groups.[24] More interestingly, branches in a terminal alkyl chain such as methyl, fluoro and cyano moieties are sometimes referred to as lateral substituents as well.[9]

Intuitively, it may be considered that anything that sticks out at the side of a molecule obviously disrupts molecular packing and therefore reduces liquid crystal phase stability. Indeed such disruption nearly always occurs through lateral substitution, but the situation is very subtle. Accordingly, in some cases this disruption to the molecular packing turns out to be advantageous for the mesomorphic and physical properties required for applications, and some very interesting and useful materials have been generated by the appropriate use of lateral substitution. Lateral substitution is important in both nematic and smectic systems: however, because of the particular disruption to the lamellar packing, necessary for smectic phases, lateral substitution always reduces smectic phase stability (particularly the more ordered smectic phases) more than nematic phase stability.

For lateral substitution, three factors need to be considered: size, polarity and position of the substituent. The most commonly used lateral substituent is the fluoro substituent which is only slightly larger than hydrogen and thus can exert a limited steric effect. Additionally, the fluoro substituent is of high polarity. This unique combination of steric and polarity effects enables some significant engineering of physical properties without too much disruption to the liquid crystal phase stability. The lateral fluoro substitution can lower $\Delta\varepsilon$ and in some

extreme cases, liquid crystals with negative $\Delta\varepsilon$ have even been prepared. Other lateral substituents are larger, and most of them have a significant effect in depressing the mesophase stability of the liquid crystals. For alkyl chains, this effect levels off with the increase of the length of the chain because it tends to lie along the long molecular axis. The position of the substitution is also of importance. Changing the position of the substituent on the same ring can even affect the phase properties of the liquid crystal, which is seen in many instances. When the lateral substituents are situated in such positions that they can make the previously conjugated aromatic rings twist to disrupt the coplanarity of the system, the physical properties such as dielectric anisotropy and birefringence can be lowered significantly.

3.4. Preliminary results of liquid crystals for IR application

Compounds with electron-donating and electron-withdrawing (push-pull) groups separated by a conjugated system, such as N, N-dimethyl-4-nitroaniline, are often used in non-linear optics applications. They have large molecular dipole moments, which result in optical absorption tailing into the near-IR region, high birefringence and large dielectric anisotropy. Liquid crystal dyes (Figure 3.8) bearing push-pull groups have been synthesized in this laboratory,[25-27] and they exhibit high dielectric anisotropy and large birefringence which extends into the IR region better than commercial liquid crystal mixtures, for example, E7 (Figure 3.9). However, their usage is limited to guest-host display since they are monotropic and have only narrow nematic ranges.

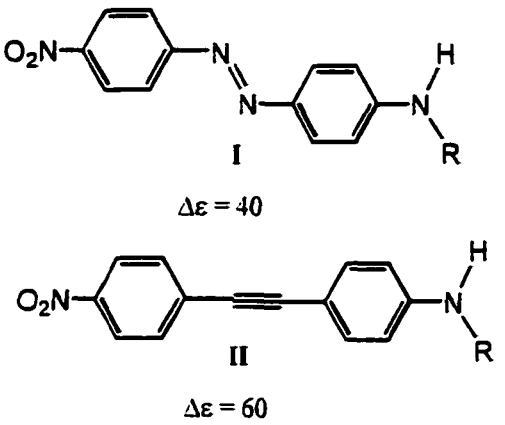

Figure 3.8. Two liquid crystal dyes synthesized in this laboratory.[25-27]

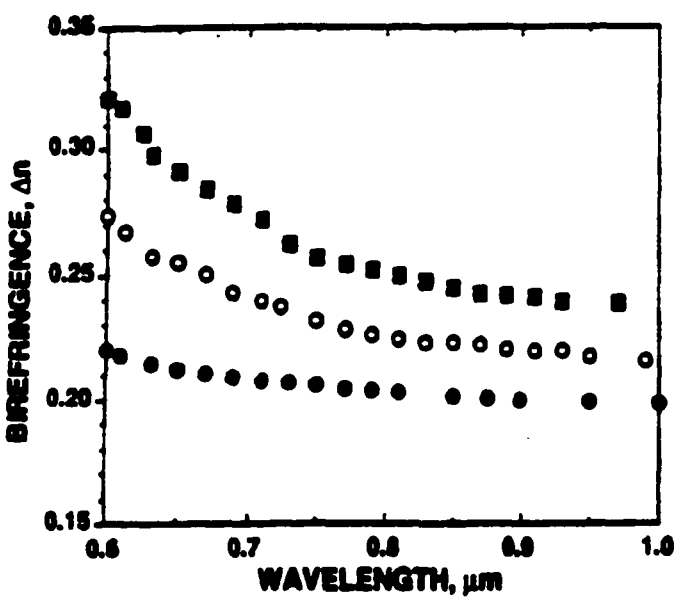

Figure 3.9. Wavelength-dependent birefringence of E7 (filled circles), 10% **I** (R = C_6H_{13}) in E7 (open circles), and 20% **I** in E7 (filled squares).[26]

Lengthening mesogenic cores normally results in better liquid crystalline properties, and the introduction of lateral substitutions can overcome the

accompanying problem of an undesirable increase in the melting point.[28-29] Some four-ring nematic liquid crystals with a lateral alkoxy branch (**III** and **IV**) have been synthesized,[30] and they have wide nematic ranges. Unfortunately, when used in guest-host display devices, they behaved differently from liquid crystal hosts, the reason of which is most likely due to the presence of the lateral alkoxy chains.

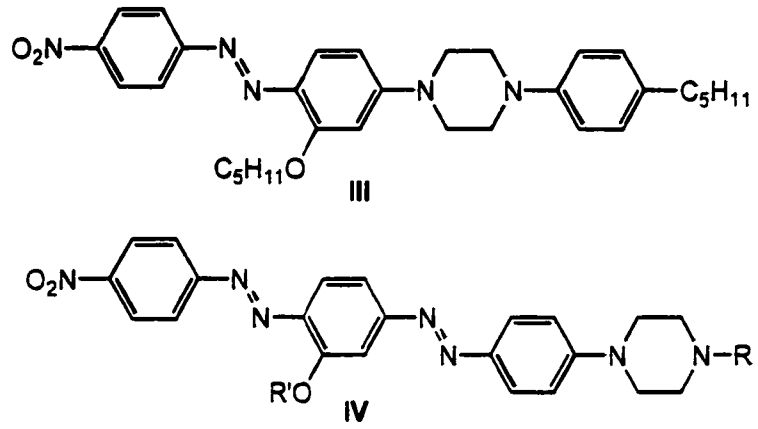

Figure 3.10. Some 4-ring nematic liquid crystals synthesized in this laboratory.[30]

In this work, the synthesis, mesomorphic and physical properties of some new liquid crystalline compounds containing three rings with relatively small lateral substituents such as fluoro-, chloro- and methyl groups on the central phenyl ring will be presented. The core of these compounds bears an electron-withdrawing nitro group at one end and an electron-donating group in the form of piperazine ring at the other end. The properties of these compounds are compared with those of the parent (non-substituted) liquid crystals. The effect of size, polarity and position of the substituents on the phase behavior and other physical properties can then be analyzed and used for further modification to prepare similar liquid crystals. For each series, the chain length changes from C5 to C8.

Because longer chain length normally favors smectic phase, liquid crystals with chains longer than C8 are not synthesized.

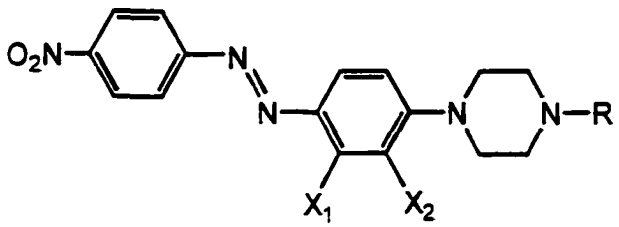

X_1= F, Cl, Me: X_2 = F, Cl, Me

V

Since liquid crystals with cyano group are very commonly used, cyano analogs of the above liquid crystals with relatively low phase transition temperatures were also synthesized to evaluate the possibility of obtaining liquid crystals with lower phase transition temperatures.

Inspired by the fact that many liquid crystals with the following structure at one end have rather large dielectric anisotropy, two other series were also

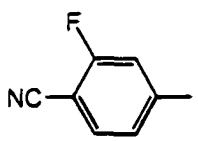

synthesized. Because the mono-fluorinated compounds in the first series are all smectic, another fluorine atom was introduced to disrupt the lamellar arrangement, forming the second homologous series.

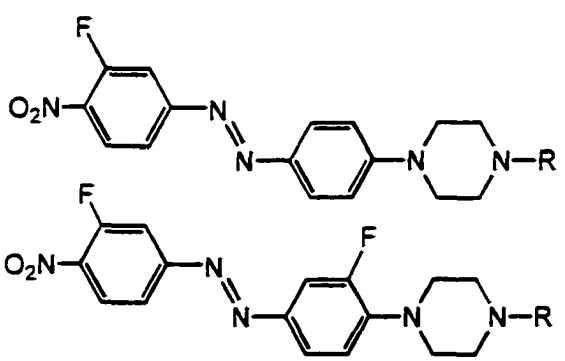

In the following sections, the synthesis and mesophoric, absorption and physical properties of all these liquid crystals will be discussed.

3.5. Experimental

3.5.1. Synthesis of liquid crystals

After many unsuccessful attempts (Appendix A.4), the following synthetic routes were adopted to make the desired liquid crystals.

3.5.1.1. Synthesis of 2-methyl-1-(4'-nitrophenylazo)-4-(4''-*n*-octylpiperazinyl)-benzene, **12**

Scheme 3.1

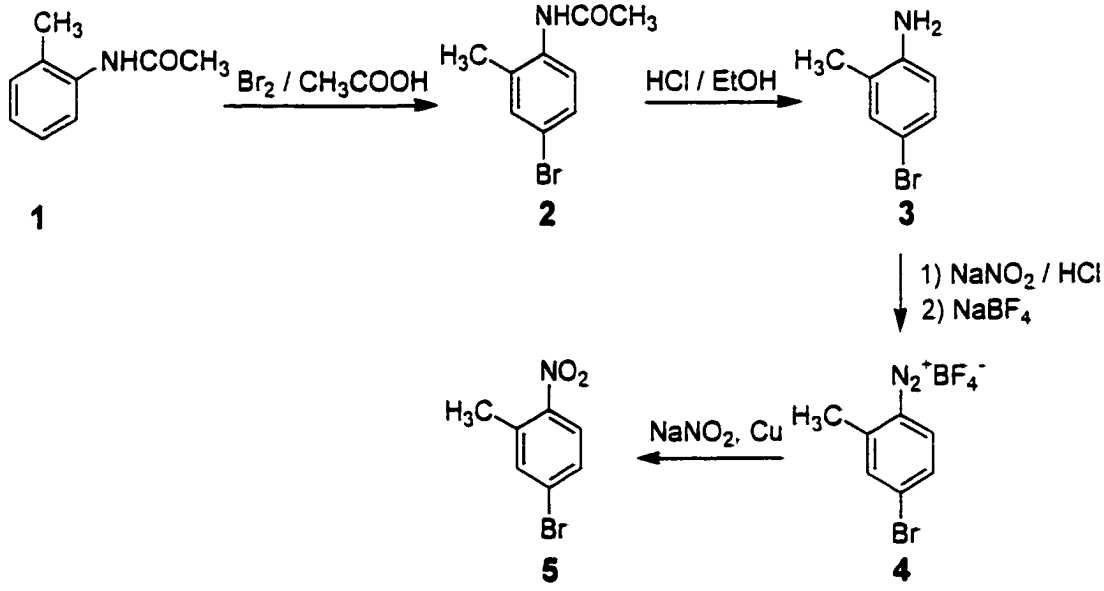

Scheme 3.2

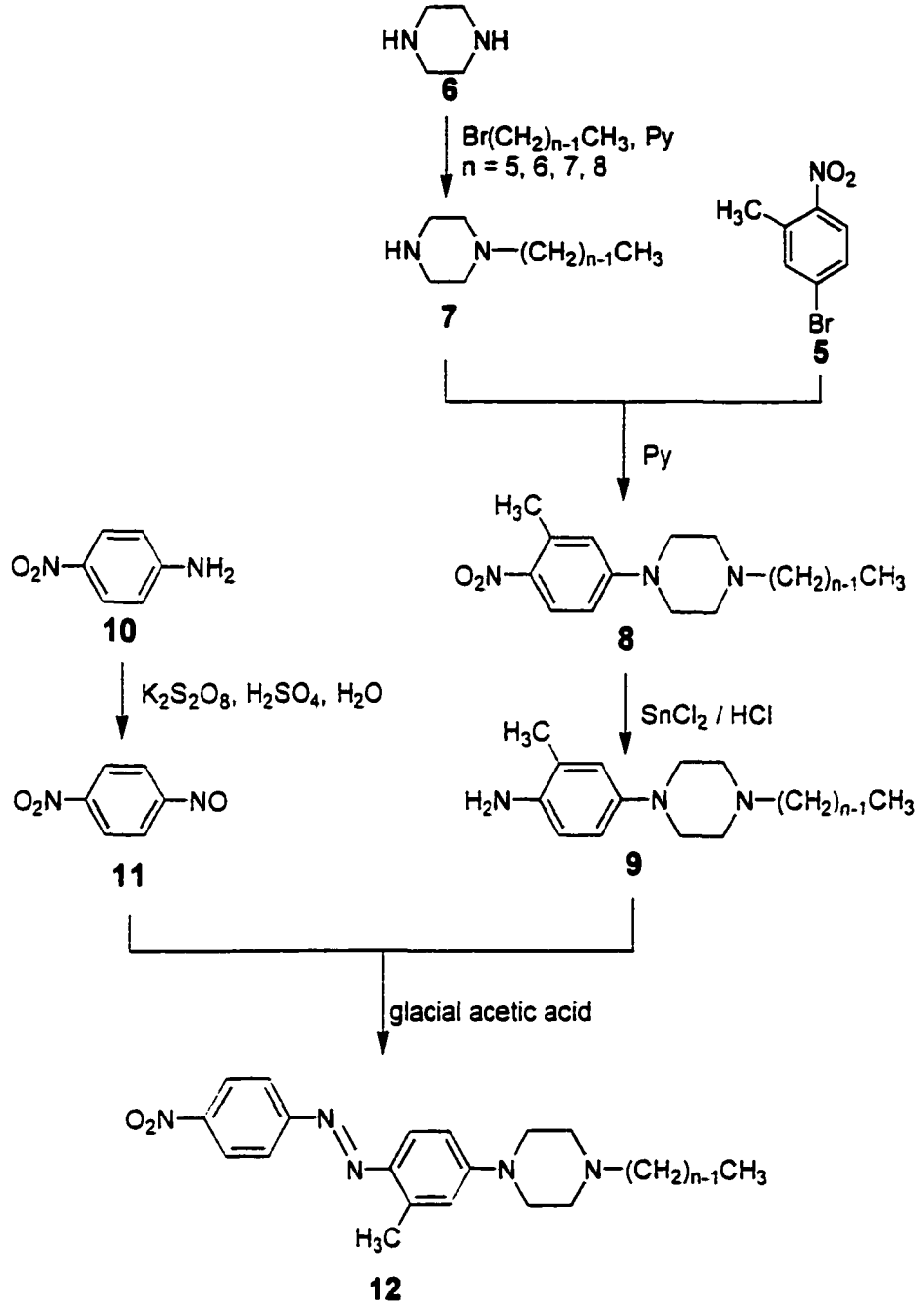

3.5.1.1.1. 3-Bromo-6-acetamidotoluene, **2**[31]

A 500 mL round bottom flask was charged with a solution of acetyl *o*-toluidine **1** (14.8 g, 0.10 mol) in acetic acid (45 mL). With the aid of a pressure-equalizing dropping funnel, a solution of Br_2 (17.0 g, 0.11 mol) in acetic acid (25

mL) was added dropwise into the flask with continuous stirring at room temperature. After completion of the addition, the solution was allowed to stay at room temperature for another 30 minutes. Then the reaction mixture was poured into water (400 mL) and well stirred. The solid **2** (white crystals) was collected by filtration.

3.5.1.1.2. 4-Bromo-2-methylaniline, **3**[31]

The crystals **2** from last step were dissolved in boiling ethanol (35 mL) contained in a 500 mL flask equipped with a reflux condenser. Concentrated hydrochloric acid (22 mL) was added to the solution via a pressure-equalizing dropping funnel. The mixture was then allowed to reflux for another 30 minutes until a test portion remained clear when diluted with water. The solution was then diluted with water (150 mL) and the flask was fitted with a condenser set for distillation. After the collection of 100 mL of distillate, the residue was poured into ice-water (100 mL) and neutralized with 5% sodium hydroxide until just alkaline. The yellow crystals **3** were collected with filtration and dried in air.

Yield, 16.8 g (90%); yellow crystals; 400-MHz ^{1}H NMR ($CDCl_3$) 7.19 (d, J = 2.3 Hz, 1H), 7.11 (d, J = 8.3 Hz, 2.3 Hz, 1H), 6.54 (d, J = 8.3 Hz, 1H), 3.59 (s, 2H), 2.13 (s, 3H); 100-MHz ^{13}C NMR ($CDCl_3$) 143.6, 132.8, 129.5, 124.4, 116.3, 110.0, 17.2.

3.5.1.1.3. 4-Bromo-2-methylphenyldiazonium tetrafluoroborate, **4**

4-Bromo-2-methylaniline **3** (8.84 g, 0.048 mol) was dissolved in a 1:1 mixture of HCl and H_2O (27 mL) with heating when necessary and the resultant solution was cooled with ice-salt bath. A pre-cooled solution of sodium nitrite (3.86 g, 0.056 mol) in H_2O (8 mL) was added dropwise to above solution and the mixture was then allowed to sit for 15 minutes. Another pre-cooled solution of sodium tetrafluoroborate (8.37 g, 0.078 mol) in H_2O (8 mL) was added to above mixture below 10 °C. The mixture was stirred for 10 more minutes and the solid product was collected by filtration and then washed by ethyl ether. Yield, 10.5 g (78%); white crystals.

3.5.1.1.4. 3-Bromo-6-nitrotoluene. **5**[31]

4-Bromo-2-methylphenyldiazonium tetrafluoroborate **4** (9.0 g, 0.037 mol) was dispersed in a solution of sodium nitrite (40.0 g, 0.58 mol) in H_2O (200 mL) mixed with freshly activated copper bronze (8 g) contained in a 400 mL beaker. The system was well stirred mechanically. Ether was added from time to time to destroy the froth. The mixture was then extracted with chloroform (200 mL x 3), the organic portions were combined and dried over anhydrous sodium sulfate. The solvent was removed and the residue was purified by silica gel column chromatography using hexane. Orange crystals **5** were obtained.

Yield, 2.0 g (20% for two steps): orange crystals; MS spectrum: m/z (DIP, 70 eV) = 214.8 (17.6), 216.8 (18.4); 400-MHz ^{1}H NMR ($CDCl_3$) 7.87 (d, J = 8.7 Hz, 1H), 7.51 (d, J = 2.2 Hz, 1H), 7.47 (d, J = 8.7 Hz, 2.2 Hz, 1H), 1.55 (s, 3H); 100-MHz ^{13}C NMR ($CDCl_3$) 147.0, 135.7, 135.5, 130.1, 127.7, 126.2, 20.4.

3.5.1.1.5. 1-*n*-Octylpiperazine, **7**

A round bottom flask equipped with a refluxing condenser was charged with piperazine **6** (30.16 g, 0.30 mol), 1-bromooctane (13.52 g, 0.070 mol) and pyridine (80 mL) and heated to reflux overnight. After being cooled to room temperature, the flask was transferred into a freezer for further cooling. The white precipitate (excess piperazine and resultant pyridinium salt) was then filtered off and washed with acetone. The acetone wash was combined with the previous filtrate and the solvents were removed with a rotary evaporator. The residue was heated at about 100 °C under moderate vacuum overnight, and then fractionally distilled under vacuum. Yellowish oil was obtained.

Yield. 9.8 g (71%); yellowish oil; bp 115 – 117 °C / 20 mm Hg; 400-MHz ^{1}H NMR ($CDCl_3$) 2.93 (t, J = 4.8 Hz, 4H), 2.44 (br s, 4H), 2.33 (m, 2H), 1.52 (m, 3H), 1.32 (br, 10H), 0.91 (t, J = 6.7 Hz, 3H); 100-MHz ^{13}C NMR ($CDCl_3$) 59.4, 54.6, 46.1, 31.7, 29.5, 29.2, 27.5, 26.6, 22.5, 14.0.

3.5.1.1.6. 2-Methyl-4-(4'-*n*-octylpiperazinyl)nitrobenzene, **8**[32]

3-Bromo-6-nitrotoluene **5** (0.40 g, 1.4 mmol), 1-*n*-octylpiperazine **7** (0.29 g, 1.5 mmol), potassium carbonate (0.55 g, 4.0 mmol) and pyridine (20 mL) were added to a 50 mL flask and refluxed. The reaction was monitored by TLC. After removal of the solvent, purification of the residue by silica gel column chromatography using 1:1 mixture of hexane/ethyl acetate afforded **8**.

Yield: 0.25 g (50%); Yellow crystals; 400-MHz ^{1}H NMR ($CDCl_3$) 8.07 (d, J = 9.2 Hz, 1H), 6.91 (dd, J = 9.2 Hz, 2.6 Hz, 1H), 6.62 (d, J = 2.6 Hz, 1H), 3.39

(t, J = 5.1 Hz, 4H), 2.63 (s, 3H), 2.56 (t, J = 5. 1 Hz, 4H), 2.37 (t, J = 7.6 Hz, 2H), 1.51 (br s, 2H); 1.27 (br m, 10H); 0.88 (t, J = 7.2 Hz, 3H); 100-MHz ^{13}C NMR ($CDCl_3$) 153.8, 139.2, 137.1, 127.7, 116.1, 111.1, 58.7, 52.7, 47.0, 31.8, 29.5, 29.2, 27.5, 26.8, 22.6, 22.6, 14.1.

3.5.1.1.7. 2-Methyl-4-(4'-*n*-octylpiperazinyl)aniline, **9**[33, 34]

A mixture of 2-methyl-4-(4'-*n*-octylpiperazinyl)nitrobenzene **8** (1.12 g, 3.4 mmol), stannous chloride dihydrate $SnCl_2{\cdot}2H_2O$ (2.92 g, 12.4 mmol) and hydrochloric acid (56.7 mL) was refluxed until a drop of the reaction mixture became clear when diluted with distilled water (1 mL). The reaction mixture was transferred into a flask and chloroform (100 mL) was then added. After cooling, the mixture was basified with 35% ammonium hydroxide slowly with stirring till it was highly alkaline. The organic part was separated and the aqueous layer was further extracted with chloroform (50 mL x 3). The organic portions were combined, dried over anhydrous potassium carbonate and then filtered. After removal of the solvent, purification of the residue by silica gel column chromatography using ethyl acetate afforded **9**.

Yield, 0.65 g (64%): yellow crystals; 400-MHz ^{1}H NMR ($CDCl_3$) 6.69 (d, J = 2.2 Hz, 1H), 6.65 (dd, J = 8.4 Hz, 2.2 Hz, 1H), 6.54 (d, J = 8.4 Hz, 1H), 3.32 (s, 2H), 3.03 (t, J = 4.4 Hz, 4H), 2.56 (t, J = 4.4 Hz, 4H), 2.35 (t, J = 7.8 Hz, 2H), 2.10 (s, 3H), 1.51 (br m, 2H), 2.28 (br m, 10H), 0.88 (t, J = 7.0 Hz, 3H); 100-MHz ^{13}C NMR ($CDCl_3$) 144.5, 138.4, 123.2, 120.0, 116.0, 115.8, 58.9, 53.5, 51.0, 31.9, 29.6, 29.3, 27.7, 26.9, 22.7, 17.8, 14.2.

3.5.1.1.8. 4-Nitrosonitrobenzene, **11**[35,36]

Potassium persulfate (5.0 g, 18.5 mmol) was added to pre-cooled concentrated sulfuric acid (3.5 mL) with continuous stirring. After the formation of a white paste, ice (50 g) was added. After the ice had completely melted, the pH of the resulting solution was adjusted to 3 with potassium carbonate. The white solid precipitated during the neutralization was filtered off and *p*-nitroaniline **10** (0.207 g, 1.5 mmol) was added to the collected filtrate at room temperature. After stirring for 3 hours, the yellow solid formed in the mixture was filtered and then purified by silica gel column chromatography using ethyl acetate / hexane (1:200).

Yield, 0.164 g (72%); yellow powder; 400-MHz ^{1}H NMR ($CDCl_3$) 8.52 (d, J = 8.8 Hz, 2H), 8.06 (d, J = 8.8 Hz, 2H); 100-MHz ^{13}C NMR ($CDCl_3$) 121.3, 125.5 (quaternary carbons missing).

3.5.1.1.9. 2-Methyl-1-(4'-nitrophenylazo)-4-(4''-*n*-octylpiperazinyl)benzene, **12**[37]

A mixture of 2-methyl-4-(4'-*n*-octylpiperazinyl)aniline **9** (0.65 g, 2.15 mmol), 4-nitrosonitrobenzene **11** (0. 33 g, 2.2 mmol) and glacial acetic acid (30 mL) was heated at about 100 °C with stirring, and the reaction was monitored by TLC. The solvent was then removed under reduced pressure. The residue was first neutralized with saturated sodium bicarbonate solution and then extracted with ethyl acetate (20 mL x 2). The solvent was removed and purification of the residue by silica gel column chromatography using ethyl acetate / hexane (1:3) afforded **12**, which was then recrystallized from hexanes.

Yield, 0.40 g (43%); dark red crystals, mp 124-126 C°; MS spectrum: m/z (DIP, 70 eV) = 437.3 (72.6); 400-MHz ^{1}H NMR ($CDCl_3$) 8.32 (d, J = 9.1 Hz, 2H), 7.92 (d, J = 9.1 Hz, 2H), 7.77 (d, J = 9.9 Hz, 1H), 6.77-6.78 (br, 2H), 3.43 (t, J = 4.8 Hz, 4H), 2.72 (s, 3H), 2.60 (br s, 4H), 2.39 (t, J = 7.4 Hz, 2H), 1.54 (br s, 2H), 1.28-1.31 (br m, 10H), 0.89 (t, J = 6.5 Hz, 3H); 100-MHz ^{13}C NMR ($CDCl_3$) 156.9, 153.9, 142.6, 124.6, 122.8, 117.1, 115.0, 112.4, 58.7, 52.9, 47.3, 31.8, 29.5, 29.2, 27.5, 26.8, 22.6, 18.2, 14.1.

3.5.1.2. Synthesis of 3-chloro-1-(4'-nitrophenylazo)-4-(4''-*n*-octylpiperazinyl)-benzene. **16d**

The same scheme (Scheme 3.3) can be utilized to synthesize many other liquid crystals with other types of substituents and the operations of the actual syntheses were very similar to that of **16d**. For simplification, only the synthesis of **16d** is shown below as an example.

Scheme 3.3

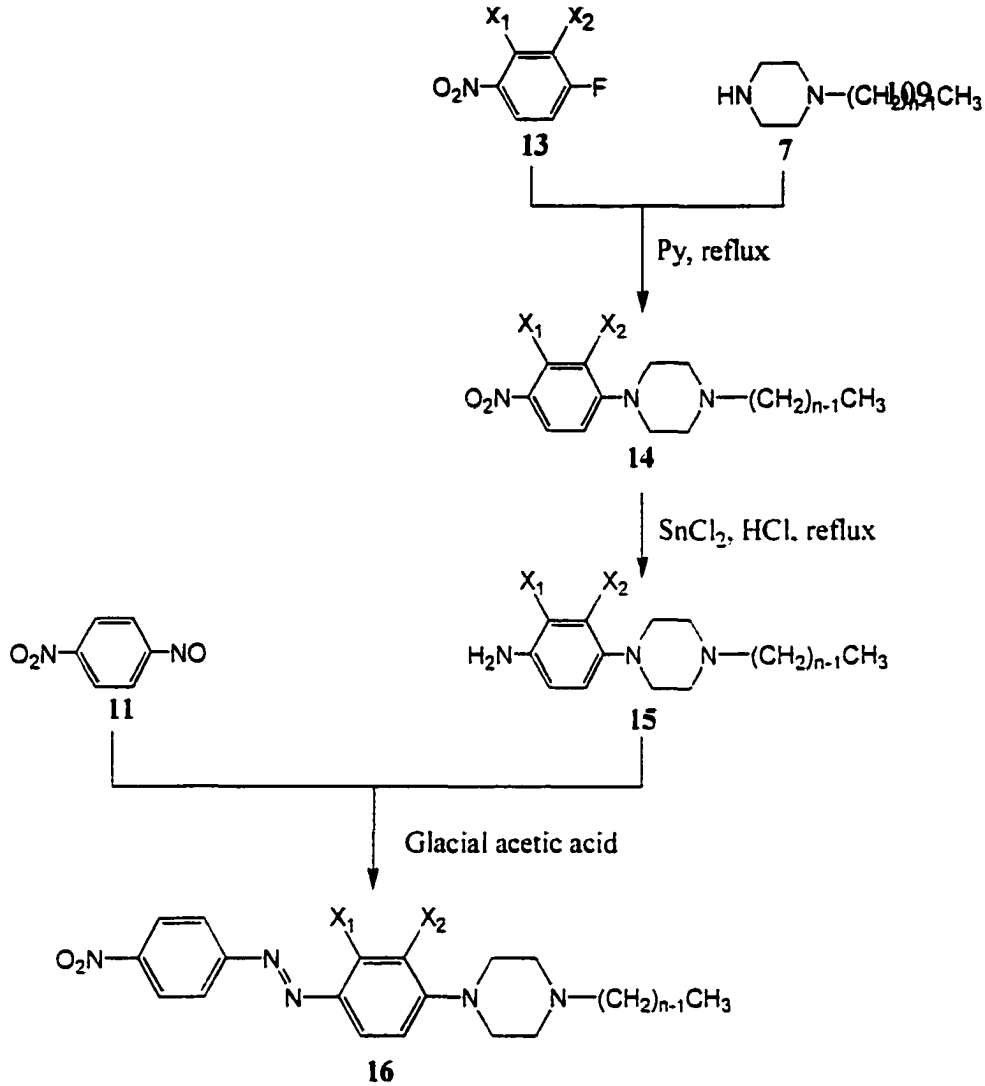

Series a: X_1 = H, X_2 = H; Series b: X_1 = H, X_2 = F;
Series c: X_1 = H, X_2 = CH_3; Series d: X_1 = H, X_2= Cl;

3.5.1.2.1. 3-Chloro-4-(4'-*n*-octylpiperazinyl)nitrobenzene, **14d**[38]

A mixture of 3-chloro-4-fluoronitrobenzene **13d** (0.64 g, 3.7 mmol), 1-*n*-octylpiperazine **7** (0.72 g, 3.7 mmol) and pyridine (20 mL) were added to a round bottom flask fitted with a condenser and refluxed overnight. After cooling, the white precipitate was filtered off. Then the solvent was removed with a rotary

evaporator, and purification of the residue by silica gel column chromatography using ethyl acetate / hexane (1:4) afforded **14d**.

Yield: 1.13g (88%); yellow crystals; 400-MHz ^{1}H NMR ($CDCl_3$) 8.24 (d, J = 2.6 Hz, 1H), 8.09 (dd, J = 8.9 Hz, 2.6 Hz, 1H), 7.04 (d, J = 8.9 Hz, 1H), 3.25 (t, J = 4.7 Hz, 4H), 2.65 (t, J = 4.7 Hz, 4H), 2.41 (m, 2H), 1.53 (m, 2H), 1.32-1.28 (br m, 10H), 0.89 (t, J = 7.0 Hz, 3H); 100-MHz ^{13}C NMR ($CDCl_3$) 154.9, 141.9, 127.4, 126.6, 123.4, 119.2, 58.67, 53.0, 50.6, 31.8, 29.5, 29.2, 27.5, 26.8, 22.6, 14.1.

3.5.1.2.2. 3-Chloro-4-(4`-*n*-octylpiperazinyl)aniline, **15d**

A mixture of 3-chloro-4-(4`-*n*-octylpiperazinyl)nitrobenzene **14d** (1.13 g, 3.2 mmol), stannous chloride dihydrate $SnCl_2 \cdot 2H_2O$ (2.78 g, 12.3 mmol) and hydrochloric acid (54 mL) was refluxed until a drop of the reaction mixture became clear when diluted with distilled water (1 mL). The reaction mixture was transferred into a flask and chloroform (100 mL) was then added. After cooling, the mixture was basified with 35% ammonium hydroxide slowly with stirring till it was highly alkaline. The organic part was separated and the aqueous layer was further extracted with chloroform (30 mL x 3). The organic portions were combined, dried over anhydrous potassium carbonate and then filtered. After removal of the solvent, purification of the residue by column chromatography using ethyl acetate afforded **15d**.

Yield, 1.03 g (~100%); yellow crystals; 400-MHz ^{1}H NMR ($CDCl_3$) 6.81 (d, J = 8.5 Hz, 1H), 6.73 (d, J = 2.6 Hz, 1H), 6.55 (dd, J = 8.5 Hz, 2.6 Hz, 1H),

3.53 (br s, 2H), 2.98 (br s, 4H), 2.61 (br s, 4H), 2.39 (t, J = 7.8 Hz, 2H), 1.52 (br s, 2H), 1.30 (br m, 10H), 0.88 (t, J = 6.9 Hz, 3H); 100-MHz ^{13}C NMR ($CDCl_3$) 142.8, 141.1, 129.8, 121.3, 117.1, 114.2, 58.9, 53.6, 51.8, 31.8, 29.5, 29.2, 27.6, 26.9, 22.6, 14.1.

3.5.1.2.3. 3-Chloro-1-(4'-nitrophenylazo)-4-(4''-*n*-octylpiperazinyl)benzene, **16d**

A mixture of 3-chloro-4-(4'-*n*-octylpiperazinyl)aniline **15d** (0.38 g, 1.2 mmol), 4-nitrosonitrobenzene **7** (0.178 g,1.2 mmol) and glacial acetic acid (25 mL) was heated at about 100 °C with stirring, and the reaction was monitored by TLC. The solvent was then removed under reduced pressure. The residue was first neutralized with saturated sodium bicarbonate solution and then extracted with ethyl acetate (20 mL x 2). The solvent was then removed and the residue was purified by silica gel column chromatography using ethyl acetate / hexane (1:3) and then recrystallized from hexanes.

Yield. 0.33 g (62%); orange crystals, mp 57-59 °C; MS spectrum: m/z (EI, 12 eV) = 459.3 (4.3), 457.3 (22.7); 400-MHz ^{1}H NMR ($CDCl_3$) 8.36 (d, J = 5.0 Hz, 2H), 8.00 (d, J = 5.0 Hz, 2H), 7.98 (d, J = 2.4 Hz, 1H), 7.89 (dd, J = 8.5 Hz, 2.4 Hz, 1H), 7.15 (d, J = 8.5 Hz, 1H), 3.25 (br s, 4H), 2.67 (br s, 4H), 2.43 (t, J = 7.8 Hz, 2H), 1.54 (m, 2H), 1.32 (br m, 10H), 0.89 (t, J = 7.0 Hz, 3H); 100-MHz ^{13}C NMR ($CDCl_3$) 155.7, 152.9, 148.5, 147.7, 128.3, 125.1, 124.7, 124.4, 123.3, 119.9, 58.8, 53.1, 50.9, 31.8, 29.5, 29.2, 27.6, 26.9, 22.6, 14.1.

The homologous series of compounds **16a**, **16b**, **16c** were synthesized by following the same scheme and the data were listed below.

16a (n = 8): red crystals, mp 128-130 °C; MS spectrum: m/z (DIP, 12 eV) = 423.1 (58.8); 400-MHz ^{1}H NMR ($CDCl_3$) 8.34 (d, J = 7.0 Hz, 2H), 8.00 (m, overlapping, 4H), 6.96 (d, J = 9.4 Hz, 2H), 3.44 (t, J = 5.1 Hz, 4H), 2.60 (t, J = 5.1 Hz, 4H), 2.39 (t, J = 7.8 Hz, 2H), 1.53 (m, 2H), 1.31 (br m, 10H), 0.89 (t, J = 7.0 Hz, 3H); 100-MHz ^{13}C NMR ($CDCl_3$) 156.5, 153.9, 147.6, 144.9, 125.7, 124.6, 122.8, 113.9, 58.7, 52.9, 47.3, 31.8, 29.5, 29.2, 27.6, 26.9, 22.6, 14.1.

16b (n = 8): red crystals, mp 93-95 °C; MS spectrum: m/z (FAB) = 442.2 (M + 1, 81.3), 441.2 (M, 37.8); 400-MHz ^{1}H NMR ($CDCl_3$) 8.36 (d, J = 9.0 Hz, 2H), 7.97 (d, J = 9.0 Hz, 2H), 7.79 (d, J = 8.3 Hz, 1H), 7.66 (d, J = 14.2, 2.2 Hz, 1H), 7.03 (t, J = 9.0 Hz, 1H), 3.32 (t, J = 4.5 Hz, 4H), 2.65 (t, J = 4.5 Hz, 4H), 2.41 (t, J = 8.0 Hz, 2H), 1.54 (m, 2H), 1.30 (br m, 10H), 0.89 (t, J = 7.0 Hz, 3H); 100-MHz ^{13}C NMR ($CDCl_3$) 156.0, 148.2, 147.1, 143.9, 124.6, 124.3, 123.1, 122.8, 117.7, 108.1, 58.8, 53.1, 49.8, 31.8, 29.5, 29.2, 27.6, 26.9, 22.6, 14.1.

16c (n = 8): red crystals, mp 87-90 °C; MS spectrum: m/z (DIP, 70 eV) = 437.2 (11.5); 400-MHz ^{1}H NMR ($CDCl_3$) 8.36 (d, J = 6.8 Hz, 2H), 7.97 (d, J = 6.8 Hz, 2H), 7.80 (m, overlapping, 2H), 7.10 (d, J = 9.2 Hz, 1H), 3.08 (t, J = 4.6 Hz, 4H), 2.65 (br s, 4H), 2.42 (t, J = 7.2 Hz, 2H), 1.54 (m, 2H), 1.30 (br m, 10H), 0.89 (t, J = 7.0 Hz, 3H); 100-MHz ^{13}C NMR ($CDCl_3$) 156.1, 155.9, 148.2, 144.1, 132.6, 125.5, 124.7, 123.7, 123.0, 118.8, 58.9, 53.5, 51.2, 31.8, 29.5, 29.2, 27.6, 26.9, 22.6, 14.1.

3.5.1.3. Synthesis of 2-chloro-1-(4'-nitrophenylazo)-4-(4''-*n*-octylpiperazinyl) benzene, **19**

Scheme 3.4

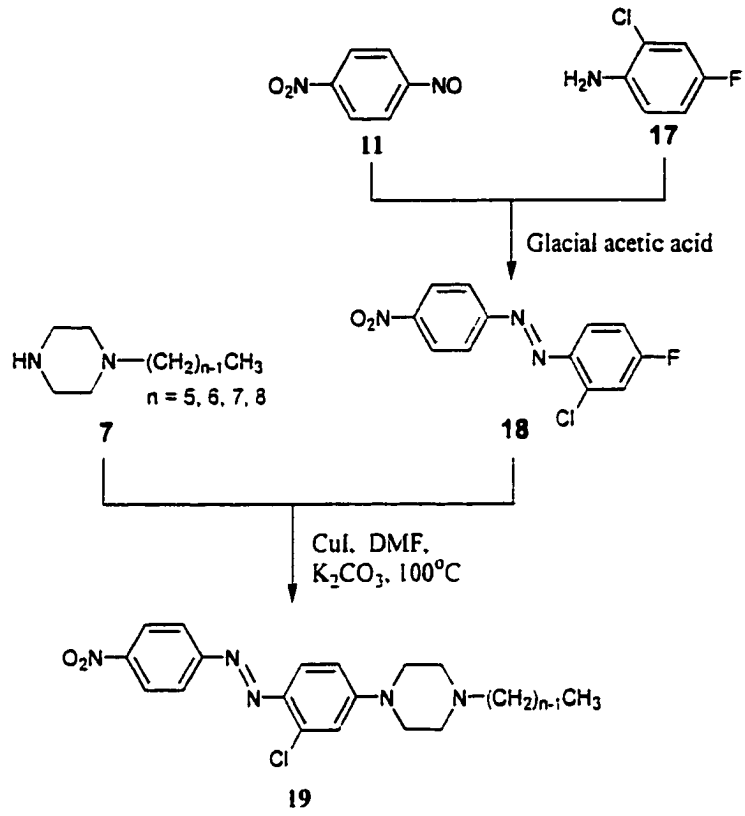

3.5.1.3.1. 4-(2'-Chloro-4'-fluorophenylazo)nitrobenzene, **18**

The procedure to make this compound is similar to that for making **16d**. A mixture of 2-chloro-4-fluoroaniline **17** (1.00 g, 6.9 mmol), 4-nitrosonitrobenzene **11** (1.04 g, 6.9 mmol) and glacial acetic acid (35 mL) was heated at 100 °C with stirring, and the reaction was monitored by TLC. After removal of glacial acetic acid, neutralization with sodium bicarbonate solution, extraction with ethyl acetate (20 mL x 2) and distillation of ethyl acetate, the residue was subjected to silica gel column chromatographic separation using ethyl acetate / hexane (1:20).

Yield, 1.65 g (85%); orange crystals; 400-MHz ^{1}H NMR ($CDCl_3$) 8.40 (d, J = 8.3 Hz, 2H), 8.07 (d, J = 8.3 Hz, 2H), 7.83 (dd, J = 9.1 Hz, 6.0 Hz, 1H), 7.35 (dd, J = 9.1 Hz, 2.8 Hz, 1H), 7.11 (m, 1H); 100-MHz ^{13}C NMR ($CDCl_3$) 166.0, 163.4, 151.9, 143.5, 138.4, 124.8, 123.9, 119.0, 118.1, 115.0.

3.5.1.3.2. 2-Chloro-1-(4'-nitrophenylazo)-4-(4''-*n*-octylpiperazinyl)benzene, **19**[39]

4-(2'-Chloro-4'-fluorophenylazo)nitrobenzene **18** (0.77 g, 2.7 mmol), 1-*n*-octylpiperazine **7** (0.60 g, 3.0 mmol), cuprous iodide (0.57 g, 3.0 mmol), potassium carbonate (0.42 g, 3.0 mmol) and dry DMF (30 mL) were charged into a flask which was then sealed and heated at 100 °C with stirring overnight. After cooling, the solvent was distilled off under reduced pressure and the residue was purified with silica gel column chromatography using ethyl acetate / hexane (1:10), followed by ethyl acetate / hexane (1:3). The product **19** was then recrystallized from a mixture of ethyl acetate and hexanes.

Yield, 0.35 g (28%); orange crystals, mp 77-79 °C; MS spectrum: m/z (EI, 12 eV) = 459.3 (12.2), 457.3 (34.0); 400-MHz ^{1}H NMR ($CDCl_3$) 8.35 (d, J = 7.0 Hz, 2H), 7.99 (d, J = 7.0 Hz, 2H), 7.82 (d, J = 9.4 Hz, 1H), 6.99 (d, J = 2.6 Hz, 1H), 6.81 (dd, J = 9.4 Hz, 2.6 Hz, 1H), 3.44 (t, J = 5.0 Hz, 4H), 2.59 (t, J = 5.0 Hz, 4H), 2.39 (t, J = 7.6 Hz, 2H), 1.53 (m, 2H), 1.31 (br m, 10H), 0.89 (t, J = 6.6 Hz, 3H); 100-MHz ^{13}C NMR ($CDCl_3$) 156.5, 154.1, 147.9, 140.2, 140.0, 124.7, 123.2, 118.5, 114.2, 112.6, 58.6, 52.7, 47.1, 31.8, 29.5, 29.2, 27.5, 26.8, 22.6, 14.1.

3.5.1.4. Synthesis of 4-[3'-fluoro-4'-(4''-*n*-octylpiperazinyl)phenylazo]benzonitrile, **22**

Scheme 3.5

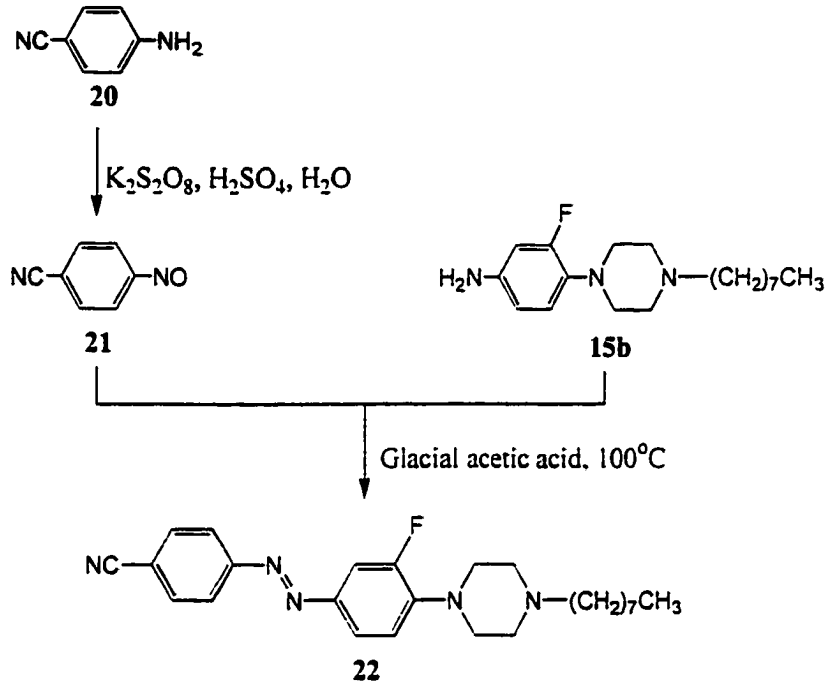

3.5.1.4.1. 4-Nitrosobenzonitrile, **21**

Potassium persulfate (5.0 g, 18.5 mmol) was added to pre-cooled concentrated sulfuric acid (3.5 mL) with continuous stirring. After the formation of a white paste, ice (50 g) was added. After the ice had completely melted, the pH of the resulting solution was adjusted to 3 with potassium carbonate. The white solid precipitated during the neutralization was filtered off and *p*-aminobenzonitrile **20** (0.18 g, 1.5 mmol) was added to the collected filtrate at room temperature. After stirring for 3 hours, the pale yellow solid formed in the mixture was filtered off and then purified by silica gel column chromatography using ethyl acetate / hexane (1:200).

Yield, 0.10 g (50%); pale yellow crystals; 400-MHz ^{1}H NMR ($CDCl_3$) 7.97 (s); 100-MHz ^{13}C NMR not available due to the low solubility in $CDCl_3$.

3.5.1.4.2. 4-[3'-Fluoro-4'-(4''-*n*-octylpiperazinyl)phenylazo]benzonitrile, **22**

A mixture of 3-fluoro-4-(4-*n*-octylpiperazinyl)aniline **15b** (0.127 g, 0.41 mmol), 4-nitrosobenzonitrile **21** (0.12 g, 0.91 mmol) and glacial acetic acid (25 mL) was heated at 100 °C with stirring, and the reaction was monitored by TLC. The solvent was then removed under reduced pressure. The residue was first neutralized with saturated sodium bicarbonate solution and then extracted with ethyl acetate (20 mL x 2). The solvent was then removed and the residue was purified by silica gel column chromatography using ethyl acetate / hexane (1:3), followed by ethyl acetate / hexane (1:1). The product **22** was then recrystallized from a mixture of ethyl acetate and hexanes.

Yield: 0.10 g (57%); orange crystals. mp 79-80 °C; MS spectrum: m/z (EI. 12 eV) = 422.3 (25.7). 400-MHz ^{1}H NMR ($CDCl_3$) 7.92 (d, J = 8.8 Hz, 2H), 7.75-7.80 (m, 3H), 7.64 (dd, J = 2.2 Hz. 14.2 Hz. 1H), 7.02 (t, J = 8.8 Hz. 1H). 3.30 (t. J = 5.0 Hz, 4H), 2.64 (t, J = 5.0 Hz, 4H). 2.40 (t, J = 7.7 Hz, 2H), 1.53 (m. 2H); 1.26-1.31 (br, 10H), 0.89 (t, J = 7.1 Hz. 3H); 100-MHz ^{13}C NMR ($CDCl_3$) 154.6. 133.1, 132.8, 126.0, 124.1. 123.1, 118.3. 117.8. 113.3. 108.2. 108.0, 58.7. 52.8. 47.2. 31.8, 29.5, 29.2, 27.5, 26.8. 22.7, 14.1.

3.5.1.5. Synthesis of 4-[3'-chloro-4'-(4''-*n*-octylpiperazinyl)phenylazo]benzonitrile, **23**

Scheme 3.6

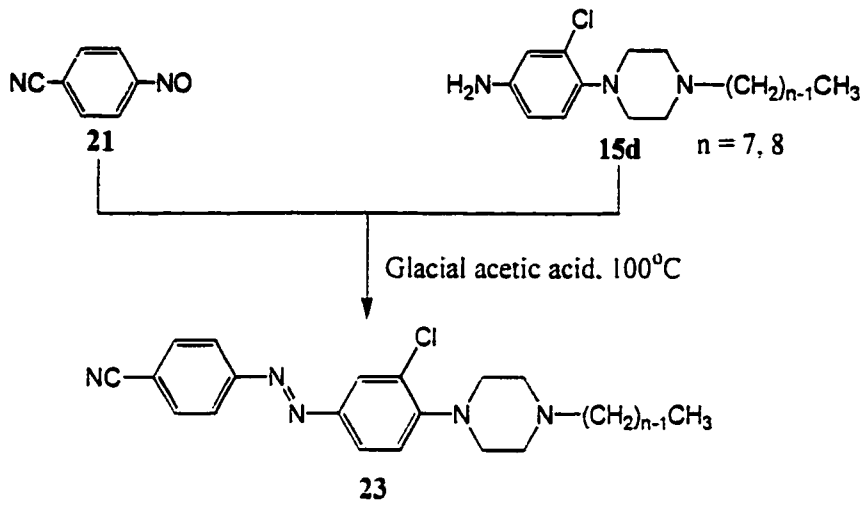

3.5.1.5.1. 4-[3'-Chloro-4'-(4''-*n*-octylpiperazinyl)phenylazo]benzonitrile, **23**

A mixture of 3-chloro-4-(4'-*n*-octylpiperazinyl)aniline **15d** (0.20 g, 0.62 mmol), 4-nitrosobenzonitrile (0.10 g, 0.62 mmol) and glacial acetic acid (25 mL) was heated at 100 °C with stirring, and the reaction was monitored by TLC. The solvent was then removed under reduced pressure. The residue was first neutralized with saturated sodium bicarbonate solution and then extracted with ethyl acetate (20 mL x 2). The solvent was removed and the residue was purified by silica gel column chromatography using ethyl acetate / hexane (1:5) and then recrystallized from hexanes.

Yield, 0.22 g (81%); orange crystals, mp 76-78 °C; MS spectrum: m/z (EI, 12 eV) = 439.2 (5.9), 437.2 (15.9); 400-MHz ^{1}H NMR ($CDCl_3$) 7.98 (d, J = 2.2

Hz, 1H), 7.94 (d, J = 8.4 Hz, 2H), 7.86 (dd, J = 2.2 Hz, 8.6 Hz, 1H), 7.80 (d, J = 8.4 Hz, 2H), 7.14 (d, J = 8.6 Hz, 1H), 3.24 (br s, 4H), 2.67 (br s, 4H), 2.43 (t, J = 7.8 Hz, 2H), 1.54 (br s, 2H), 1.26-1.32 (br, 10H), 0.89 (t, J = 6.8 Hz, 3H); 100-MHz ^{13}C NMR ($CDCl_3$) 154.5, 152.7, 147.7, 133.2, 128.7, 124.9, 124.3, 123.2, 122.8, 119.9, 118.5, 58.8, 53.2, 50.9, 31.8. 29.5, 29.2. 27.6, 26.9, 22.7, 14.1.

3.5.1.6. Synthesis of 1-(3'-fluoro-4'-nitrophenylazo)-4-(4''-*n*-octylpiperazinyl) benzene, **29**

Scheme 3.7

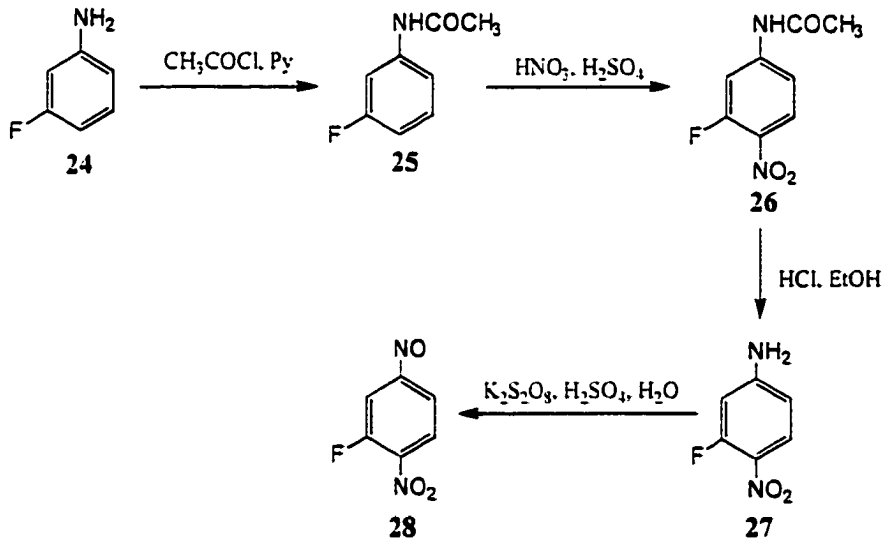

Scheme 3.8

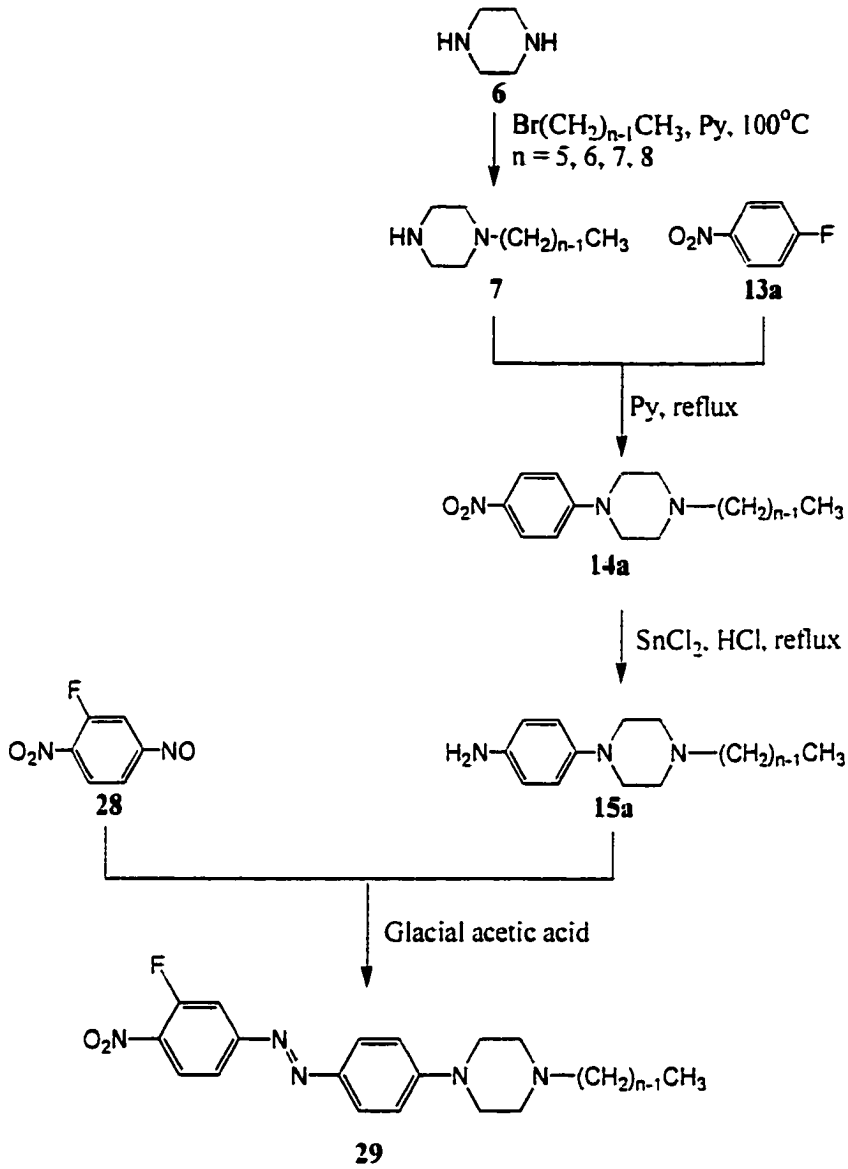

3.5.1.6.1. 3-Fluoroacetanilide, **25**[31]

3-Fluoroaniline **24** (5.02 g, 0.045 mol) was dissolved in about 30 mL pyridine and the mixture was then cooled in an ice bath. Acetyl chloride (4.26 g, 0.054 mol) was dissolved in 1,4-dioxane (15 mL) and the resultant solution was added to the previous mixture dropwise with constant stirring. After completion of addition, the mixture was then heated with a water bath at 60 °C for an hour.

After cooling, the solvents were removed with a rotary evaporator and the residue was dissolved in chloroform and the solution was washed with 10% HCl (30 mL x 2), water (50 mL x 2), Na_2CO_3 solution (30 mL x 2) successively and dried over anhydrous Na_2SO_4. After filtration and distillation of chloroform, white crystals were obtained. The product was used directly in the following step without further purification.

Yield, 4.72 g (68%); white crystals; 400-MHz ^{1}H NMR ($CDCl_3$) 7.66 (br s, 1H); 7.47 (d, J = 11.0 Hz, 1H); 7.23 (m, 1H); 7.13 (d, J = 8.1 Hz, 1H); 6.79 (dt, J = 2.5 Hz, 8.4 Hz); 2.17 (s, 3H).

3.5.1.6.2. 3-Fluoro-4-nitroacetanilide. **26**[31]

A 150 mL round bottom flask was charged with nitric acid (5 mL), and concentrated sulfuric acid (7 mL) was introduced into the flask slowly. The mixture was then cooled with 0 °C water with stirring. 3-Fluoroacetanilide **25** (4.72 g, 0.031 mol) was added to the above mixture in small portions. The resultant mixture was heated in a water bath at 55 °C (not appreciably higher) for 45 minutes. The reaction mixture was poured into a beaker charged with a mixture of water and ice (100 mL) with vigorous stirring and the precipitate was collected and purified by column chromatography using 1:1 hexane/ethyl acetate.

Yield, 1.34 g (22%); yellow crystals; 400-MHz ^{1}H NMR ($CDCl_3$) 8.08 (dd, J = 8.4 Hz, 8.9 Hz, 1H), 7.82 (dd, J = 2.3 Hz, 13.2 Hz, 1H), 7.56 (br s, 1H), 7.22 (ddd, J = 1.2 Hz, 2.3 Hz, 9.0 Hz, 1H), 2.25 (s, 3H); 100-MHz ^{13}C NMR ($CDCl_3$) 127.3, 114.0, 108.2, 24.8 (quaternary carbons missing).

3.5.1.6.3. 3-Fluoro-4-nitroaniline (**27**)

3-Fluoro-4-nitroacetanilide **26** (1.34g, 6.8 mmol) was dissolved in boiling ethanol (5 mL). With the aid of pressure-equalizing dropping funnel, concentrated hydrochloric acid (1 mL) was added into the solution and the mixture was refluxed for another hour. Water (10 mL) was added and the mixture was then subject to distillation under reduced pressure with rotary evaporator. The residue was added with water (20 mL) and the solid was collected and recrystallized from dilute ethanol. Brown crystals **27** were obtained.

Yield. 1.0 g (95%); brown crystals; 400-MHz ^{1}H NMR ($CDCl_3$) 7.98 (dd, J = 7.9 Hz. 8.9 Hz. 1H), 6.43-6.37 (m, 2H), 4.47 (br s. 2H).

3.5.1.6.4. 2-Fluoro-4-nitrosonitrobenzene. **28**

Potassium persulfate (15.0 g, 0.056mol) was added to pre-cooled concentrated sulfuric acid (17.5 mL) with continuous stirring. After the formation of a white paste. ice (150 g) was added. After the ice had completely melted, the pH of the resulting solution was adjusted to 3 with potassium carbonate. The white solid precipitated during the neutralization was filtered off and 3-fluoro-4-nitroaniline **27** (1.0 g, 6.4 mmol) was added to the collected filtrate at room temperature. After stirring for 3 hours, a yellow solid formed in the mixture was filtered off and then purified by silica gel column chromatography using ethyl acetate / hexane (1:200).

Yield: 0.51 g (47%); bright yellow crystals; 400-MHz ^{1}H NMR ($CDCl_3$) 8.44 (dd, J = 2.0 Hz, 4.9 Hz, 1H), 8.04 (ddd, J = 1.2 Hz, 2.0 Hz, 8.8 Hz, 1H), 6.58

(dd, J = 6.4 Hz, 8.8 Hz, 1H); 100-MHz ^{13}C NMR not available due to the low solubility in $CDCl_3$.

3.5.1.6.5. 1-(3'-Fluoro-4'-nitrophenylazo)-4-(4''-*n*-octylpiperazinyl)benzene, **29**

A mixture of 4-(4'-*n*-octylpiperazinyl)aniline **15a** (0.0447 g, 0.155 mmol), 2-fluoro-4-nitrosonitrobenzene **28** (0.0234 g, 0.141 mmol) and glacial acetic acid (5 mL) was stirred at room temperature, and the reaction was monitored by TLC. The solvent was then removed under reduced pressure. The residue was first neutralized with saturated sodium bicarbonate solution and then extracted with ethyl acetate (20 mL x 2). The solvent was then removed and the residue was purified by silica gel column chromatography using ethyl acetate / hexane (1:3) and then recrystallized from a mixture of etheyl acetate and hexanes.

Yield, 0.0617g (99%); red crystals, mp 94-96 °C; MS spectrum: m/z (EI, 12 eV) = 441.2 (40.0); 400-MHz ^1H NMR ($CDCl_3$) 7.67-8.18 (m, 5H), 6.94 (d, J = 9.2 Hz, 2H), 3.46 (t, J = 5.1Hz, 4H), 2.60 (t, J = 5.1 Hz, 4H), 2.39 (t, J = 7.7 Hz, 2H), 1.53 (m, 2H), 1.28-1.31 (br, 10H), 0.885 (t, J = 6.7 Hz, 3H); 100-MHz ^{13}C NMR ($CDCl_3$) 154.2, 145.3, 126.2, 126.1, 119.8, 118.3, 113.7, 112.9, 110.3, 100.02, 58.7, 52.8, 47.2, 31.8, 29.5, 29.2, 27.5, 26.8, 22.7, 14.1.

3.5.1.7. Synthesis of 3-fluoro-1-(3'-fluoro-4'-nitrophenylazo)-4-(4''-*n*-octyl-piperazinyl)benzene, **30**

Scheme 3.9

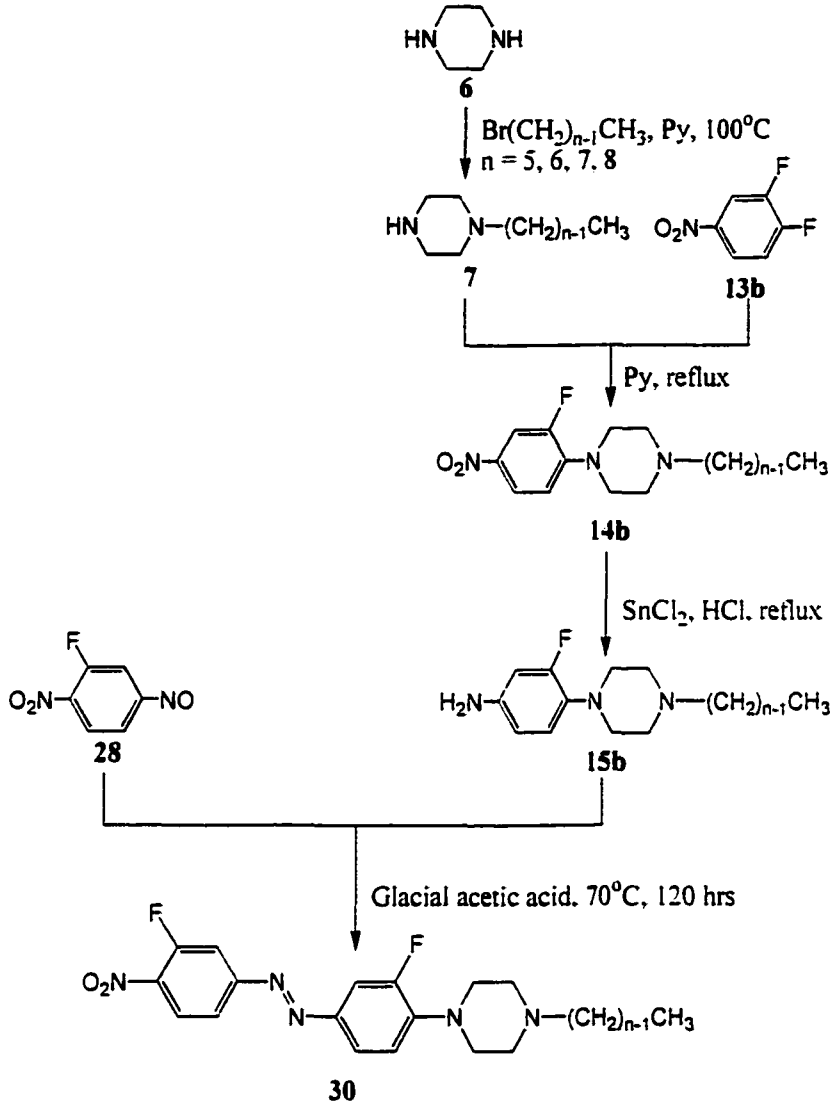

3.5.1.7.1. 3-Fluoro-1-(3'-fluoro-4'-nitrophenylazo)-4-(4''-*n*-octylpiperazinyl)benzene, **30**

A mixture of 3-fluoro-4-(4'-*n*-octylpiperazinyl)aniline **15b** (0.0341 g, 0.11 mmol), 2-fluoro-4-nitrosonitrobenzene **28** (0.0158 g, 0.093 mmol) and glacial acetic acid (5 mL) was heated with a water bath at 70 °C with stirring, and the reaction was monitored by TLC. The solvent was then removed under reduced pressure. The residue was first neutralized with saturated sodium bicarbonate

solution and then extracted with ethyl acetate (20 mL x 2). The solvent was then removed and the residue was purified by silica gel column chromatography using ethyl acetate / hexane (1:3) and then recrystallized from hexanes.

Yield, 0.0363 g (71%); red crystals, mp 76-78 °C; MS spectrum: m/z (EI, 12 eV) = 459.2 (16.9); 400-MHz ^{1}H NMR ($CDCl_3$) 8.08-8.23 (m, 2H), 7.63-7.87 (m, 3H), 6.94 (dt, J = 1.8 Hz, 9.2 Hz, 1H), 3.34 (t, J = 4.8 Hz, 4H), 2.64 (t, J = 4.8 Hz, 4H), 2.41 (t, J = 7.7 Hz, 2H), 1.53 (m, 2H), 1.28-1.31 (br, 10H), 0.89 (t, J = 6.6 Hz, 3H); 100-MHz ^{13}C NMR ($CDCl_3$) 127.0, 124.9, 119.8, 119.6, 118.5, 117.6, 113.3, 113.0, 110.8, 110.6, 108.6, 108.4, 58.8, 53.1, 49.8, 31.8, 29.5, 29.3, 27.6, 26.8, 22.7, 14.1.

3.5.2.Measurement of absorption properties of synthesized liquid crystals

The absorption properties of the synthesized liquid crystals were recorded on a Shimadzu UV-160 UV-vis spectrophotometer. Two solvents were used in the measurement. DMSO was selected when plastic cells were used. When quartz cells were applied, acetonitrile was utilized.

3.5.3. Phase behaviors of the synthesized liquid crystals

The phase transition temperatures were determined using a Perkin Elmer DSC7 differential scanning calorimeter and the nature of phases was checked using an Olympus BH-2 polarizing optical microscope.

3.5.4. Other physical property measurements of synthesized liquid crystals

The dielectric anisotropy and elastic constant ratio measurements were performed on APT III automated LC property tester purchased from Displaytech, Inc.

The birefringence measurements were carried out in a home-built instrument with an optical path shown in Figure 3.11. The light from the lamp is made monochromic by an optical grating (the wavelength of the light can be controlled by a palm-top computer). When it passes through the polarizer, it becomes plane polarized light. The intensity of the light can be modulated by the analyzer and detected by a photodetector. The liquid crystal cell is situated in between the two polarizers. By changing the amplitude of the driving voltage, the retardation can be measured and used to calculate the birefringence. The change of the driving voltage was facilitated by the APT III instrument. The same voltage scanning technique is used in the measurement of dielectric anisotropy and elastic constant ratio. To improve the intensities of the signals, a pair of condenser lenses are put between the polarizer and LC cell and between the cell and the analyzer.

The lamp, monochromator, palm-top computer and photodector were all purchased from CVI instrument group. The polarizer and analyzer (for visible and near-IR) were purchased from Edmund Scientific Co.

The signals from the photodetector are analog signals which are then transformed into digital signals with the help of an A/D converter (obtained from Digi-Key corporation). The data acquisition part uses the parallel port of a PC

computer with the aid of a Quick Basic program. The configuration and principle of its operation can be found in Appendix A.5.

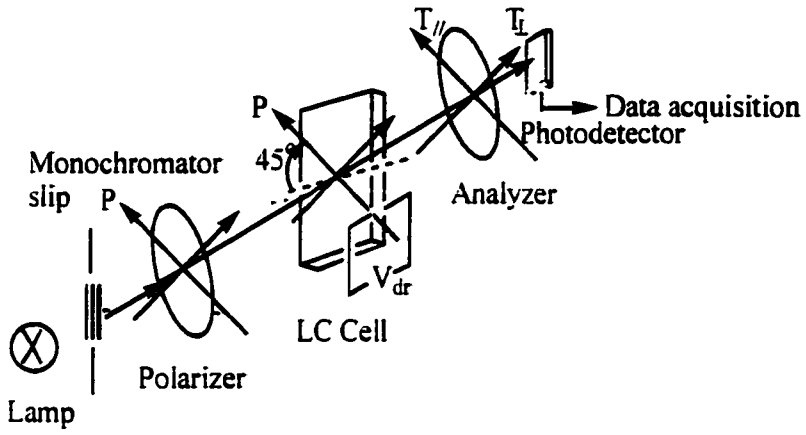

Figure 3.11. Setup for birefringence measurement.

3.6. Results and discussion

Ten series of liquid crystals with push-pull structures were synthesized and studied in this work. In most of the schemes of the synthesis, the diazo linkage was formed by coupling a *para*-substituted nitroso benzene derivative with a suitably substituted aniline. The results of all the measurements are listed in the subsequent sections. The structures of most of the synthesized liquid crystals has the general formula as **VI.** and two other series have the structure **VII.**

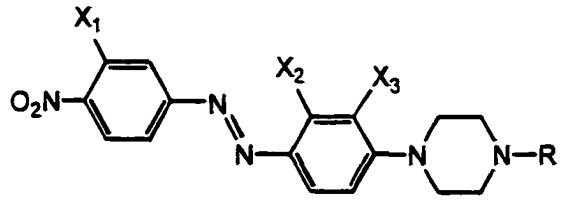

VI

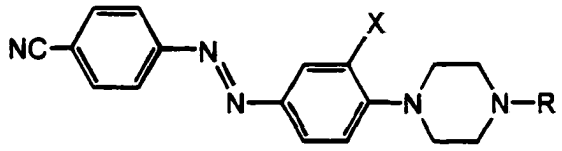

VII

3.6.1. Phase behavior

As expected, the presence of lateral substituents depresses the melting point and the clearing point of all the liquid crystals because lateral substitution interferes with the packing of molecules in crystalline and liquid crystalline phases. The position of substitution is important in affecting the phase transition temperatures. When the substituents are *ortho* to the piperazine ring, the liquid crystals have lower melting points but higher clearing points. namely broader liquid crystalline ranges, than the corresponding *meta*-substituted liquid crystals. It can be found that when the substituent is located *meta* to the piperazine ring, the group is more shielded by other part of the molecule and its steric effect on the melting points is less obvious (compared to corresponding *ortho*-compounds). In the *meta*-fluorinated case (compound *), although the steric effect is somewhat shielded, intermolecular interactions are sufficient to cause smectic arrangements.

Table 3.1. Phase transition temperatures of the liquid crystals substituted with different groups on the central ring.

Compound	X_2	X_3	n	K	S	N	I
16a	H	H	5	-	148.2	194.8	
			6	-	147.5	227.0	
			7	-	145.1	230.9	
			8	-	128.4	229.2	
16b	H	F	5	-	98.6	194.2	
			6	-	81.2	183.0	
			7	-	91.9	180.7	
			8	93.0	168.8	184.7	
16d	H	Cl	5	-	91.3	154.4	
			6	-	76.9	146.7	
			7	-	74.0	148.6	
			8	-	57.6	135.1	
16c	H	CH_3	5	-	117.0	165.8	
			6	-	86.7	154.9	
			7	-	83.8	151.0	
			8	-	87.7	149.0	
*	F	H	5	103.2	131.8	190.3	
			6	82.9	154.4	184.2	
			7	88.4	164.7	181.0	
			8	81.8	175.8	181.2	
19	Cl	H	5	-	91.5	139.8	
			6	-	84.2	127.5	
			7	-	93.0	120.7	
			8	-	77.7	128.3	
12	CH_3	H	5	-	124.5	146.8	
			6	-	108.0	146.3	
			7	-	102.3	131.2	
			8	-	109.8	132.6	

* This series of compounds were synthesized by Wing Shun Cheung, a postdoc in our laboratory.

For substituents on the *ortho* (X_3) position, the extent of melting point depression (compared to the non-substituted compound, **16a**) is Cl > CH_3 > F, while the extent of clearing point depression is CH_3 > Cl > F. For substituents on the *meta* position (X_2), the extent of melting ponit depression (compared with **16a**) is F > Cl > CH_3, while the extent of clearing point depression is Cl > CH_3 > F. Melting points are mainly determined by the packing of molecules as well as intermolecular interactions in the solid lattice; therefore, the melting point depression is a combinative effect of polar and steric factors.

The effect of fluorine substitution at different positions are shown in Table 3.2. Regardless of the position of substitution, all fluorinated compounds with a pentyl chain have wider mesomorphic ranges than the parent compound (**16a**). Substitution at the position *ortho* to the piperazine ring (**16b**, **16c**, **16d**) has the most significant influence on the melting point depression of the liquid crystals. Substitution at other positions (* and **29**) has less effect, plus another disadvantage of inducing the formation of a S_A phase. However, when another fluorine atom is introduced into compound **29**, the disruption of the lamellar arrangement can be visualized again (compound **30**). This is in accordance with the observation that the incorporation of the second fluorine atom does not guarantee an enhancement of smectic phases.[40] From other physical measurements to be discussed later, it appears that the introduction of a fluorine atom onto the position *ortho* to the nitro groups is a rather promising method to obtain liquid crystals with large birefringence and lower melting points. If the electron-withdrawing group like fluorine neighboring to the nitro group is a must

for good physical properties, larger groups can be incorporated in the X_3 position in structure **VI** to further lower the melting points of the liquid crystals.

Table 3.2. Phase transition temperatures of liquid crystals **VI** with fluorination at different positions.

Compound	X_1	X_2	X_3	n	K	S	N	I
16a	H	H	H	5	-		148.2	194.8
				6	-		147.5	227.0
				7	-		145.1	230.9
				8	-		128.4	229.2
16b	H	H	F	5	-		98.6	194.2
				6	-		81.2	183.0
				7	-		91.9	180.7
				8	93.0		168.8	184.7
*	H	F	H	5	103.2		131.8	190.3
				6	82.9		154.4	184.2
				7	88.4		164.7	181.0
				8	81.8		175.8	181.2
29	F	H	H	5	109.8		154.1	183.2
				6	99.0		158.8	182.9
				7	94.0		169.8	182.8
				8	94.8		175.5	180.8
30	F	H	F	5	-		69.9	160.6
				6	-		75.4	150.6
				7	-		88.8	152.1
				8	76.0		138.0	150.0

For the three liquid crystals with a cyano group (**22** and **23**, n = 7, 8), their phase transition temperatures are listed in Table 3.3. For the sake of comparison, their nitro analogs (**16d** and **16b**) are also listed. The results show that, although all the cyano liquid crystals have higher nematic stability than their nitro analogs, the change of the terminal group has an ambiguous effect on the liquid crystal system. For instance, **22** has lower melting point than **16b** (n = 8), but **23** has higher melting points than corresponding **16d**. This really makes the study much more complicated, so the investigation of effect of end groups was not further pursued.

Table 3.3. Phase transition temperatures of three cyano liquid crystals **VII** (**22**, X = F; **23**, X = Cl) and their nitro analogs **VI** (**16b**, $X_1 = X_2 = H$, $X_3 = F$; **16d**, $X_1 = X_2 = H$, $X_3 = Cl$).

Compound	n	K	S	N	I
22	8	-		79.0	192.1
23	7	-		106.2	157.1
23	8	-		76.5	167.5
16b	8	93.0		168.8	184.7
16d	7	-		74.0	148.6
16d	8	-		57.6	135.1

3.6.2. UV-vis absorption

The λ_{max} values of the nitro compounds in DMSO solutions are listed in Table 3.4. The data show that the substituents have considerable effect on the optical absorption of the liquid crystals. For compounds with only one substituent on the central aromatic ring, the values of λ_{max} for *meta* substitution (with respect to the piperazine ring) increase compared with the parent liquid crystals (**16a**) and the bathochromic effect is CH_3 > Cl > F. When the substituents are situated *ortho* to the piperazine ring, the values of λ_{max} decrease and the hypsochromic effect is CH_3 < Cl < F. The presence of a fluorine atom at the X_1 position increases the λ_{max} values of corresponding compounds (from 480 nm in **16a** to 493 nm in **29** and from 435 nm in **16b** to 448 nm in **30**).

Table 3.4. λ_{max} values of liquid crystals **VI** in DMSO.

	16a	**12**	**19**	*	**16c**	**16d**	**16b**	**29**	**30**
X_1	H	H	H	H	H	H	H	F	F
X_2	H	CH_3	Cl	F	H	H	H	H	H
X_3	H	H	H	H	CH_3	Cl	F	H	F
λ_{max} / nm	480	493	483	482	406	418	435	493	448

These results can be explained as follows. Because the piperazine ring prefers a chair conformation, the nitrogen atom directly bonded onto the phenyl ring cannot adopt sp^2 hybridization, but the conjugative stabilization will force the ring to adopt a conformation to allow partial overlapping of the lone pair on the nitrogen atom with the π electrons on the phenyl ring. The presence of a lateral

substituent on the *ortho* position (**16c**, **16d** and **16b**) would invoke strong steric interactions between the substituent and the piperazine ring, which would force the ring to rotate along the N-C bond connecting the piperazine ring to the phenyl ring to relieve the steric repulsion. This would diminish the conjugation of the system, causing a broadening of the energy gap between n and π^* orbitals and results in an increase of the $n \rightarrow \pi^*$ excitation energy. An increase in the size of the substituent would increase the magnitude of steric interaction, so the hypsochromic effect shows the trend $CH_3 > Cl > F$.

When the substituents are neighboring the azo linkage (*meta* to the piperazine ring; **12**, **19**, and *), an opposite trend is observed. The steric interaction may force the 4-nitrophenyldiazene moiety to rotate away from the coplanar conformation with respect to the central phenyl ring. Quantum mechanical calculations by Forber[41] *et al.* showed that there is a strong anti-bonding interaction between the substituents and the azo linkage. It increases the energy of the n orbital on the nitrogen,[41,42] thus lowering the energy of the $n \rightarrow \pi^*$ transition. Basically the effect of the substituent at the *meta* position with respect to the piperazine ring is due to the steric factor, but it must also have an electronic component. This is manifested by the fact that the λ_{max} values for **16a**, **19**, and * are almost the same in spite of the large differences in the sizes of H, Cl, and F. Thus, the electronic interaction works against the steric factor in these compounds. Our other work[40] to incorporate a second fluorine atom onto the other ortho position of the piperazine ring caused the λ_{max} to decrease from 483 nm to 448 nm (not listed in Table 3.4).

A comparison of the difference of λ_{max} values of the non-substituted and corresponding substituted compounds suggests that the deconjugation perturbance is larger in magnitude than the perturbance of the increasing energy level of the nitrogen atom in the azo linkage. For example, the difference between **12** and **16a** is only 13 nm, while that between **16c** and **16a** is -74 nm.

The fluorine neighboring the nitro group also has bathochromic effect. This effect can be ascribed as resulting from the fluorine atom, a strong electron-withdrawing group, which together with the nitro group can make better conjugation in this push-pull system than a single nitro functionality. Interestingly enough, the increments from **16a** to **29** and from **16b** to **30** are both 13 nm.

DMSO is not a commonly used solvent for UV-vis measurements. It was chosen because other solvents dissolve plastic sample cells that were used in the initial study. To obtain better UV-vis spectra and precisely obtain the molar extinction coefficients, acetonitrile, which has a cut-off wavelength of 210 nm. was chosen as a solvent later, and quartz cells were used in the measurements. The data are listed in Table 3.5.

Table 3.5. λ_{max} and logε values for liquid crystals **VI** in acetonitrile.

	16a	**12**	**19**	*	**16c**	**16d**	**16b**	**29**	**30**
X_1	H	H	H	H	H	H	H	F	F
X_2	H	CH_3	Cl	F	H	H	H	H	H
X_3	H	H	H	H	CH_3	Cl	F	H	F
λ_{max} / nm	456	455	465	453	413	406	392	474	434
logε	4.36	4.40	4.60	4.47	4.29	4.08	4.41	4.41	4.37

It is widely accepted that λ_{max} values change with the solvents.[43] However, it is rather surprising that the trend of wavelength change with the substituents is also solvent dependent. Careful comparison between the data in Tables 3.4 and 3.5 shows that the case is really complicated. When the substituent is *ortho* to the piperazine ring (**16c, 16d, 16b**), the trends in acetonitrile and DMSO are just the opposite. When the substituent is *meta* to the piperazine (*ortho* to the diazo linkage), only the chloro group increases the λ_{max} value; methyl and fluoro substitution actually slightly decrease the λ_{amx} values. In this case it can be concluded that the electronic effect plays a much more important role than in the DMSO case. In the extreme case (**16c, 16d. 16b**, *ortho*-substitution to the piperazine ring), electronic effect can completely dominate over the steric one and invert the trend of the wavelength change.

It should be kept in mind that the fluoro group neighboring the piperazine ring substantially decreases the λ_{max} of the liquid crystal. However, the fluorine atom neighboring the nitro group on the outer aromatic ring increases the λ_{max} value (from 456 nm of **16a** to 474 nm of **29,** and from 392 nm of **16b** to 434 nm of **30**). This can only be attributed to the better delocalization of electrons of the whole conjugation system due to the help of the fluorine atom. In other words, the newly introduced fluorine atom makes a better push-pull system.

3.6.3. Dielectric anisotropy

The measurement of dielectric anisotropy must be made in the liquid crystalline phase. However, none of the synthesized liquid crystals has liquid

crystalline phase at room temperature. To measure the genuine dielectric anisotropy of the pure liquid crystal samples, a hot stage with precise temperature control compatible with the LC cells used in the APT III automated LC property tester would be necessary. However, in practical applications, LCDs are operated at ambient temperatures.

To avoid this problem, the dielectric anisotropy measurements were made by dissolving the LC samples in E7, a commercially available liquid crystal mixture, to form 10 wt% "solutions". E7 is a mixture of cyano biphenyls and terphenyls; it has a large nematic range, and is widely used as a standard for electro-optic studies of liquid crystals at room temperature. The results of these liquid crystal mixtures are summarized below in Table 3.6.

From physics, the dielectric constant ε of a mixture of two substances (with dielectric constants, ε_1 and ε_2, respectively) can be related to ε_1 and ε_2 by the following relation.

$$\varepsilon = x_1 \varepsilon_1 + x_2 \varepsilon_2 \qquad (3.23)$$

where X_1 and X_2 are the mole fraction of the two components. At low frequency, for liquid crystal mixtures, the same relation can be applied to the case of parallel and perpendicular components. However, in our measurement, the applied frequency is 1.0 kHz, and this relation does not strictly hold. Although calculations cannot be carried out, Eq.3.23 can still be used to estimate the properties of pure LC materials.

The data in Table 3.6 show that only samples **19**, * and **16c** have larger dielectric anisotropy than that of E7. However, as discussed in the introduction

part of this chapter, it is the ratio of $\Delta\varepsilon/\varepsilon_{\perp}$ that really affects the switching time of liquid crystals.[9] Therefore, the most promising sample seems to be compound **30** because this compound has smaller value of $\varepsilon_{//}$ but larger $\varepsilon_{\perp}$ than those of E7 and consequently a smaller value of $\Delta\varepsilon/\varepsilon_{\perp}$. It is worth to note that the data listed in the table are the data for the 10 wt% LC mixtures in E7. The molecular weights of the synthesized liquid crystals are larger than those of different components of E7, so the molar ratios are actually smaller than 10%. Pure **30** should have smaller $\varepsilon_{//}$ and larger $\varepsilon_{\perp}$ than the data listed in Table 3.6 and the $\Delta\varepsilon/\varepsilon_{\perp}$ for pure **30** should be even smaller.

Table 3.6. Dielectric anisotropy of 10% liquid crystals in E7.

compound	n	$\varepsilon_{//}$	$\varepsilon_{\perp}$	$\Delta\varepsilon$	$\Delta\varepsilon/\varepsilon_{\perp}$
E7		18.39	5.33	13.06	2.45
16a	8	17.56	4.75	12.81	2.69
12	8	19.26	5.10	14.16	2.78
19	8	18.30	5.04	13.26	2.63
*	8	22.33	6.05	16.28	2.69
16c	8	18.64	5.00	13.64	2.73
16d	8	17.74	4.99	12.76	2.56
16b	8	17.07	4.78	12.29	2.57
29	8	17.42	4.87	12.55	2.58
30	8	18.26	6.15	12.11	1.97

3.6.4. Elastic constant ratio

Table 3.7. Elastic constant ratio and threshold voltage of 10 wt% LC mixtures.

compound	n	d (μm)	K_{33}/K_{11}	V_{th} (V)
E7		3.83	1.05	1.55
16a	8	3.72	1.34	1.51
12	8	3.91	1.18	1.43
19	8	3.92	1.18	1.39
*	8	3.57	1.16	1.51
16c	8	4.47	1.22	1.47
16d	8	3.43	1.16	1.39
16b	8	3.47	1.14	1.51
29	8	3.34	1.12	1.51
30	8	2.56	1.06	2.25

These data are for 10 wt% LC mixture in E7. Practical LCDs require materials with low elastic constant ratio K_{33}/K_{11} and this property is determined by each component of the mixture and the interactions between them. The concentrations of the synthesized LCs are low, and the values are all very close to that of E7. They indicate that mixing the LC samples does not substantially deteriorate the elastic property of the LC mixture except for **16a**.

3.6.5. Birefringence

Birefringence measurements were performed at 633 nm (visible range) and 1050 nm (near-IR range). The samples are the same as those in the other physical property measurement. The data are summarized in Table 3.8.

Table 3.8. Birefringence of liquid crystal mixtures at two wavelengths.

Compound	n	10% LC mixture		Pure compounds	
		Δn(633)	Δn(1050)	Δn(633)	Δn(1050)
E7		0.213	0.203	0.213	0.203
16a	8	0.257	0.221	0.653	0.383
12	8	0.257	0.220	0.653	0.373
19	8	0.256	0.224	0.643	0.413
*	8	0.217	0.200	0.253	0.173
16c	8	0.243	0.220	0.513	0.373
16d	8	0.242	0.217	0.503	0.343
16b	8	0.251	0.226	0.593	0.433
29	8	0.266	0.230	0.743	0.473
30	8	0.277	0.236	0.853	0.533

For most of synthesized samples, with molar percentage lower than 10%, the obtained birefringence is already substantially higher than that for E7. For a mixture, the observed birefringence is related to the Δn_i values of the components by Eq. 3.24

$$\Delta n \approx P_1 \Delta n_1 + P_2 \Delta n_2 \qquad (3.24)$$

where P_1 and P_2 are the weight percentage of the components 1 and 2, respectively. Using the values of E7, extrapolations to the pure liquid crystals were made and the results are also listed in Table 3.8. These extrapolation values were used to estimate the birefringence for pure LCs with structure **VI**. It can be seen that except for compound *, the resulted birefringence values are very high for all the synthesized liquid crystals. The main error is not from the measurement procedure itself but weighing the mass of the compounds in the preparation of LC mixtures. Because of the high price of E7, only 45 mg and 5 mg of the synthesized compounds were used to make each mixture.

3.6.6. Rise time

The sample cells for this measurement have alignment films arranged perpendicular to each other. In other words, this measurement is just like the practical operation of TN LCDs. The measurement of rise time was performed using a 5.0 V driving voltage and 1060 nm monochromic light. After the application of the driving voltage, the transmittance change with time was recorded using a photodetector and the results are summarized in Table 3.9. In this table. 100-10% stands for the transmittance change from 100 to 10% and the time is in ms unit.

From this table, all the TN cells have rise time of the same magnitude. Although it is not suitable to compare the trend of rise time change with the substituents. it can still be concluded that all these liquid crystals are good candidates for potential IR applications. It was pointed out in 3.6.3. that **30** has the

smallest $\Delta\varepsilon/\varepsilon_{\perp}$ value, which favors a fast response. This is indeed the case, but **12** and **16c** also have the same rise time. Obviously, other factors such as viscosity must also be taken into account.

Table 3.9. Rise time of 10 wt% LC mixtures in E7.

Compound	d (μm)	100-10%
E7	3.25	13.5
16a	3.77	22
12	3.18	17.0
19	3.77	23.7
16c	3.65	17.0
16d	3.72	22.0
16b	4.29	20.2
29	3.99	23.7
30	3.52	17.0

3.7. Conclusion

The syntheses of eight series of liquid crystals carrying push-pull groups, with four homologs in each series, were carried out in this work. The effects of the substituents on the phase behavior, phase transition temperatures, optical absorption, dielectric anisotropy, elastic constant ratio and birefringence were studied.

The presence of lateral substitution depresses both melting and clearing points of the liquid crystals. Compounds with *ortho*-substitution (with respect to the piperazine ring) have broader nematic ranges than the corresponding *meta*-substituted ones. For optical properties, in DMSO, *ortho*-substitution causes red shift, while *meta*-substitution causes blue shifts. This effect originates from the steric and electronic interactions between the substituents and certain segments of the liquid crystals. This trend is solvent dependent and in acetonitrile, only *meta*-chlorination causes a red shift. Surprisingly, in DMSO and acetonitrile, *ortho* substitution has exactly the opposite trends in the λ_{max} change with respect to the parent compound.

All the liquid crystals synthesized in this study have relatively large values of birefringence. However, the dielectric anisotropy values were much lower than expected.

The incorporation of a fluorine atom onto the position neighboring the nitro group can enhance the conjugation of the push-pull system, as a result, liquid crystals with better physical properties (large birefringence, small $\Delta\varepsilon/\varepsilon_{\perp}$ ratio) can be obtained. This can then be combined with other substituents on the position ortho to the piperazine ring, and hopefully liquid crystals with both good properties and rather low melting points can be achieved. This information can be taken further advantage to guide the design and modification of liquid crystals with similar structures.

3.8. References

1. Flannery, R. E. and Miller, J. E., *Proceedings of SPIE Infrared Image Systems: Design, Analysis, Modeling, and Testing III*, **1992**, 379.
2. Joffre, P., Illiaquer, G. and Huignard, J. P., *SPIE Proceedings*, **1989**, *1126*, 13.
3. West, J. L., Doane, J. W., Domingo, Z. and Ukleja, P., *Polym. Prepr.*, **1989**, *30*, 531.
4. Shi, Y., *SPIE Proceedings*, **1990**, *1230*, 58.
5. Sharp, R. C., Resler, D. P., Hobbs, D. S. and Dorschner, T. A., *Opt. Lett.*, **1990**, *15*, 87.
6. McCarger, W., Ondris-Crawford, R. and West, J. L., *J. Electronic Imaging*, **1992**, *1*, 22.
7. Moore, A. D., *Electrostatics and Its Applications* (John Wiley & Sons), **1973**, p 26.
8. Polh, L., *Liquid Crystals, Applications and Uses* (World Scientific), ed. by Birendra Bahadur, **1990**, *Vol. 1*, p 140.
9. Collings, P. J. and Hird, M., *Introduction to Liquid Crystals* (Taylor & Francis), **1997**, p 273.
10. Klein, M. V., *Optics* (John Wiley & Sons), **1970**, p 496.
11. Khoo, I. and Wu, S.-T., *Optics and Nonlinear Optics of Liquid Crystals* (World Scientific), **1993**, p 107.
12. Frank, F. C., *Disc. Faraday Soc.*, **1958**, *59*, 958.
13. Uchida, T. and Takahashi, Y., *Mol. Cryst. Liq. Cryst.*, **1981**, *72*, 133.
14. Gruler, H., Scheffer, T. J. and Meizer, G., *Z. Naturforsh.*, **1972**, *72a*, 966.

15. Coats, D., *Liquid Crystals, Applications and Uses* (World Scientific), ed. by Birendra Bahadur, **1990**, *Vol. 1*, p 92.

16. Hrid, M. and Toyne, K. J., *Mol. Cryst. Liq. Cryst.*, **1998**, *323*, 1.

17. Viney, C., Russell, T. P., Depero, L. E. and Twieg, R. J., *Mol. Cryst. Liq. Cyst.*, **1989**, *168*, 63.

18. Schubert, H. and Zaschke, H. J., *J. Prakt. Chem.*, **1970**, *312*, 494.

19. Haramoto, Y. and Kamogawa, H., *Chem. Lett.*, **1985**, 79.

20. Scadt, M., Buchecker, R., Leenhouts, F., Boller, A., Nilleger, A. and Petrzilka, M., *Mol. Cryst. Liq. Cryst.*, **1986**, *139*, 1.

21. Coates, D., *Liq. Cryst.*, **1987**, *2*, 63.

22. Gray, G. W., Harrison, K. J. and Nash, J. A., *Electron Lett.*, **1973**, *9*, 130.

23. de Jeu, W. H., *Philos. Trans. R. Soc. London. A*, **1983**, *309*, 217.

24. Weissflog, W. and Demus, D., *Mol. Cryst. Liq. Cryst.*, **1985**, *129*, 235.

25. Wu, S. T., Margerum, J. D., Ho, M.-S. and Fung, B. M., *Appl. Phys. Lett.*, **1994**, *64*, 2191.

26. Wu, S. T., Ho, M.-S. and Fung, B. M., *Mol. Cryst. Liq. Cryst.*, **1995**, *261*, 79.

27. Wu, S. T., Sherman, C. S., Margerum, J. D., Funkhouser, K. and Fung, B. M., *Asia Display*, **1995**, 567.

28. Osman, M. A., *Mol. Cryst. Liq. Cryst.*, **1985**, *128*, 45.

29. Bui, E., Bayle, J. P., Perez, P., Libert, L. and Courtieu, J., *Liq. Cryst.*, **1990**, *8*, 513.

30. Tong, T.-H. and Fung, B. M., *Liq. Cryst.*, **1997**, *23*, 883.

31. Furniss, B. S., Hannaford, A. J., Smith, P. W. and Tatchell, A. R., *Vogel's Textbook of Practical Organic Chemistry* (Longman), Fifth Edition, **1991**, p 918.

32. Kiritsy, J. A. and Yung, D. K., *J. Med. Chem.*, **1978**, *21*, 1301.

33. Bellamy, F. D. and Ou, K., *Tetrahedron Lett.*, **1984**, *25*, 839.

34. Dankwardt, S. M., Newman, S. R. and Krstenansky, J. L., *Tetrahedron Lett.*, **1995**, *36*, 4923.

35. Huang, S.-L. and Swern, D., *J. Org. Chem.*, **1979**, *44*, 2510.

36. Fieser, M., and Fieser, L. F., *Reagents for Organic Synthesis* (John Wiley & Sons), **1977**, *6*, 97.

37. Matsui, M., Tanka, N., Nakaya, K., Funabiki, K., Shibata, K., Muramatsu, H., Abe, Y. and Kaneko, M., *Liq. Cryst.*, **1997**, *23*, 217.

38. March, J., *Advanced Organic Chemistry, Reactions, Mechanisms and Structures* (John Wiley & Sons), Third Edition, **1985**, p 581.

39. Lindley, J., *Tetrahedron*, **1984**, *40*, 1433.

40. Sun, H., Cheung, W. S. and Fung, B. M., *Liq. Cryst.* (in press).

41. Forber, C. L., Kelusky, E. C., Bunce, N. J. and Zerner, M. C., *J. Am. Chem. Soc.*, **1985**, *107*, 5884.

42. Kobayashi, S., Yokoyama, H. and Kamei, H., *Tetrahedron*, **1987**, *138*, 333.

43. Crews, P., Rodriguez, J. and Jaspars, M., *Organic Structure Analysis* (Oxford University Press), **1997**, p 396.

Appendices

A.1. Least-squares fitting of the two phenyl rings in 7CPB

Table A.1.1. Least-squares fitting for Ring 1 (phenyl ring with heptyl chain) of 7CPB.

T/°C	1st simulation				2nd Simulation	
	$\angle H_2\text{-}C_2\text{-}C_3$	$\angle H_3\text{-}C_3\text{-}C_2$	S_{zz}	$S_{xx} - S_{yy}$	S_{zz}	$S_{xx} - S_{yy}$
25.0	120.34°	119.88°	0.662	0.0354	0.662	0.0365
30.0	120.11°	119.51°	0.637	0.0474	0.636	0.0372
35.0	120.63°	120.00°	0.595	0.0278	0.597	0.0366
39.0	120.30°	119.85°	0.576	0.378	0.575	0.0376
Average	120.34°	119.81°				

Table A.1.2. Least-squares fitting for Ring 2 (phenyl ring with cyano group) of 7CPB.

T/°C	1st simulation				2nd Simulation	
	$\angle H_2'\text{-}C_2'\text{-}C_3'$	$\angle H_3'\text{-}C_3'\text{-}C_2'$	S_{zz}	$S_{xx} - S_{yy}$	S_{zz}	$S_{xx} - S_{yy}$
25.0	121.49°	120.99°	0.699	0.0129	0.704	0.0470
30.0	120.50°	119.30°	0.687	0.0857	0.685	0.0639
35.0	120.85°	119.73°	0.654	0.0717	0.655	0.0658
39.0	120.48°	120.30°	0.643	0.940	0.631	0.0890
Average	120.83°	120.08°				

In the first fitting, 1-bond and 2-bond dipolar coupling constants were used (6-component fitting). The average values of angles were used in second fitting.

A.2. Linear correlation between order parameters and chemical shift anisotropy

Table A. 2.1. Data for the correlation of order parameters and chemical shift anisotropy for Ring 1.

T/°C	S_{zz}	Δδ /ppm			
		C1	C2	C3	C4
25.0	0.662	59.36	29.28	24.88	54.46
30.0	0.636	57.61	28.50	24.20	53.31
35.0	0.597	55.25	27.43	23.32	51.75
39.0	0.575	52.62	26.14	22.21	49.76

Table A. 2.2. Data for the correlation of order parameters and chemical shift anisotropy for Ring 2.

T/°C	S_{zz}	Δδ /ppm			
		C1'	C2'	C3'	C4'
25.0	0.704	59.36	28.64	31.08	68.08
30.0	0.685	57.66	27.87	30.20	66.08
35.0	0.655	55.27	26.84	29.08	63.37
39.0	0.631	52.33	25.60	27.70	60.09

In the actual plotting (Figures 2.6-2.13), the z denotation was dropped and as a result. S_{zz} became S.

Table A. 2.3. Data for the correlation of order parameters and chemical shift anisotropy for aliphatic carbons.

T/°C	Cα		Cβ		Cγ		Cδ	
	S	Δδ	S	Δδ	S	Δδ	S	Δδ
25.0	-0.242	-10.21	-0.188	-7.80	–0.199	–7.05	-0.173	-7.19
30.0	-0.237	-9.79	-0.177	-7.43	–0.193	–6.63	-0.161	-6.71
35.0	-0.225	-9.38	-0.166	-7.04	–0.180	–6.25	-0.150	-6.27
39.0	-0.215	-8.92	-0.152	-6.59	–0.166	–5.81	-0.139	-5.74

T/°C	Cε		Cζ		Cω	
	S	Δδ	S	Δδ	S	Δδ
25.0	-0.176	-8.09	-0.128	-2.45	-0.073	-3.20
30.0	-0.166	-7.60	-0.120	-2.31	-0.068	-2.92
35.0	-0.156	-7.05	-0.111	-2.16	-0.063	-2.69
39.0	-0.143	-6.42	-0.101	-2.01	-0.058	-2.46

A.3. Haller fitting of aromatic carbons in 7CPB

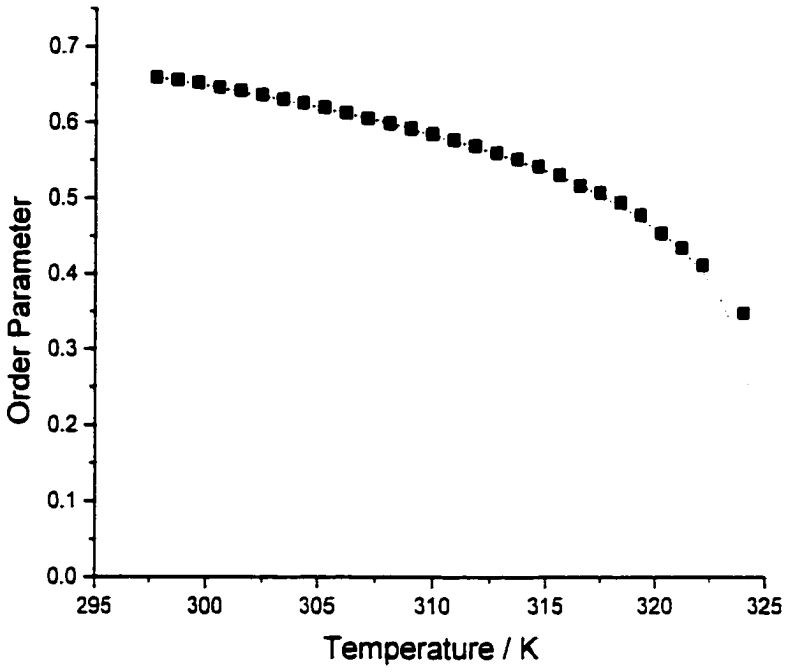

Figure A.3.1. First fitting of the temperature dependence of the order parameter of C1 in 7CPB.

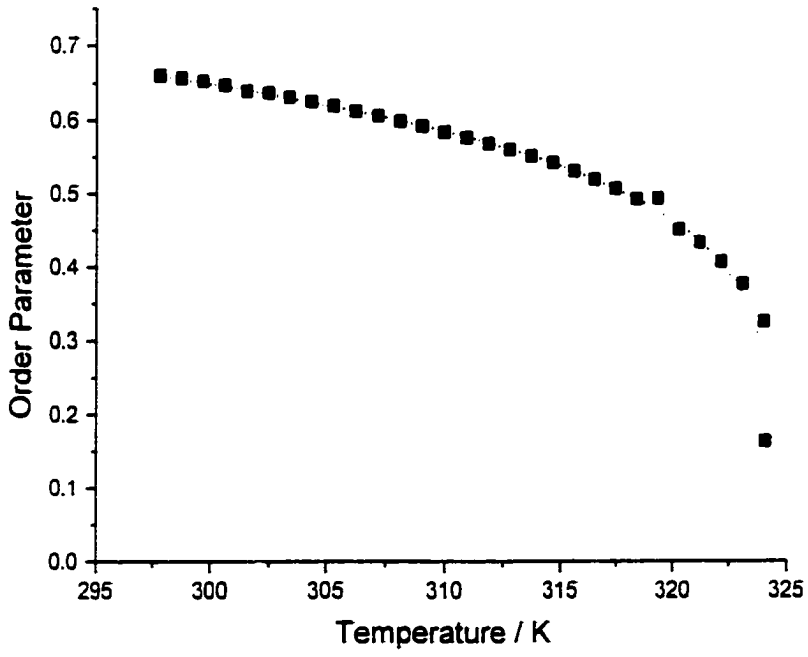

Figure A.3.2. First fitting of the temperature dependence of the order parameter of C2 in 7CPB.

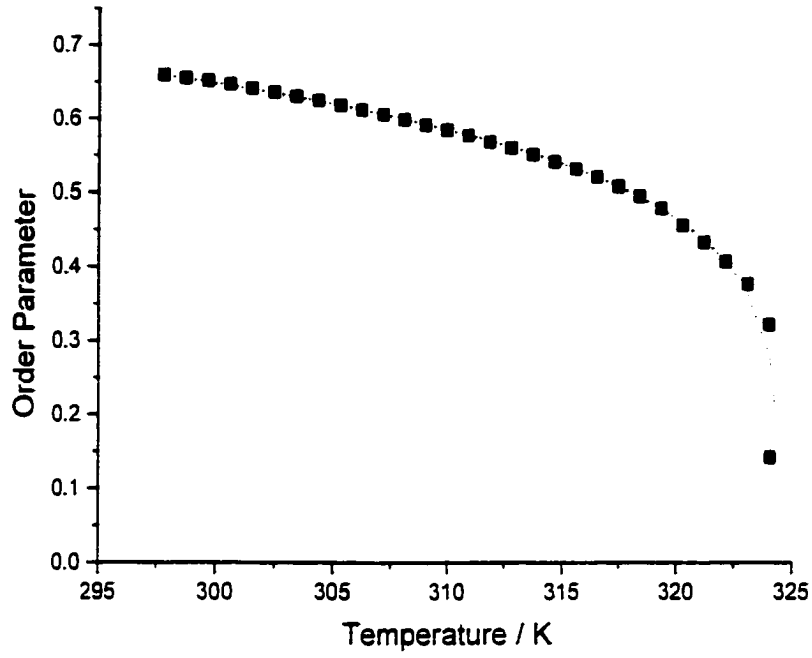

Figure A.3.3. First fitting of the temperature dependence of the order parameter of C3 in 7CPB.

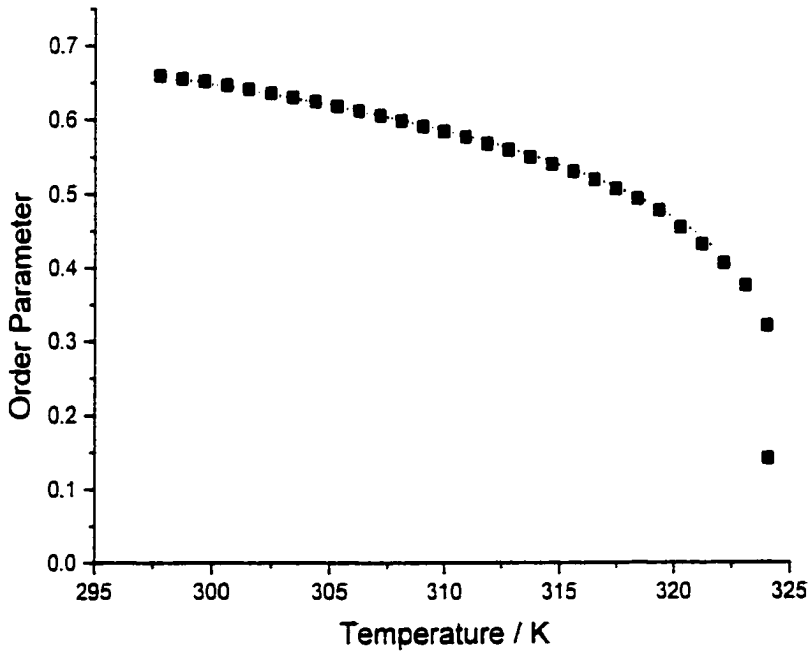

Figure A.3.4. First fitting of the temperature dependence of the order parameter of C4 in 7CPB.

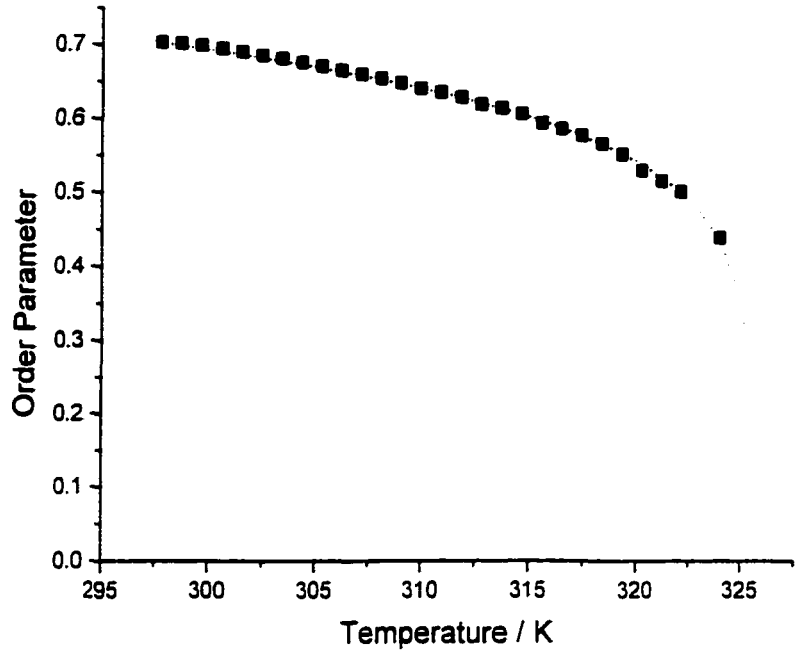

Figure A.3.5. First fitting of the temperature dependence of the order parameter of C1' in 7CPB.

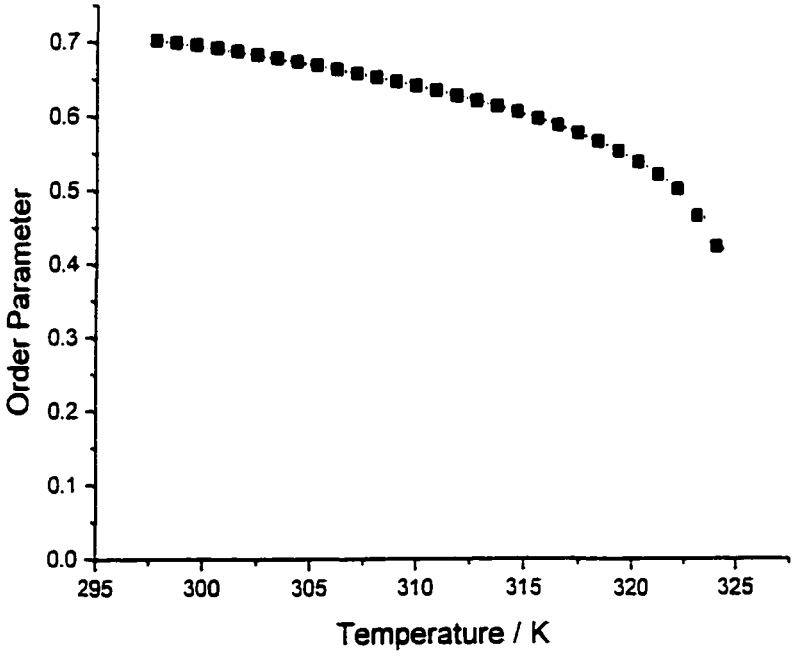

Figure A.3.6. First fitting of the temperature dependence of the order parameter of C2' in 7CPB.

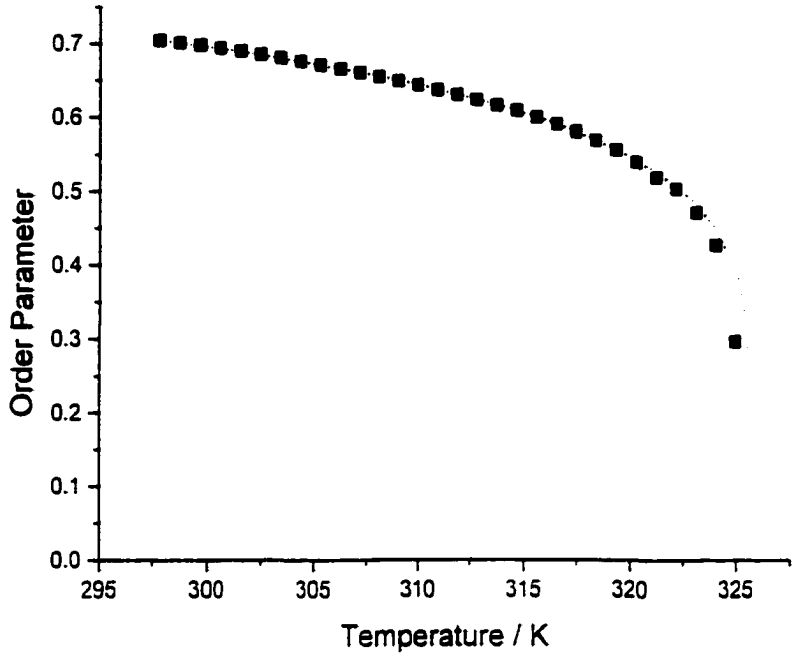

Figure A.3.7. First fitting of the temperature dependence of the order parameter of C3' in 7CPB.

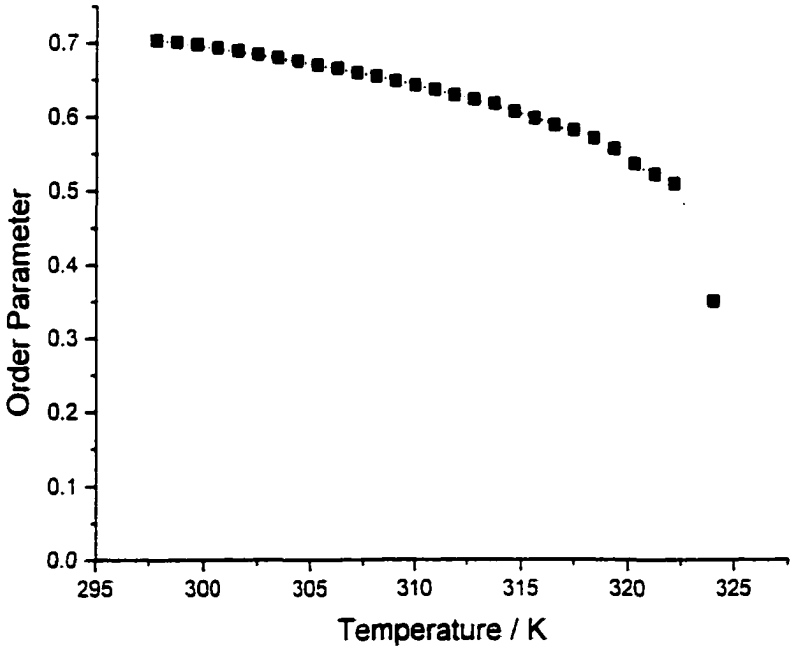

Figure A.3.8. First fitting of the temperature dependence of the order parameter of C4' in 7CPB.

The above fittings were carried out by using S_0, F and T* as three variables and the results were summarized in Tables A.3.1. and A.3.2.

Table A.3.1. S_0, F and T* from the first Haller fitting of aromatic carbons of Ring 1 of 7CPB.

Carbon	S_0	F	T*
C1	1.091	0.201	324.46
C2	1.074	0.195	324.38
C3	1.072	0.194	324.34
C4	1.008	0.194	323.79

Table A.3.2. S_0, F and T* from the first Haller fitting of aromatic carbons of Ring 2 of 7CPB.

Carbon	S_0	F	T*
C1'	1.036	0.158	325.39
C2'	1.036	0.158	325.52
C3'	1.042	0.159	325.68
C4'	1.028	0.153	324.93

The average value of T* was then used as a fixed parameter. The second fitting was then performed by treating S_0, F as two variables.The parameters thus obtained were summarized in Tables A.3.3. and A.3.4.

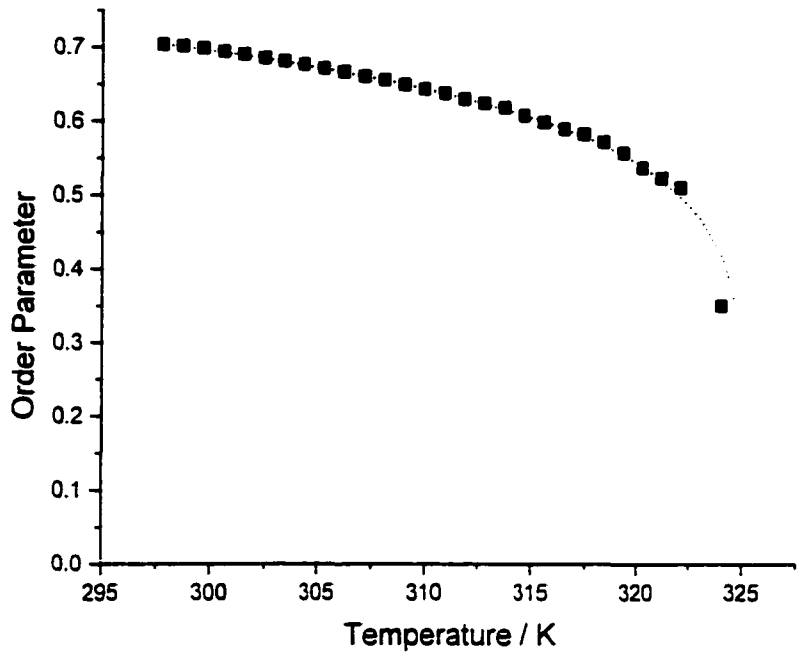

Figure A.3.9. Second fitting of the temperature dependence of the order parameter of C1 in 7CPB.

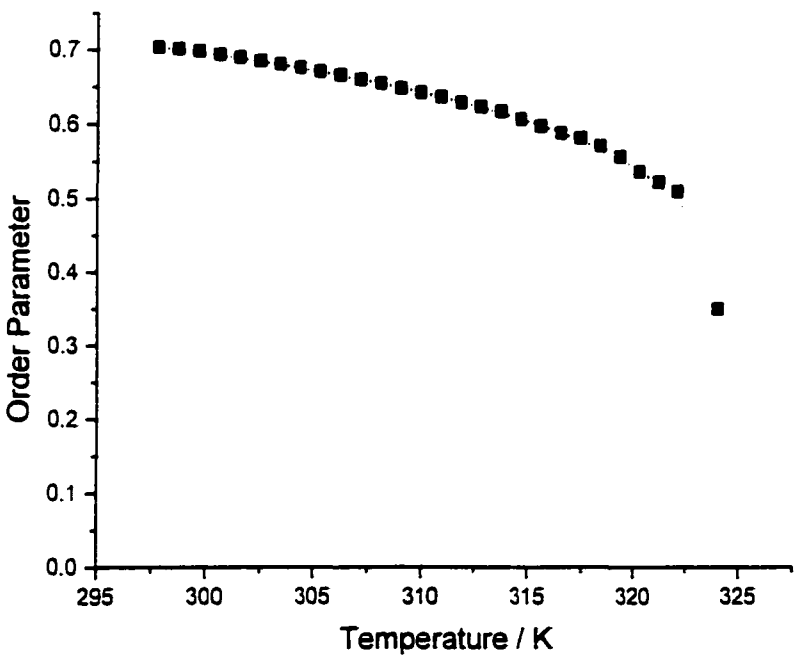

Figure A.3.10. Second fitting of the temperature dependence of the order parameter of C2 in 7CPB.

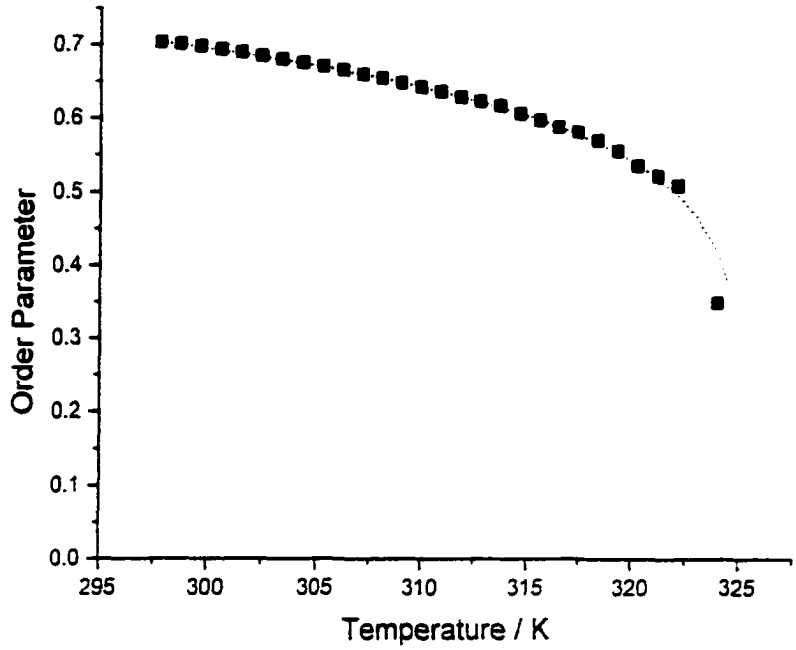

Figure A.3.11. Second fitting of the temperature dependence of the order parameter of C3 in 7CPB.

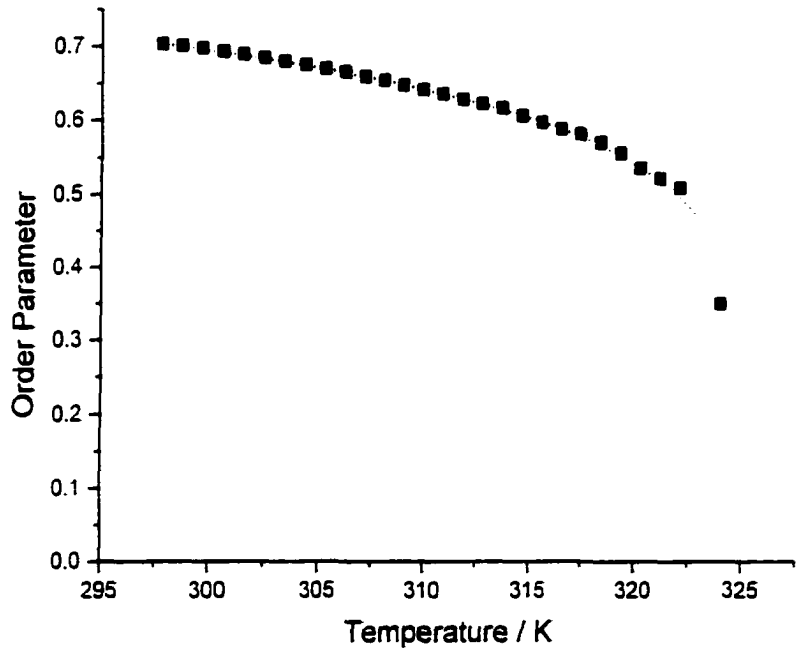

Figure A.3.12. Second fitting of the temperature dependence of the order parameter of C4 in 7CPB.

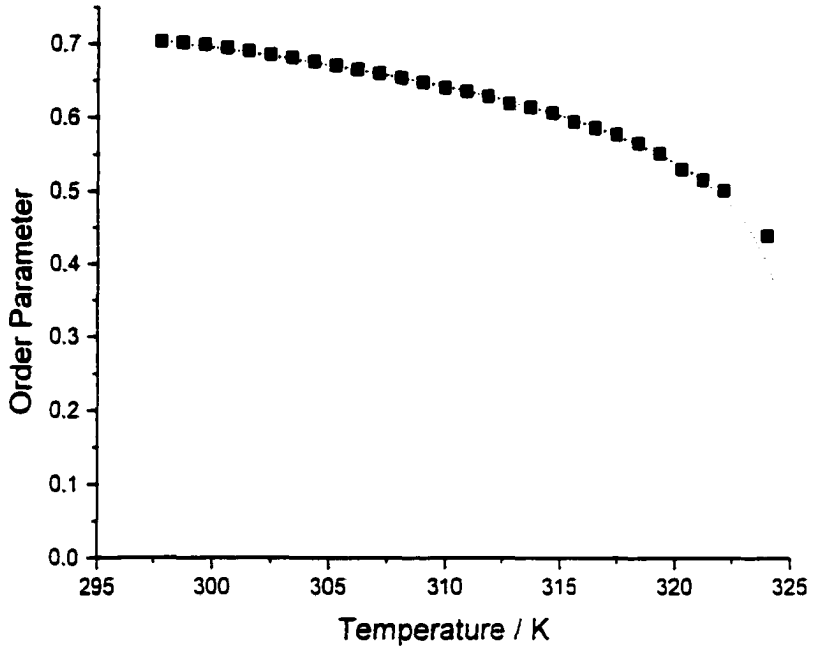

Figure A.3.13. Second fitting of the temperature dependence of the order parameter of C1' in 7CPB.

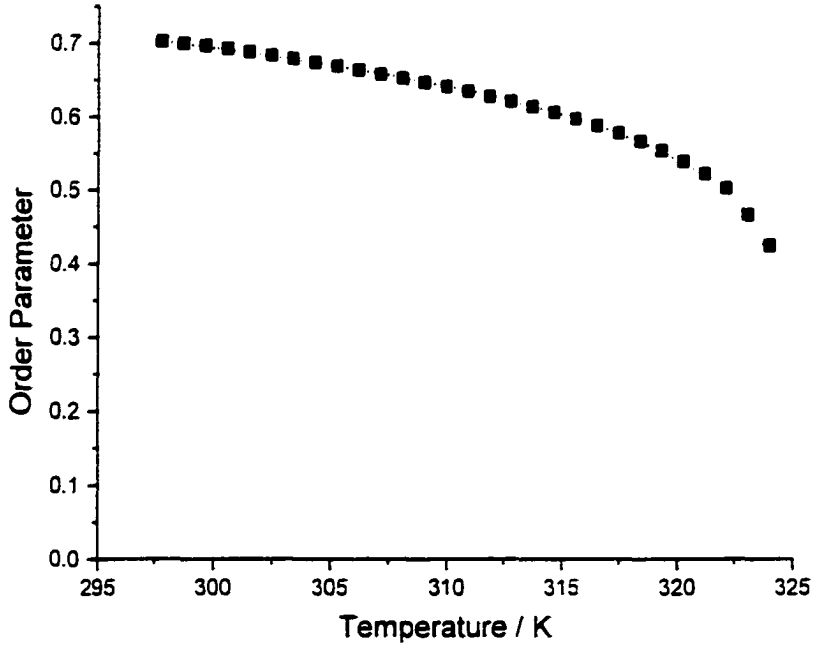

Figure A.3.14. Second fitting of the temperature dependence of the order parameter of C2' in 7CPB.

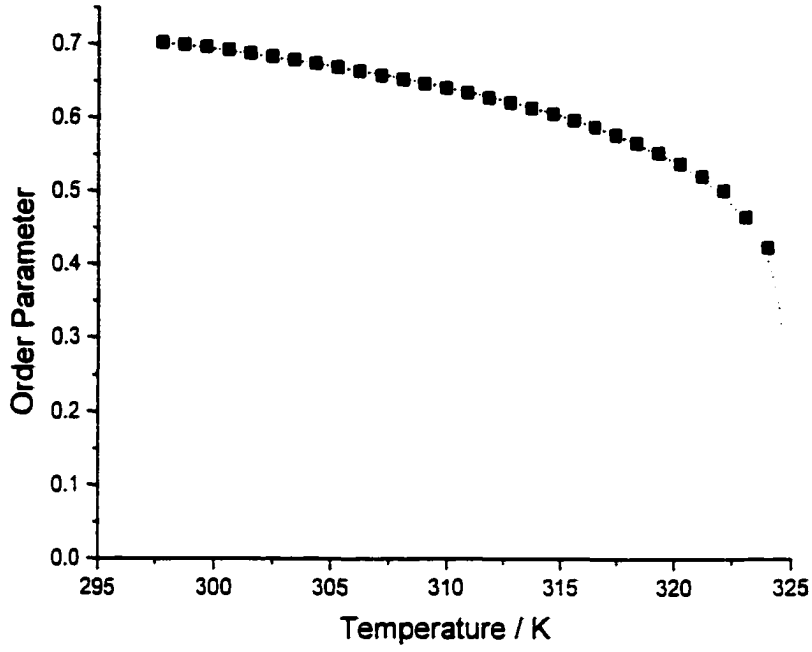

Figure A.3.15. Second fitting of the temperature dependence of the order parameter of C3' in 7CPB.

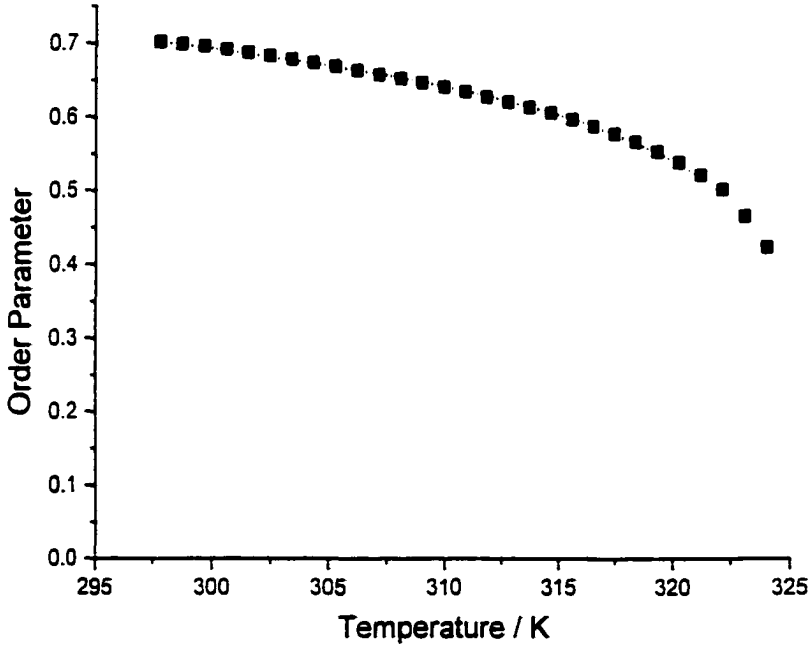

Figure A.3.16. Second fitting of the temperature dependence of the order parameter of C4' in 7CPB.

Table A.3.3. S_0, F from the second Haller fitting of aromatic carbons of Ring 1 of 7CPB.

Carbon	So	F
C1	1.100	0.205
C2	1.085	0.200
C3	1.084	0.199
C4	1.071	0.195
Average	1.09	0.20

Table A.3.4. S_0, F from the second Haller fitting of aromatic carbons of Ring 2 of 7CPB.

Carbon	So	F
C1'	1.030	0.153
C2'	1.018	0.149
C3'	1.021	0.149
C4'	1.023	0.151
Average	1.02	0.15

The average values of So and F were then used in the fitting curve shown in Chapter II.

A.4. Attempted synthesis

A.4.1. Alkylation of anilines

Scheme A.4.1

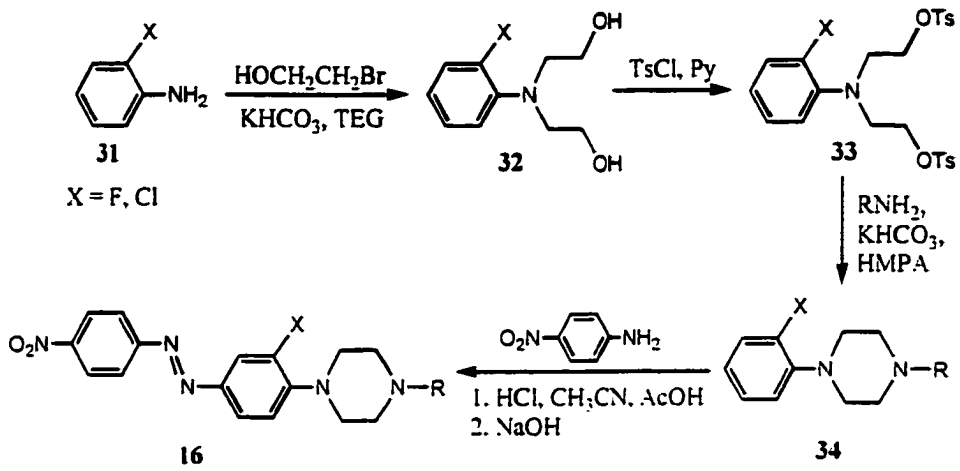

Scheme A.4.1 was first proposed to synthesize the liquid crystals by following a procedure used for dialkylation of aniline with alkoxyl goups.[1] Unfortunately, the first step (**31**→**32**) did not work. The possibility of dialkylation of substituted aniline was tested by reacting 2-chloroaniline (or 2-fluoroanline) with ethylene ditolsylate. Only monoalkylated product was obtained. The dialkylation was further tested using Scheme A.4.2. The electron-withdrawing ability of acetyl amino groups is much lower than fluorine and chlorine, but the alkylation was still not successful.

Scheme A.4.2

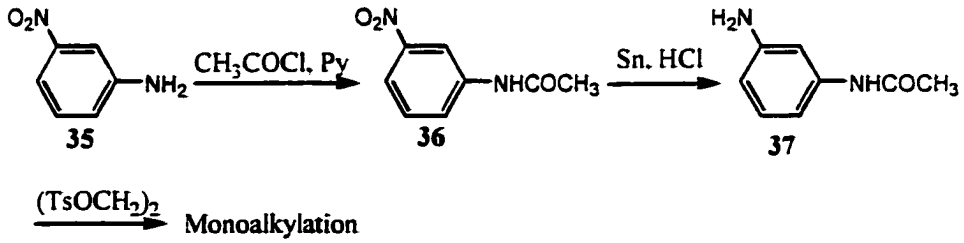

A literature procedure[2,3] was followed to make the arylpiperazine, pyridine was the solvent and K_2CO_3 was utilized as a base (Scheme A.4.3). Another procedure[4] using microwave was also attempted and there was no positive result either.

Scheme A.4.3

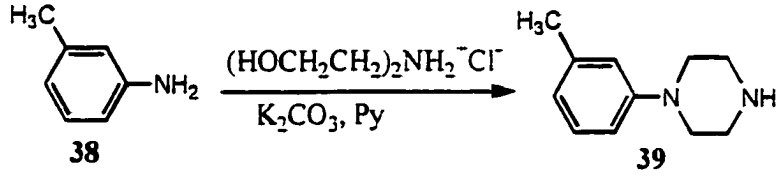

38 **39**

Since such a strong alkylating reagent as tosylate is not good enough to dialkylate the chloroaniline (or fluoroaniline or even *m*-acetylaminoaniline), probably it is not possible to prepare arylpiperazine by the way shown in Scheme A.4.1.

A.4.2. Direct coupling

To couple the alkylpiperazine with aromatic halides should be a good way to circumvent the confronted difficulty. Some methods[5-6] (Schemes A.4.4. and A.4.5) were tried to connect the aromatic ring with the piperazine ring and then manipulate with the rest functionality. Pd[7-8] has been widely reported in literature to catalyze this coupling reaction, but the expense is rather prohibitive.

Scheme A.4.4

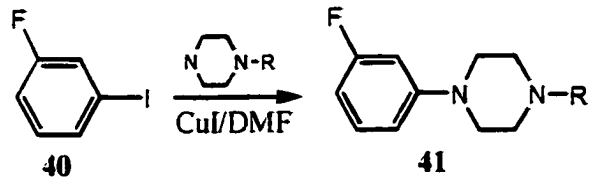

40 **41**

Scheme A.4.5

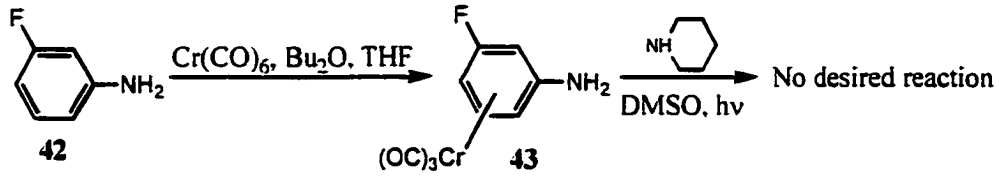

42 43

A.4.3. Aromatic nucleophilic substitution

Aromatic nucleophilic substitution[9-11] is the best candidate for the coupling of piperazine and the phenyl rings. However, it is rather frustrating to see that diazo coupling reaction fail to proceed in the presence of halogen atoms on the aromatic ring (Scheme A.4.6).

Scheme A.4.6

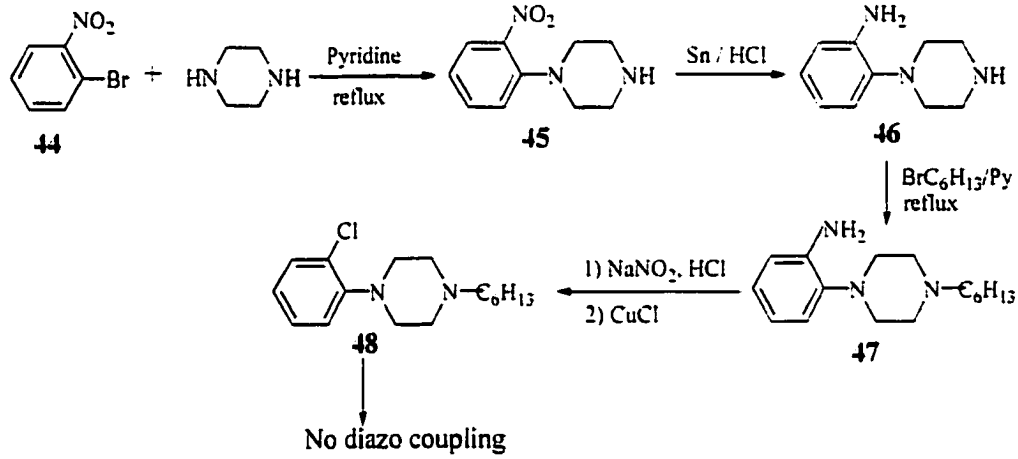

44 45 46 47 48

It took quite a while to realize that suitably substituted 4-fluoronitrobenzene can be used in this synthesis. The nitro group can facilitate the nucleophilic substitution (F as leaving group), and can then be reduced to amino group by various methods. The resultant amino group can then react with nitroso group to form diazo linkage as shown in the synthetic part in Chapter 3.

A.4.4. References

1. Tong, T.-H. and Fung, B. M., *Liq. Cryst.*, **1997**, *23*, 883.

2. Lyon, R. A., Titeler, M., McKenney, J. D., Magee, P. and Glennon, R., *J. Med. Chem.*, **1986**, *29*, 630.

3. Ennis, M. D. and Chazal, N. B., *Tetrahedron Lett.*, **1992**, *33*, 6387.

4. Jaisinghani, H. G. and Khadilkar, B. M., *Tetrahedron Lett.*, **1997**, *38*, 6875.

5. Lindley, J., *Tetrahedron*, **1984**, *40*, 1433.

6. Rausch, M. D., *J. Org. Chem.*, **1974**, *39*, 1787.

7. Kerrigan, F., Martin, C. and Thomas, G., *Tetrahedron Lett.*, **1998**, *39*, 2219.

8. Yamamoto, T., Nishiyama, M. and Koie, Y., *Tetrahedron Lett.*, **1998**, *39*, 2367.

9. Kiritsy, J. A. and Yung, D. K., *J. Med. Chem.*, **1978**, *21*, 1301.

10. March, J., *Advanced Organic Chemistry, Reactions, Mechanisms and Structures* (John Wiley & Sons), Third Edition, **1985**, 581.

11. Dankwardt, S. M., Newman, S. R. and Kristenansky, J. L., *Tetrahedron Lett.*, **1995**, *36*, 4923.

A.5. Data Acquisition

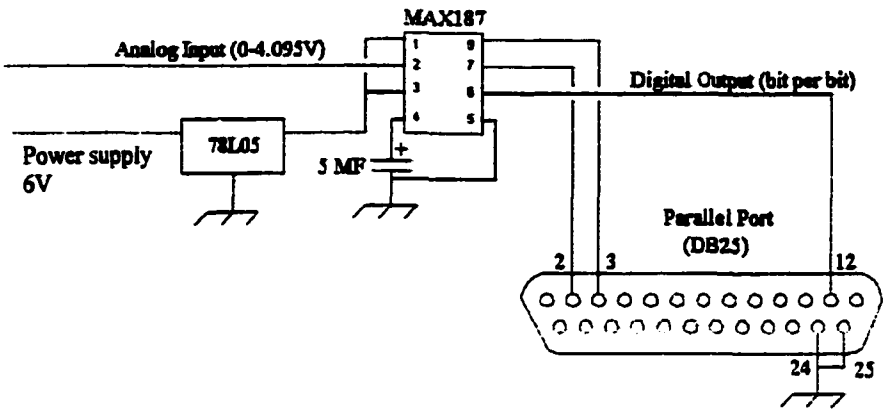

MAX187 is an A/D converter that can convert analog voltage signals to digital signals. There is an internal reference voltage that can be utilized by the converter to calculate the magnitude of the analog input. This internal reference is connected to Pin 1 of MAX187. Pins 6, 7 and 8 (of the converter) are used in the data collection. When Pin 7 receives a pulse, it initiates the conversion of the analog signal to a digital one. The resulting signal (binary) is stored in the converter. When Pin 8 receives a pulse, the converter begins to output signal bit by bit from Pin 6. In the above circuit, Pin 7 (of the converter) is connected to Pin 2 of the parallel port of a PC computer, Pin 8 (of the converter) to Pin 3 (of the parallel port) and Pin 6 (of the converter) to Pin 12 (of the parallel port).

The needed pulse can be realized by sending a number to the parallel port and its address in a PC computer is always 378H. It can be seen from the above picture that the parallel port has 25 pins. The parallel port is used to exchange data between the computer and perimeter equipment in a parallel manner, so some of the pins are used for input and output of the data. Normally, Pins 2-9 work as data bits and they are data bits 0-7 correspondingly. In current computers, one bit has

only two states, 0 and 1, which is different from each other in the voltage of the bit. When the voltage is high, it stands for 1, otherwise it is 0. Now the if we want to send a pulse to Pin2 of the port (and then to Pin 8 of the converter) to initiate the A/D conversion, we need to send first a 1 and then 0 to Pin 2. If we want to send a similar pulse to Pin 3 of the port (and then to Pin 8 of the converter) to trigger the output the data, we need to send 2, 0 to the address 378H, because Pin 3 is data bit 1, and 2 means a high voltage on Pin 3.

The output signal on Pin 12 (data bit 4 of address 379H) needs to be read out. A common way to do this is to test the voltage of this pin directly. In computer language. this is done by testing the bit with a logic command AND. This datum is only a bit of the whole binary signal (12 bits). As mentioned previously. the signal will be transferred bit by bit in decreasing significance. Then these 12 binary signals are converted to the more familiar decimal signal by following basic rules.

The practical program is written in Quick Basic as follows:

```
DIM BIT%(11)
INPUT "OPTICAL MEASUREMENT FILENAME:", OUTFILE$
OPEN OUTFILE$ FOR OUTPUT AS #1

NAVE% = 500
START& = TIMER
```

```
WHILE INKEY$ <> "!"


SIG! = 0
FOR j% = 1 TO NAVE%
OUT &H378, 1
OUT &H378, 0


FOR i% = 0 TO 11
    OUT &H378, 2
    OUT &H378, 0
    IF (INP(&H379) AND &H20) THEN
        BIT%(i%) = 1
    ELSE
        BIT%(i%) = 0
    END IF
NEXT i%


NUM% = BIT%(11) + BIT%(10) * 2 + BIT%(9) * 4 + BIT%(8) * 8 + BIT%(7) *
16 + BIT%(6) * 32 + BIT%(5) * 64 + BIT%(4) * 128 + BIT%(3) * 256 +
BIT%(2) * 512 + BIT%(1) * 1024 + BIT%(0) * 2048
SIG! = SIG! + NUM%
TIME! = TIMER - START&
NEXT j%
```

```
SIG! = SIG! / NAVE%

PRINT USING "##.##  ######"; TIME!; SIG!

PRINT #1, USING "##.##  ######"; TIME!; SIG!


WEND


CLOSE #1
```

A.6. Data for birefringence measurement for 10 wt% LC mistures

	n	d / μm	633 nm				1050 nm			
			$T_{//}$	$T_{\perp}$	m	Δn	$T_{//}$	$T_{\perp}$	m	Δn
E-7		3.83	0.387	0.620	2	**0.213**	0.481	0.532	1	**0.203**
16a	8	3.72	0.001	0.999	3	**0.257**	0.401	0.619	1	**0.221**
12	8	3.91	0.077	0.924	3	**0.257**	0.707	0.292	1	**0.220**
19	8	3.92	0.074	0.930	3	**0.256**	0.752	0.241	1	**0.224**
16c	8	4.47	0.393	0.608	3	**0.243**	0.968	0.027	1	**0.220**
16d	8	3.43	0.311	0.677	2	**0.242**	0.364	0.624	1	**0.217**
16b	8	3.47	0.141	0.868	2	**0.251**	0.504	0.521	1	**0.226**
29	8	3.34	0.090	0.897	2	**0.266**	0.445	0.558	1	**0.230**
30	8	2.56	0.860	0.140	2	**0.277**	0.054	0.950	1	**0.236**

An example of the calculation for compound **16b** at 633 nm is given below.

The following plot is somewhat different from what is shown in Figure 3.2, because in our automated measurement, we used the scanning voltage used by the APTIII instrument. The voltage begins to increase from 0.5 V in every 0.1 V interval when below 4.0 V and changes to 1.0 V interval after 4.0 V till 24.0 V. In our program we did not try to relate the voltage to time since the most important information is the values of $T_{//}(0)$, $T_{\perp}(0)$ and m (number of cycles) and they all can be obtained in this measurement.

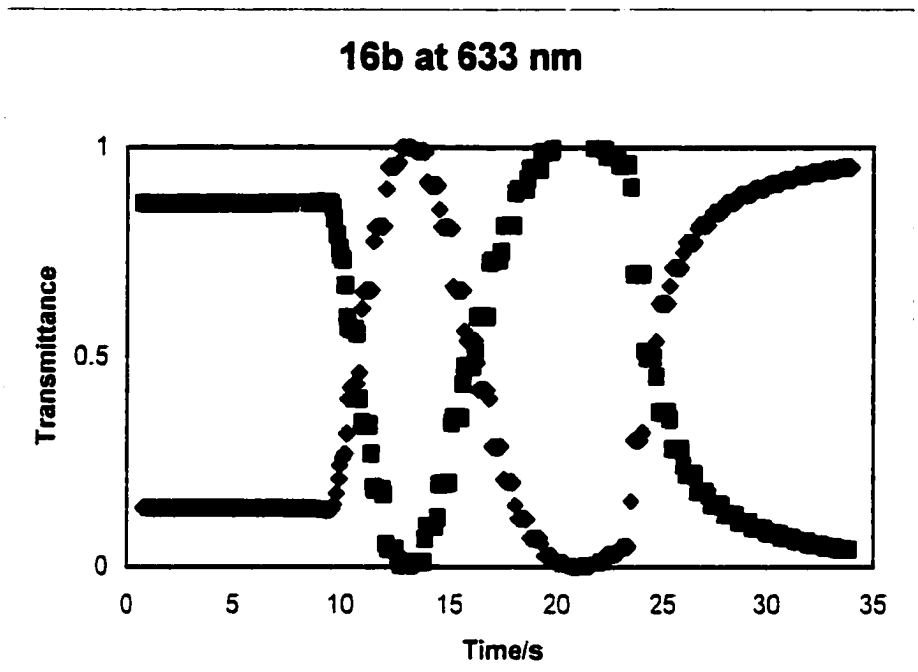

m = 2. d = 3.47 μm

$T_{//}(0) = 0.141$, $T_{\perp}(0) = 0.868$

$$\delta = 2\pi \Delta n\, d / \lambda = 2\pi + 2 \tan^{-1} \sqrt{\frac{0.868}{0.141}} = 2.756\,\pi$$

Thus,

$$\Delta n = \frac{2.756\pi \times 633 \times 10^{-9}}{2\pi \times 3.47 \times 10^{-6}} = 0.2513$$

A.7. UV-vis absorption spectra for synthesized liquid crystals

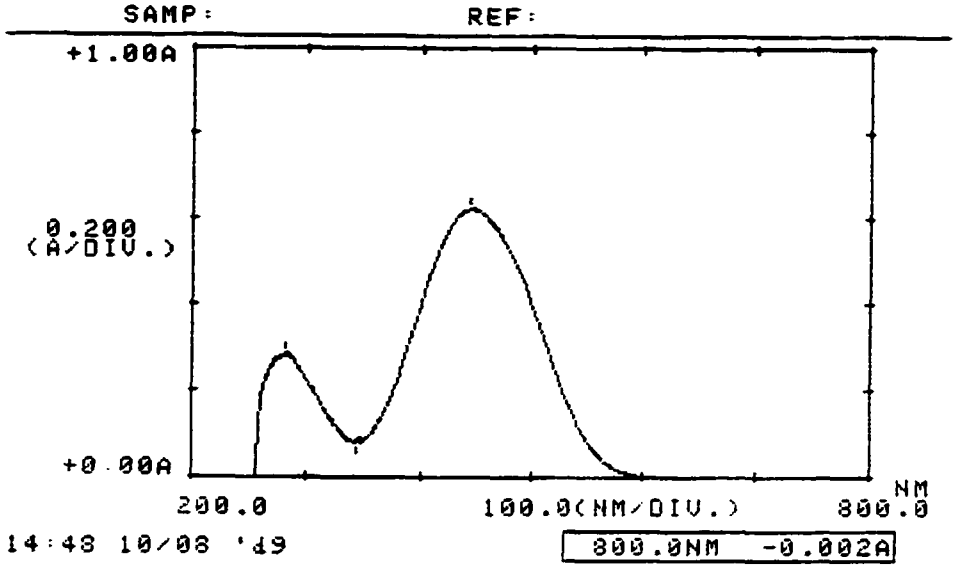

Figure A.7.1. The UV-vis spectrum of **16a** (n = 5) in DMSO (λ_{max} = 443 nm).

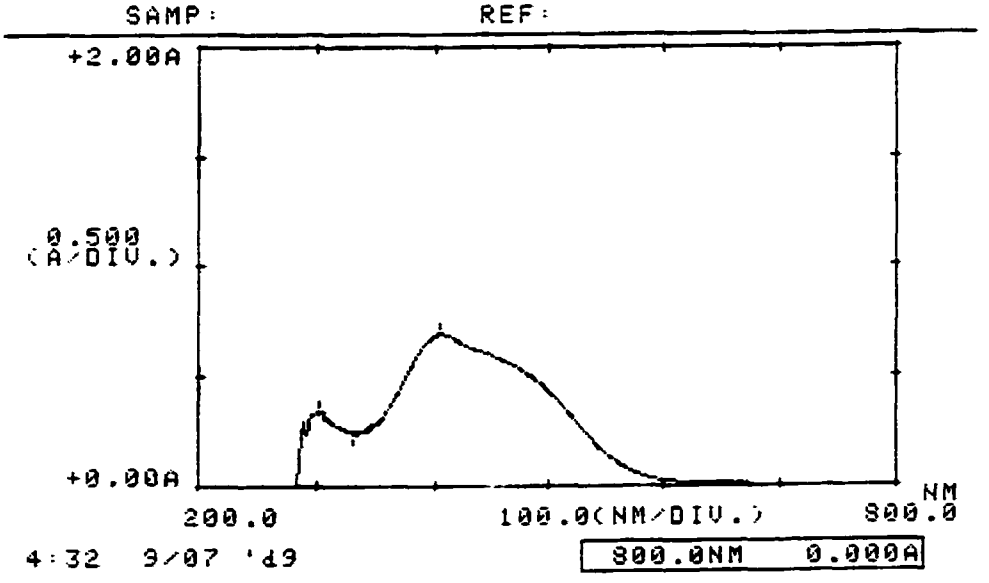

Figure A.7.2. The UV-vis spectrum of **16c** (n = 5) in DMSO (λ_{max} = 406 nm).

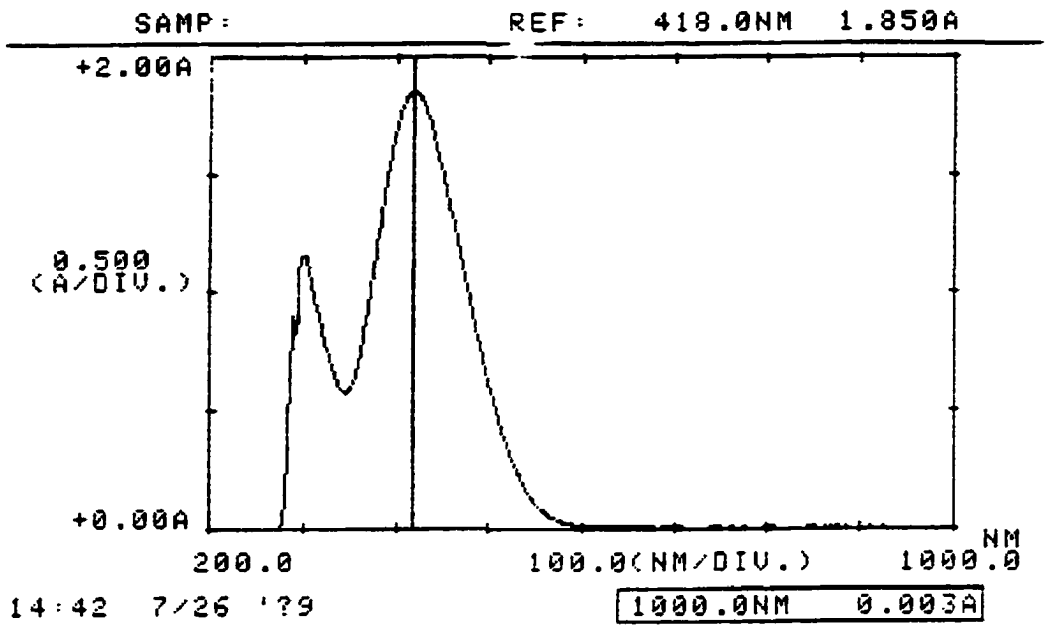

Figure A.7.3. The UV-vis spectrum of **16d** (n = 5) in DMSO (λ_{max} = 418 nm).

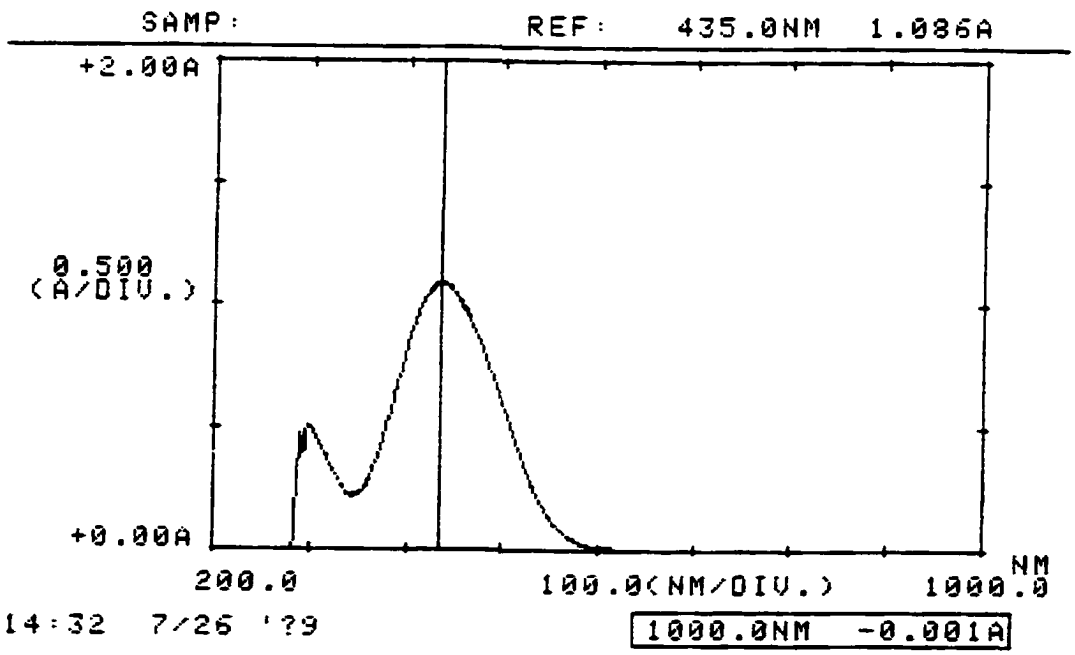

Figure A.7.4. The UV-vis spectrum of **16b** (n = 5) in DMSO (λ_{max} = 435 nm).

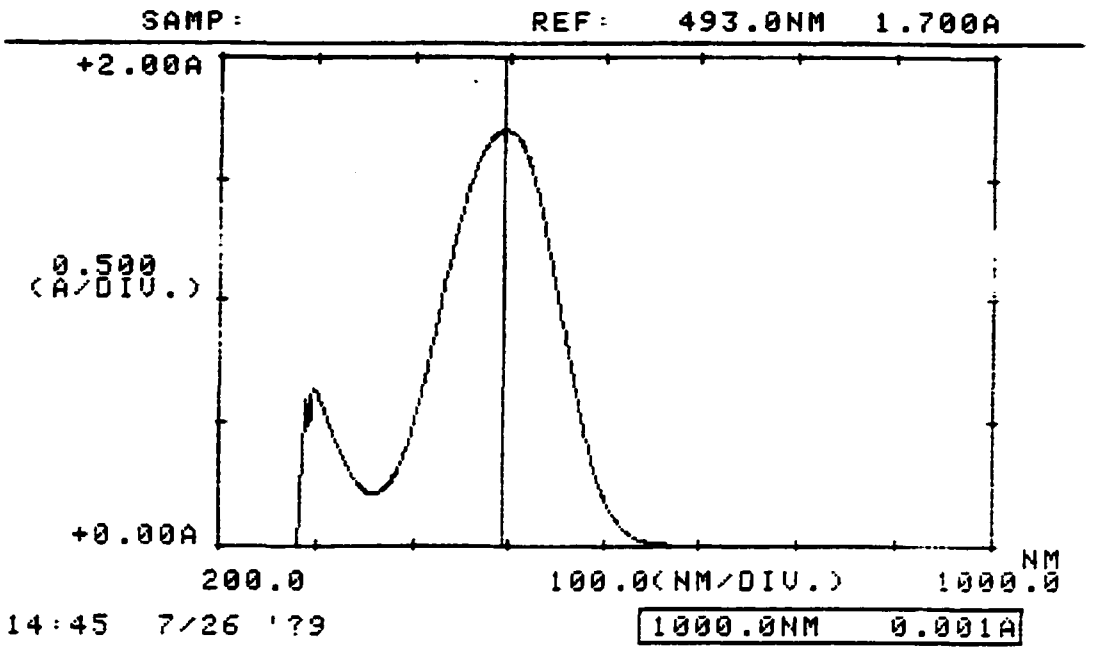

Figure A.7.5. The UV-vis spectrum of **12** (n = 5) in DMSO (λ_{max} = 493 nm).

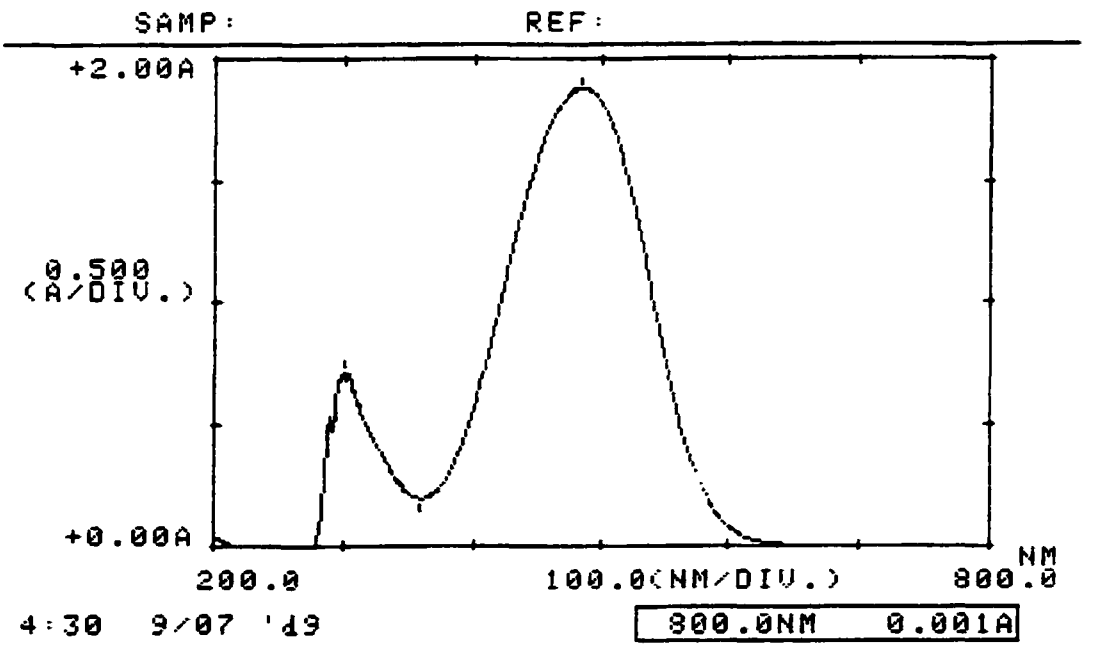

Figure A.7.6. The UV-vis spectrum of **19** (n = 5) in DMSO (λ_{max} = 483 nm).

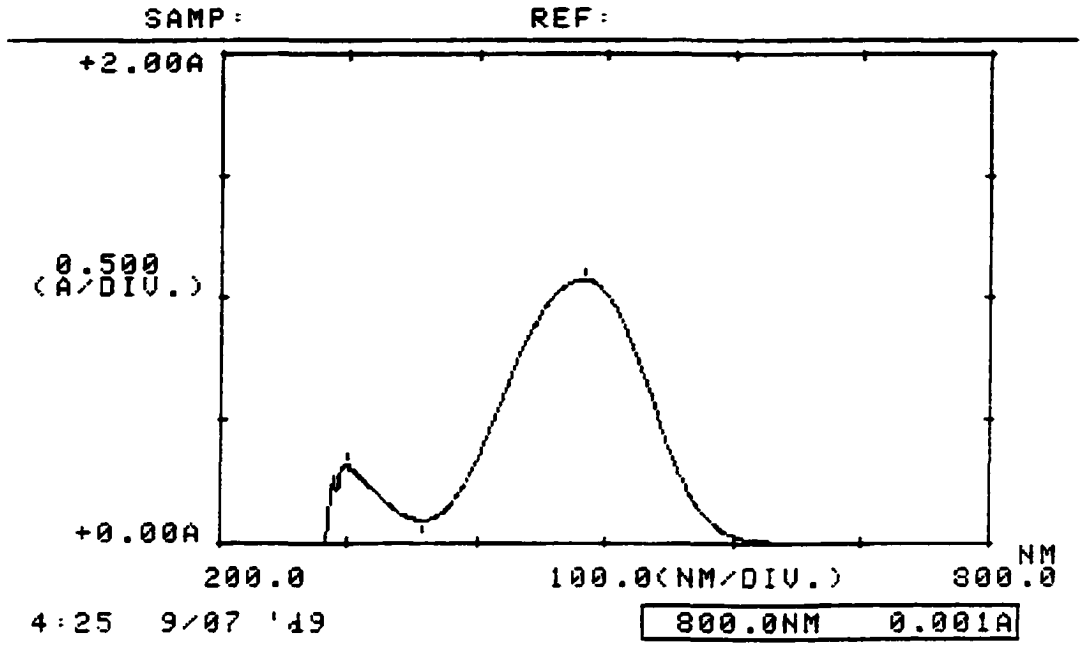

Figure A.7.7. The UV-vis spectrum of * (n = 5) in DMSO (λ_{max} = 482 nm).

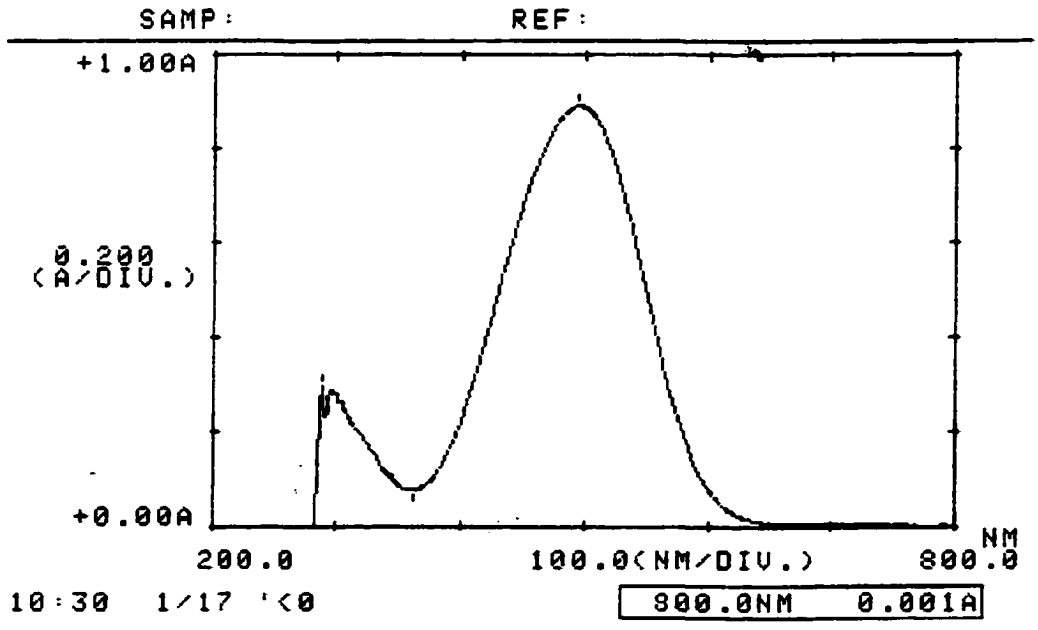

Figure A.7.8. The UV-vis spectrum of **29** (n = 5) in DMSO (λ_{max} = 493 nm).

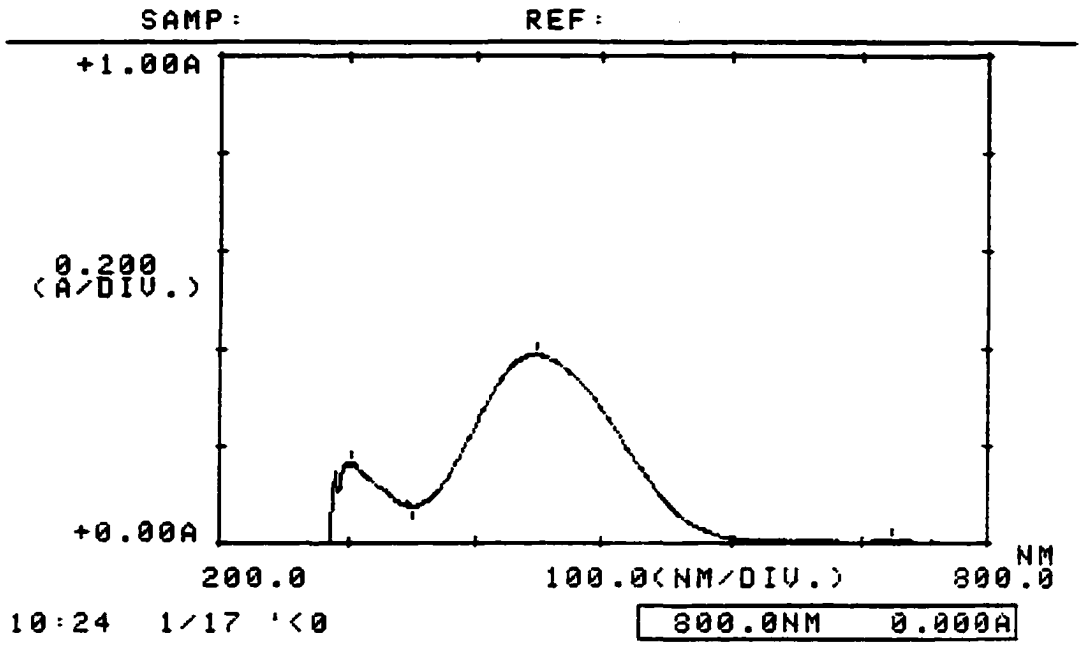

Figure A.7.9. The UV-vis spectrum of **30** (n = 5) in DMSO (λ_{max} = 485 nm).

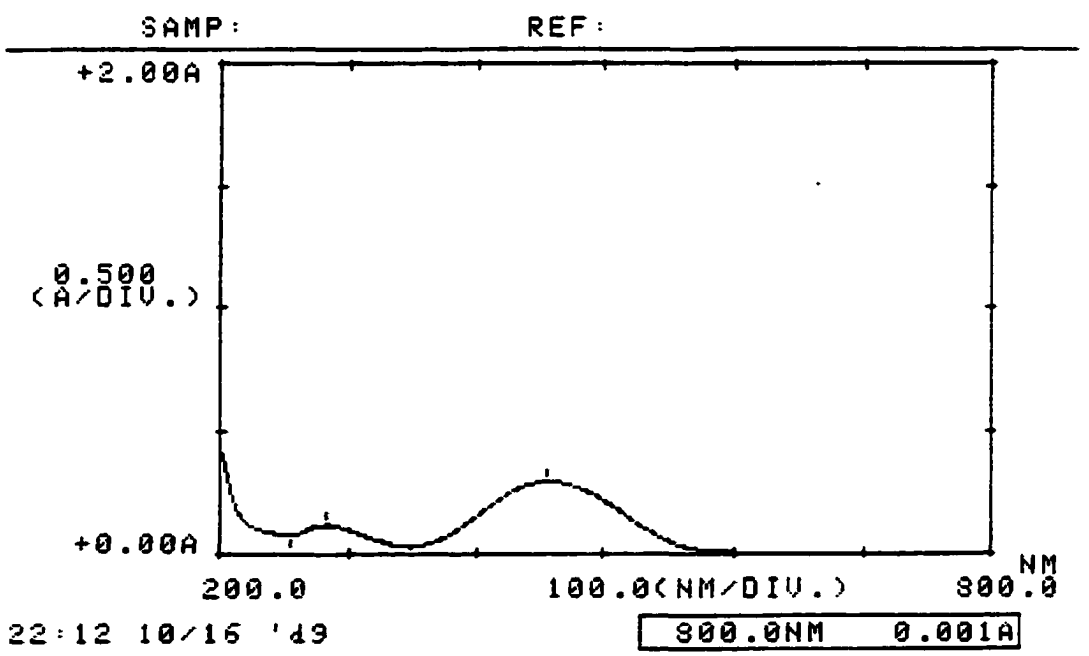

Figure A.7.10. The UV-vis spectrum of 13.0 μM **16a** (n = 5) in CH_3CN (λ_{max} = 456 nm and A = 0.296).

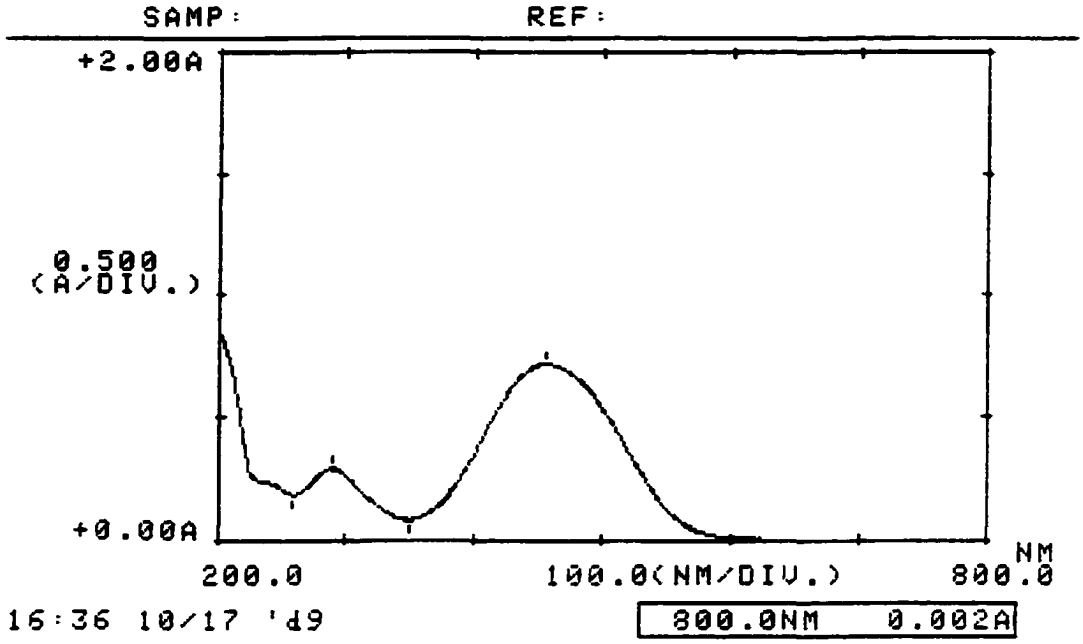

Figure A.7.11. The UV-vis spectrum of 27.8 μM **12** (n = 5) in CH_3CN (λ_{max} = 455 nm and A = 0.718).

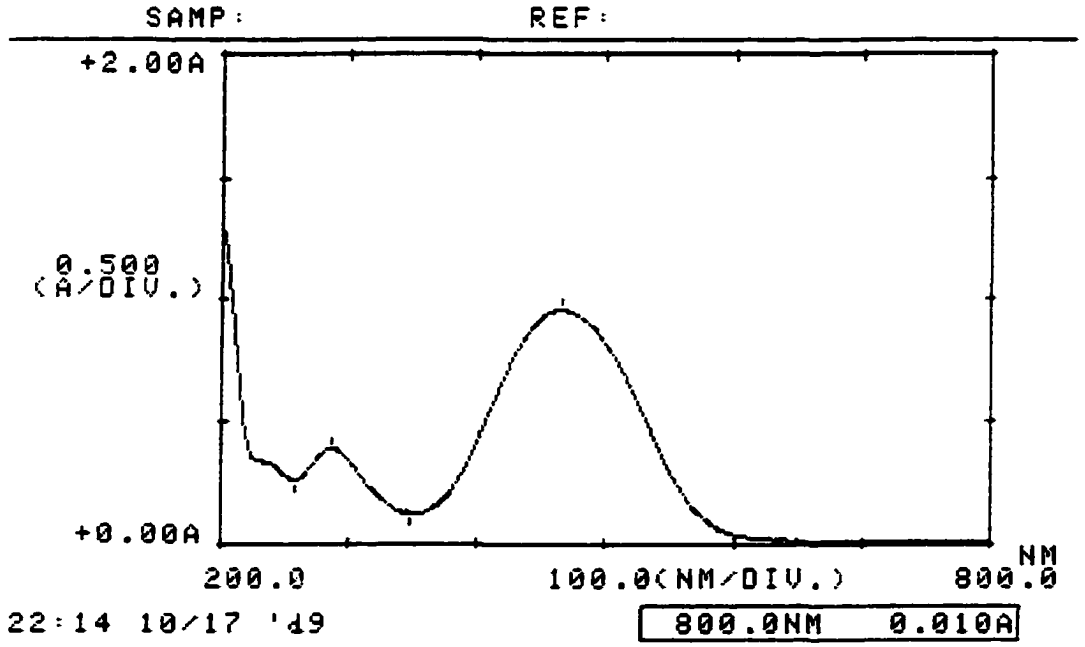

Figure A.7.12. The UV-vis spectrum of 24.1 μM **19** (n = 5) in CH_3CN (λ_{max} = 465 nm and A = 0.956).

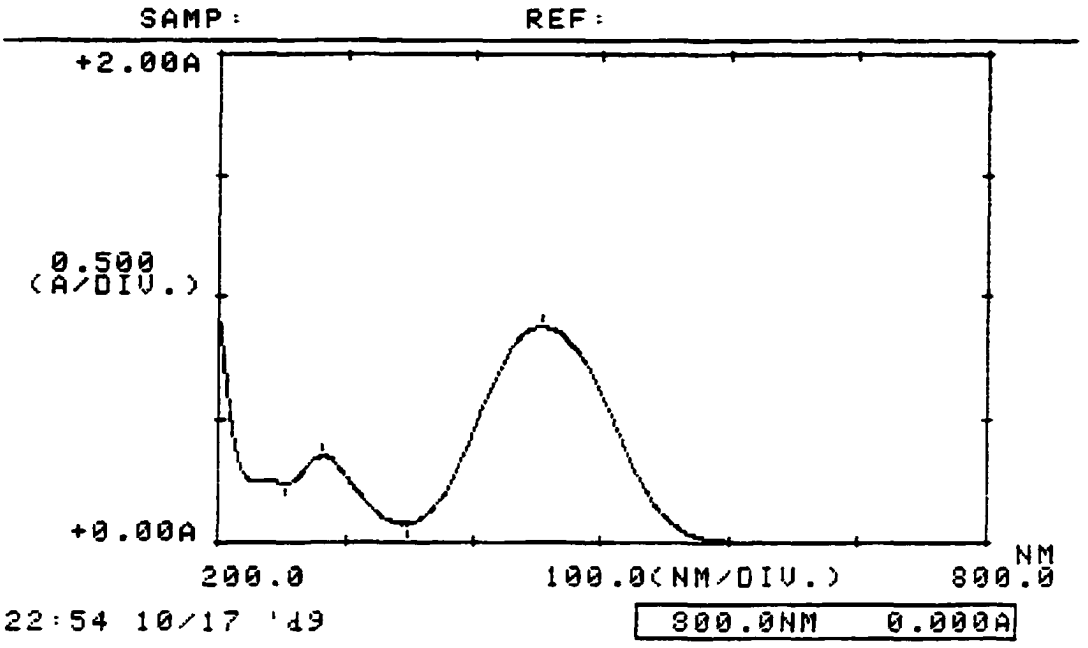

Figure A.7.13. The UV-vis spectrum of 30.0 μM * (n = 5) in CH_3CN (λ_{max} = 453 nm and A = 0.878).

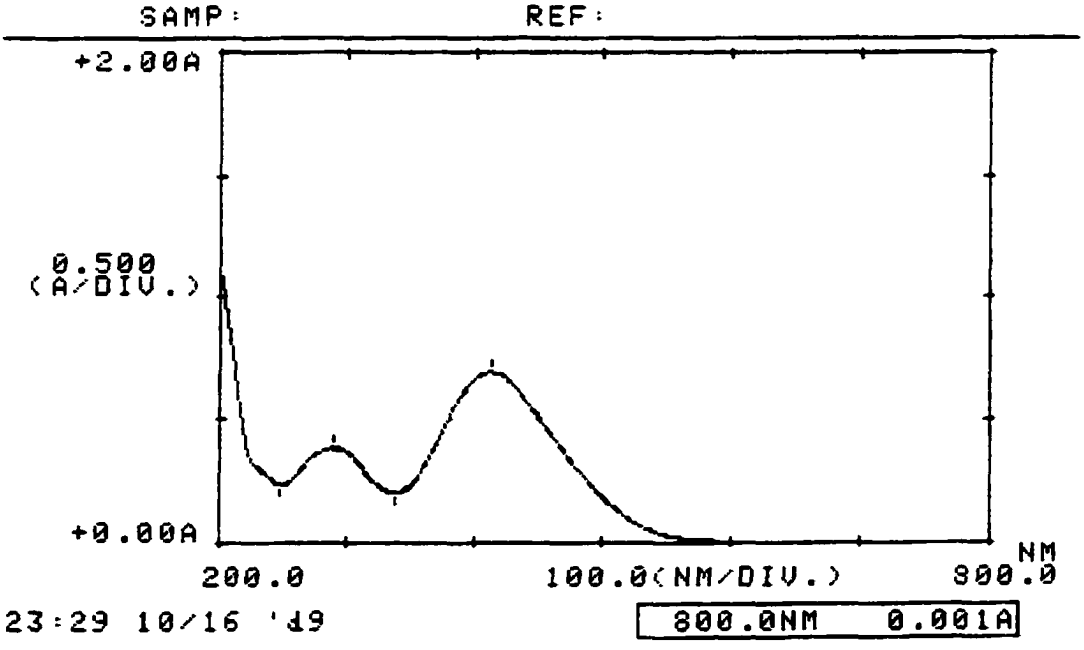

Figure A.7.14. The UV-vis spectrum of 35.4 μM **16c** (n = 5) in CH_3CN (λ_{max} = 413 nm and A = 0.692).

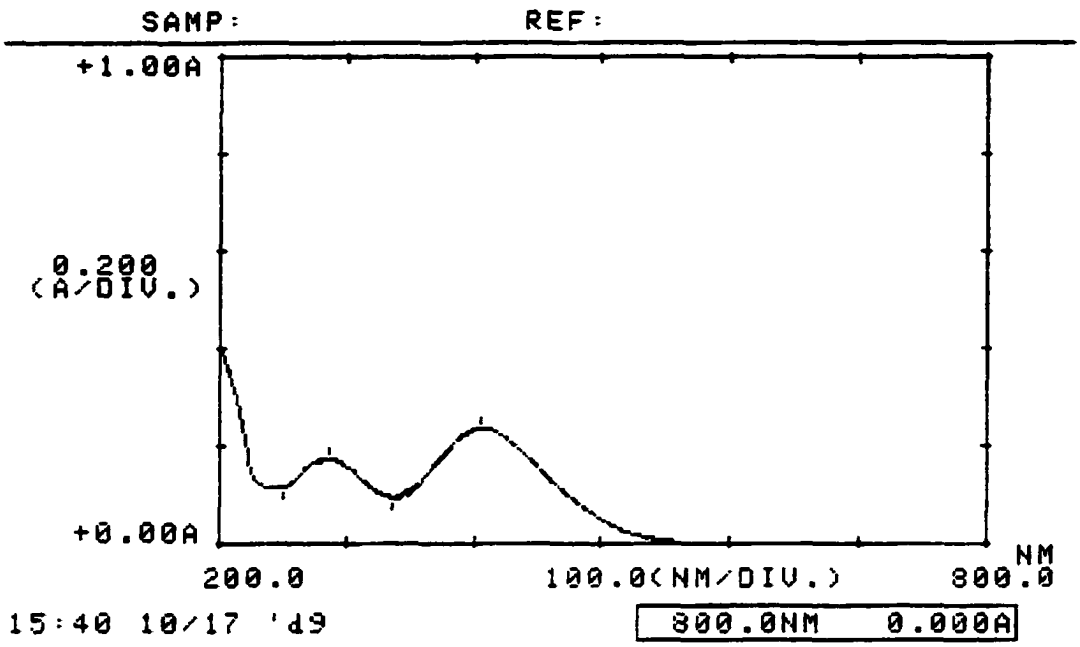

Figure A.7.15. The UV-vis spectrum of 19.3 μM **16d** (n = 5) in CH_3CN (λ_{max} = 406 nm and A = 0.234).

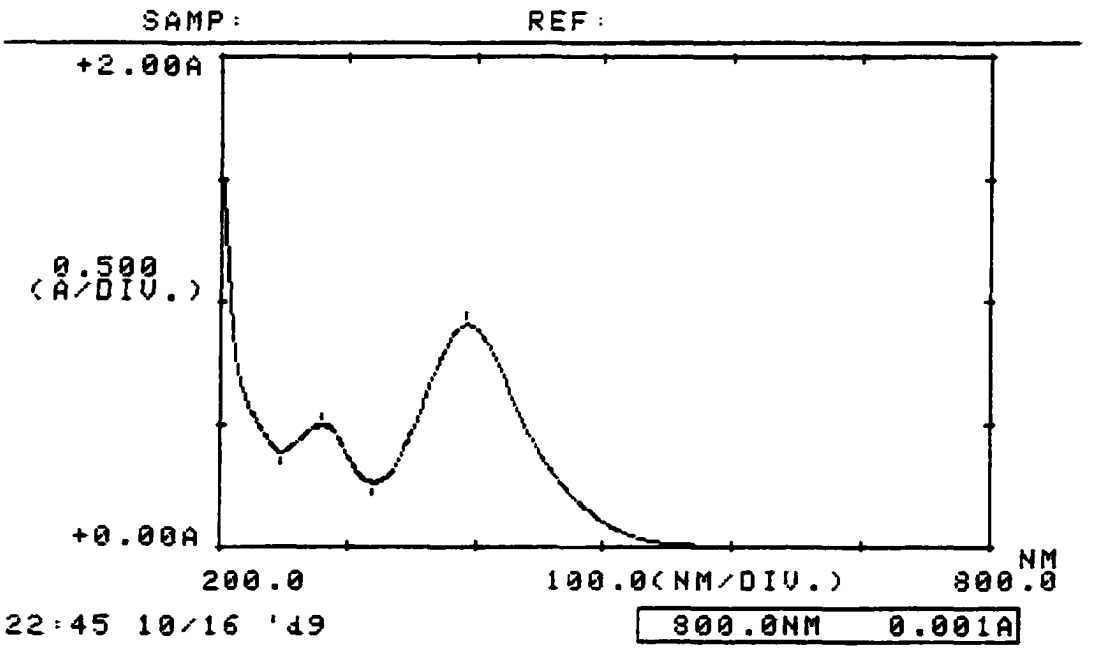

Figure A.7.16. The UV-vis spectrum of 35.1 μM **16b** (n = 5) in CH_3CN (λ_{max} = 392 nm and A = 0.911).

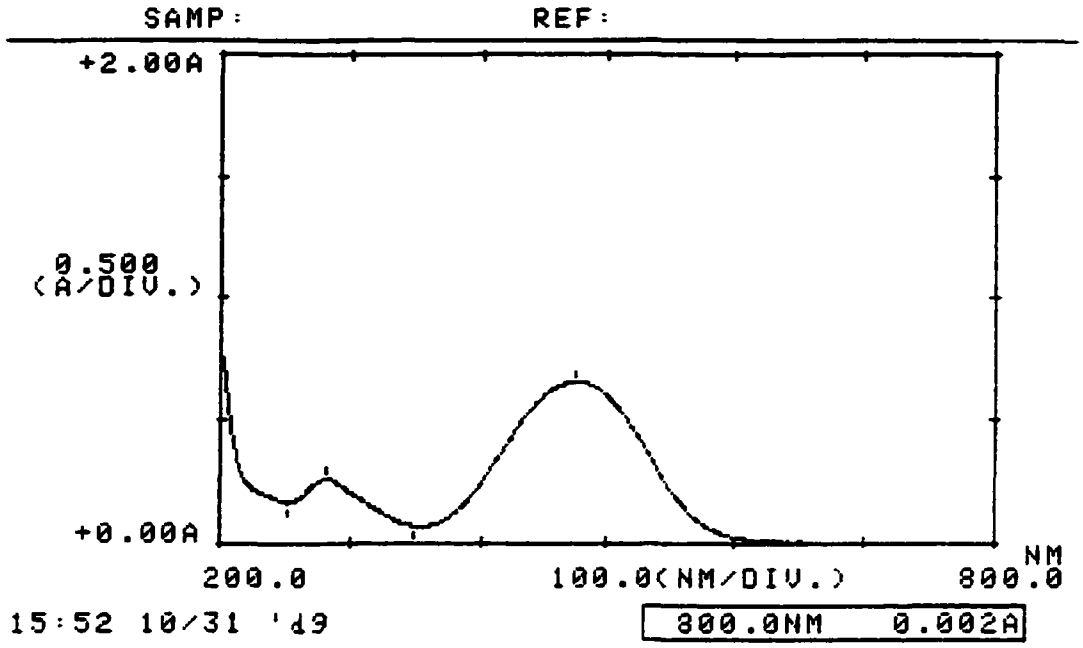

Figure A.7.17. The UV-vis spectrum of 25.1 μM **29** (n = 5) in CH_3CN (λ_{max} = 474 nm and A = 0.653).

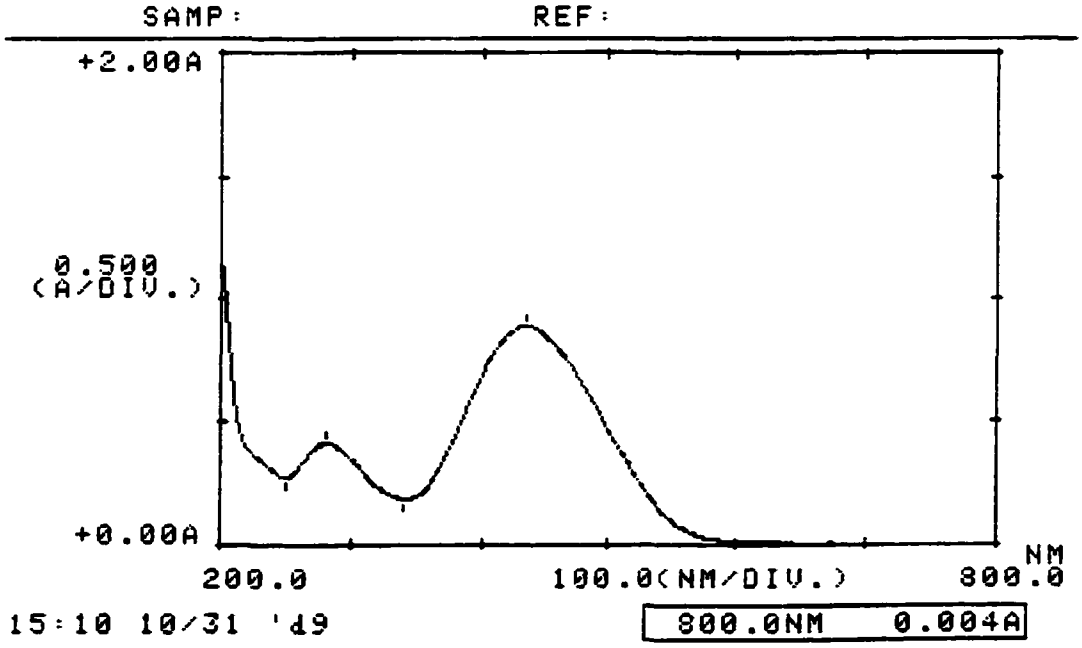

Figure A.7.18. The UV-vis spectrum of 38.4 μM **30** (n = 5) in CH_3CN (λ_{max} = 434 nm and A = 0.891).

A.8. NMR spectra for synthesized liquid crystals

Figure A.8.1. ^{1}H and ^{13}C NMR spectra of **12** (n = 8) in $CDCl_3$.

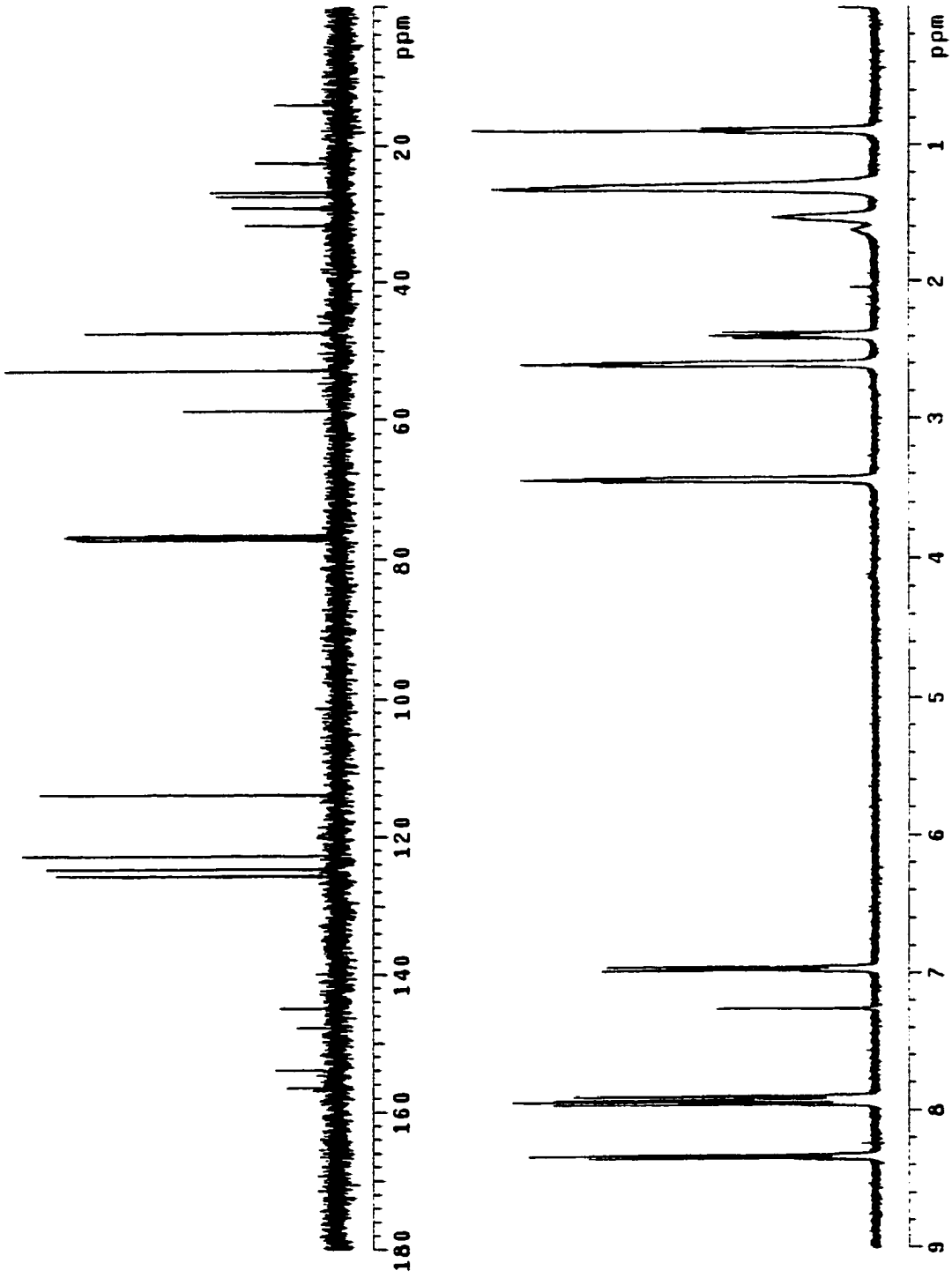

Figure A.8.2. ^{1}H and ^{13}C NMR spectra of **16a** (n = 7) in $CDCl_3$.

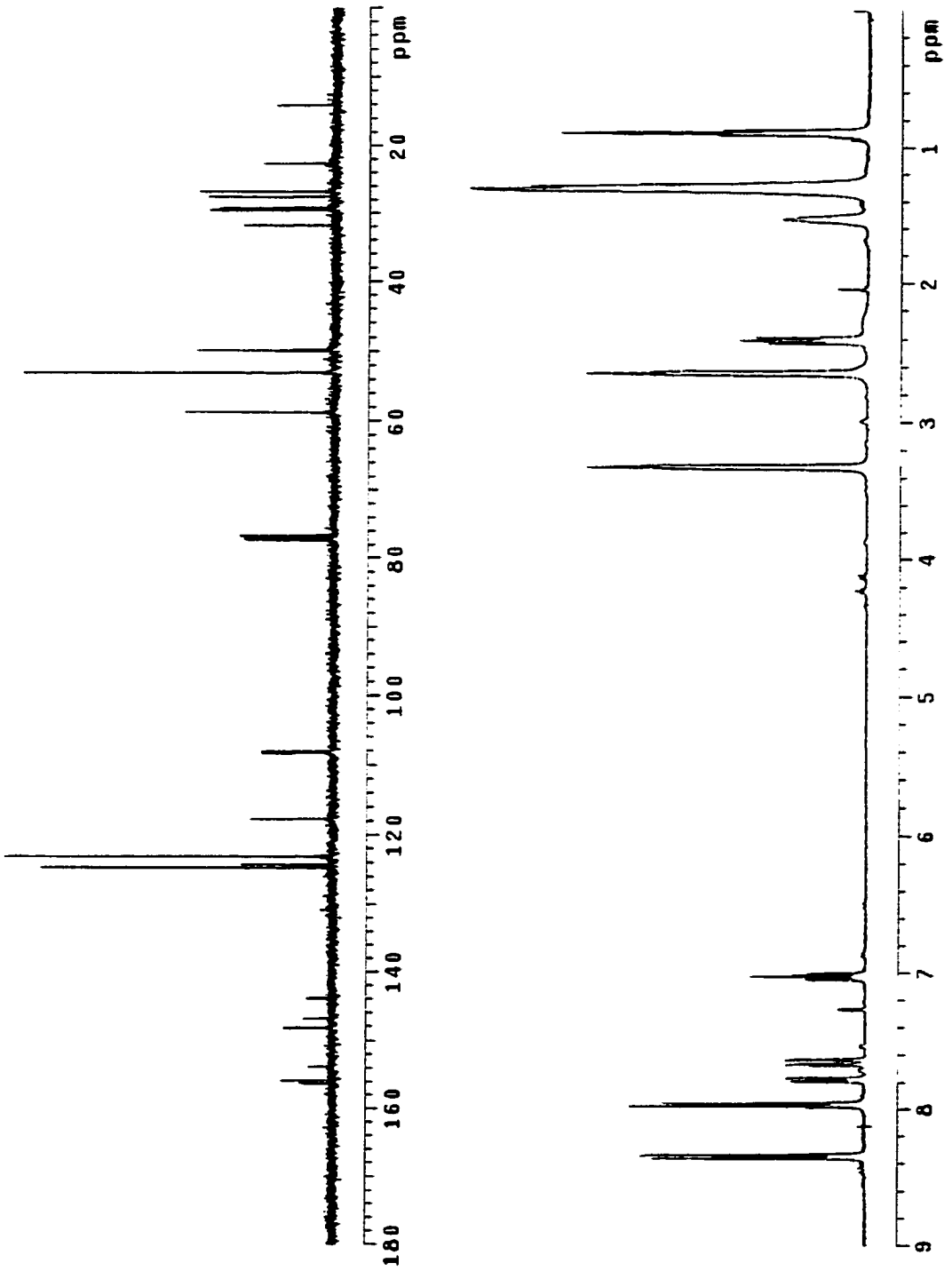

Figure A.8.3. ^{1}H and ^{13}C NMR spectra of **16b** (n = 8) in $CDCl_3$.

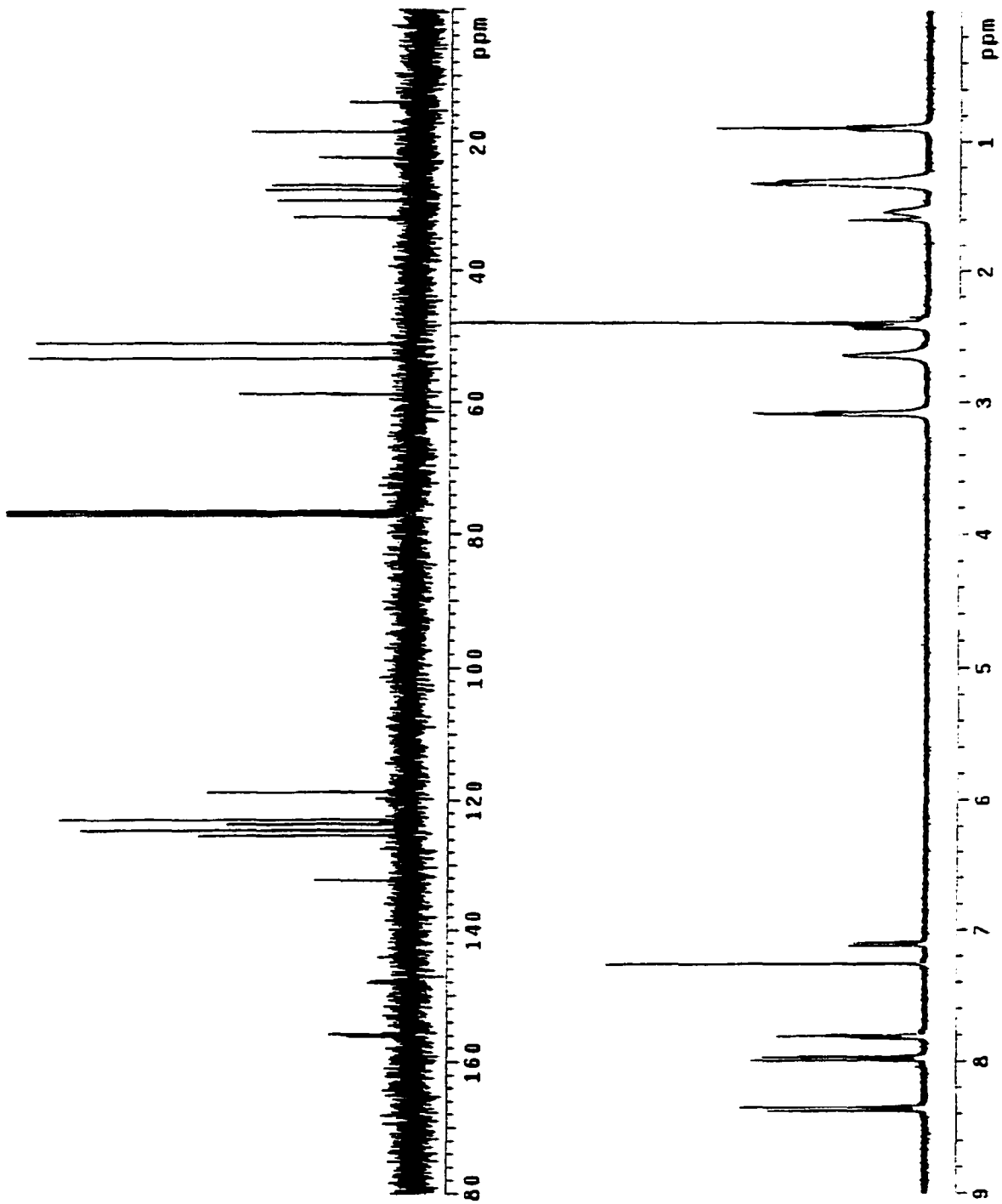

Figure A.8.4. ^{1}H and ^{13}C NMR spectra of **16c** (n = 7) in $CDCl_3$.

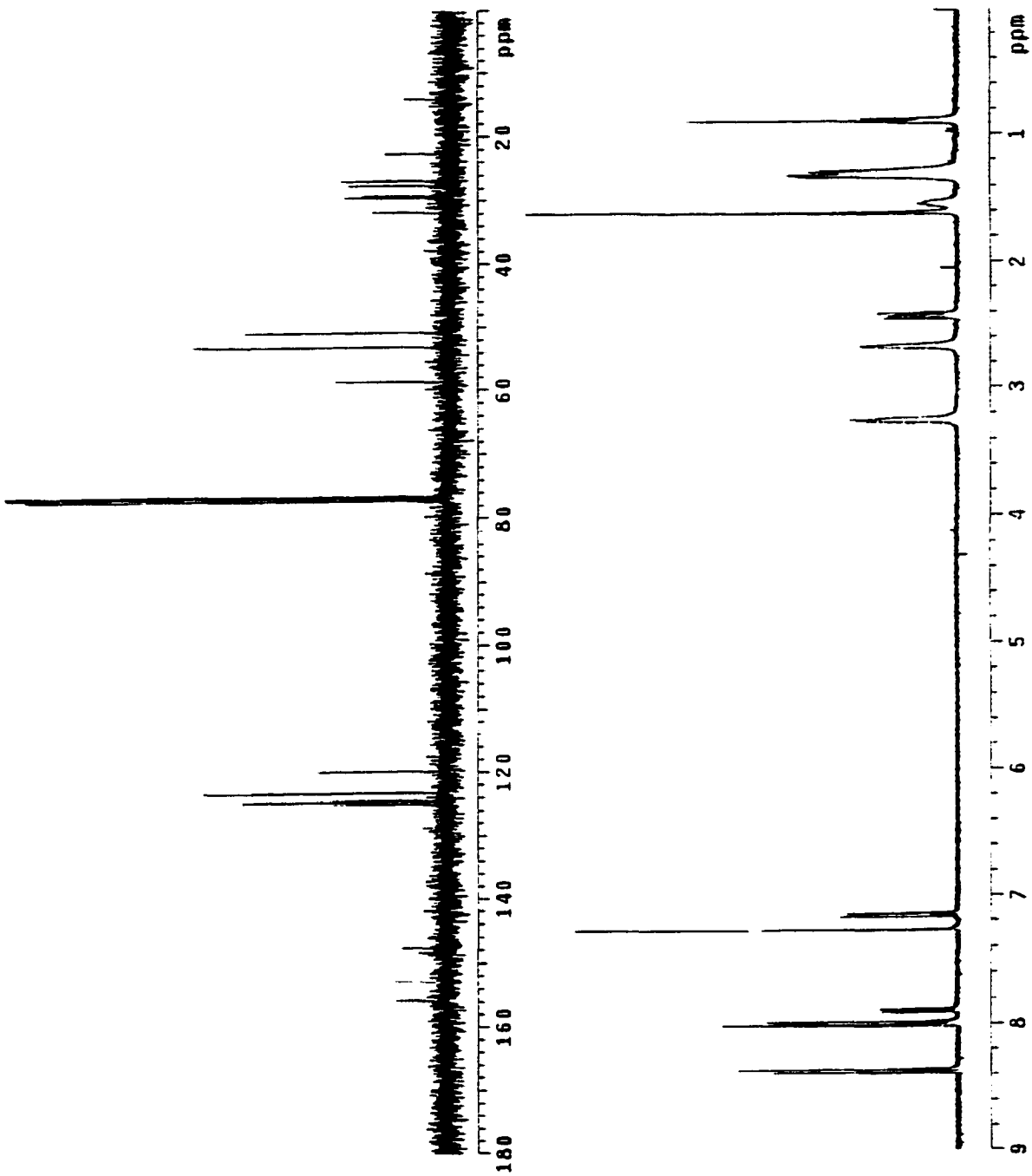

Figure A.8.5. ^{1}H and ^{13}C NMR spectra of **16d** (n = 8) in $CDCl_3$.

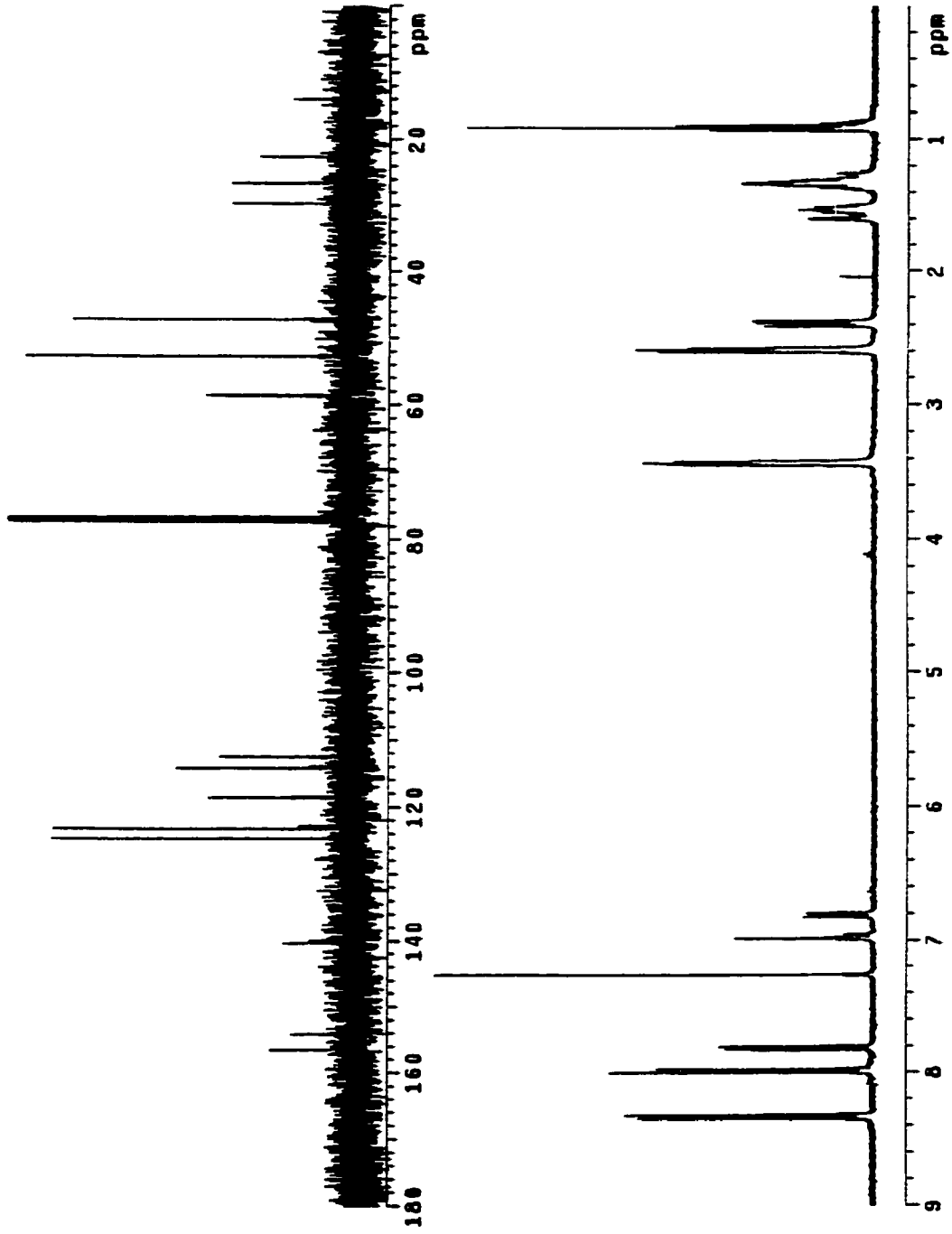

Figure A.8.6. ^{1}H and ^{13}C NMR spectra of **19** (n = 5) in $CDCl_3$.

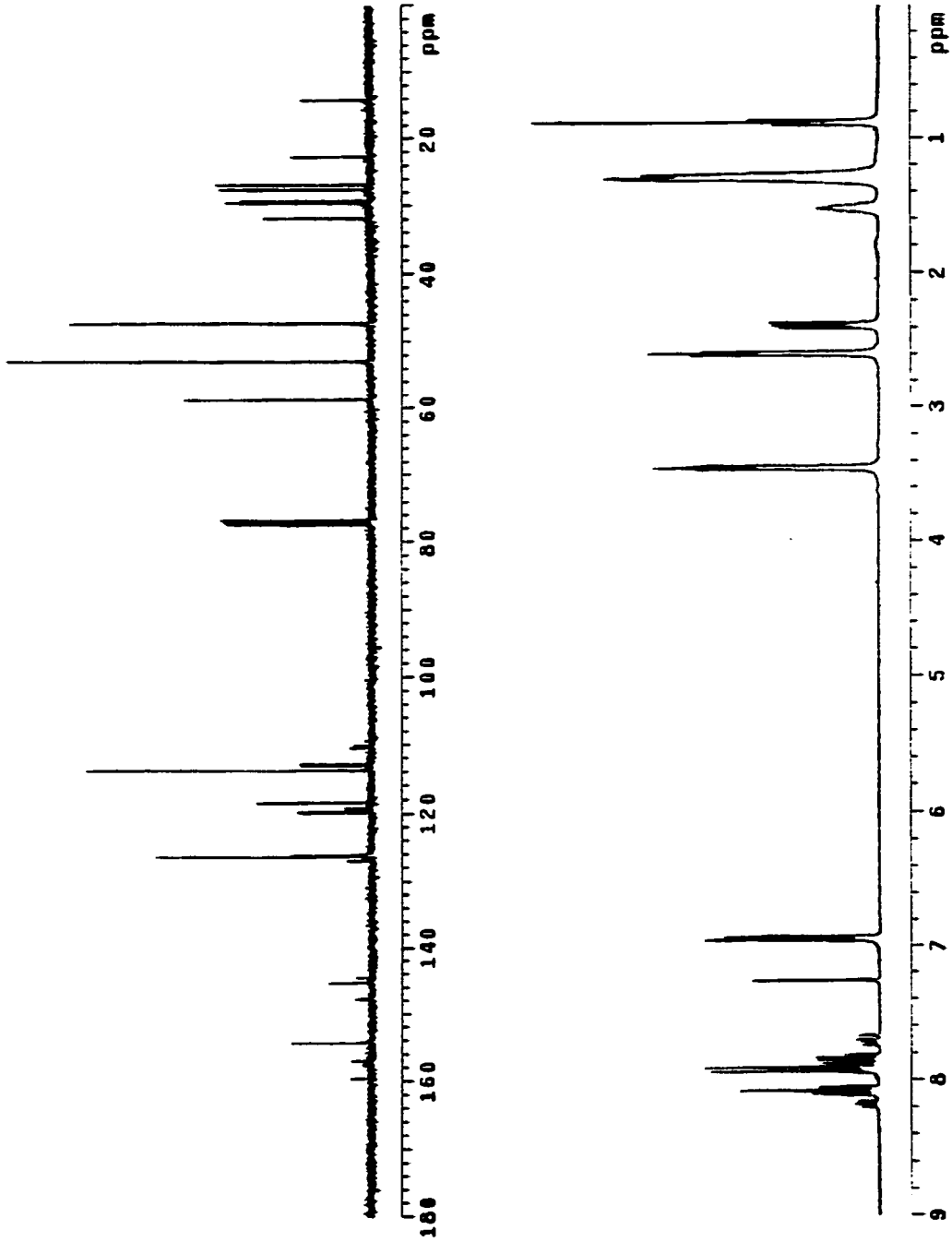

Figure A.8.7. ^{1}H and ^{13}C NMR spectra of **29** (n = 8) in $CDCl_3$.

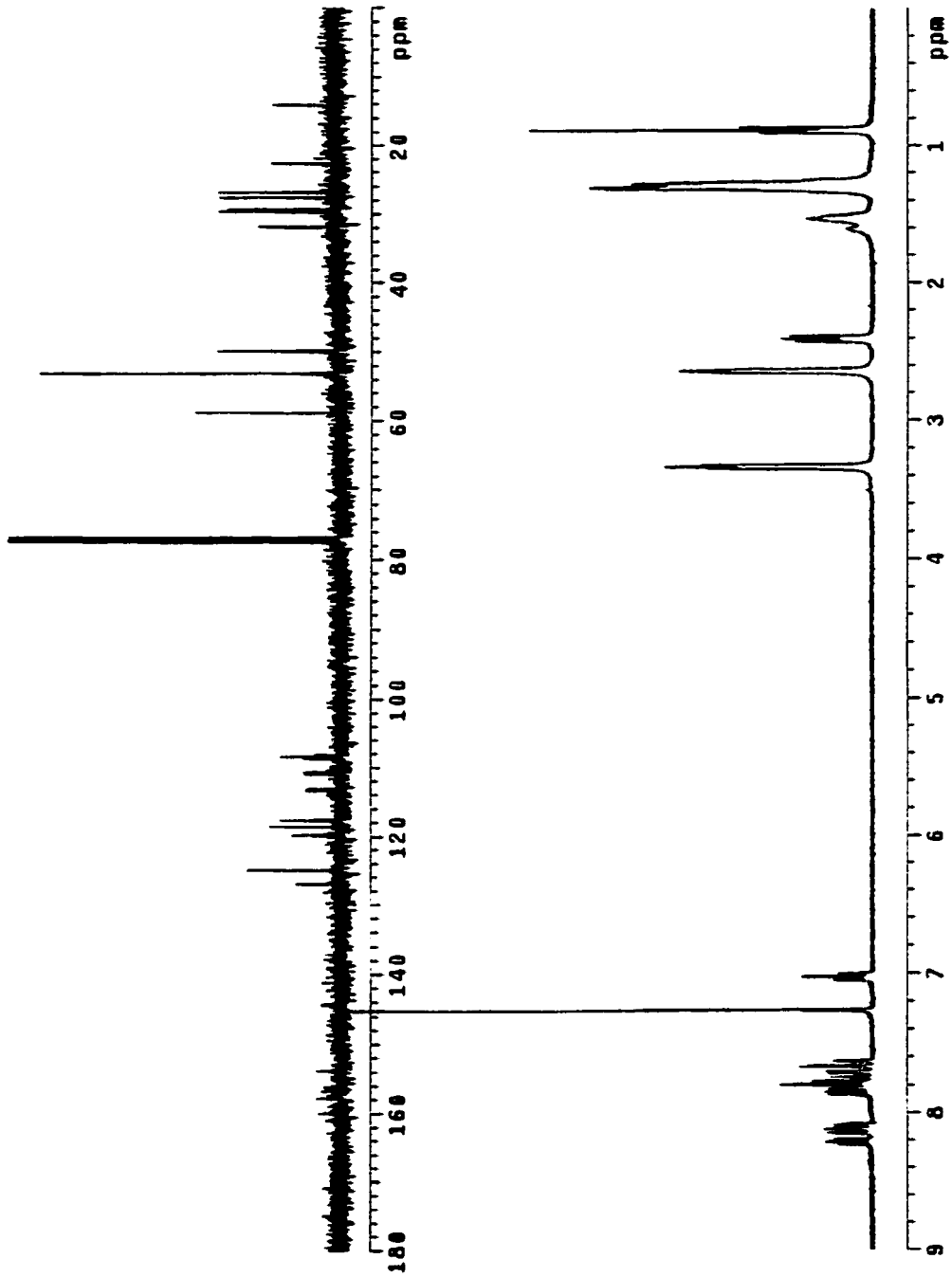

Figure A.8.8. ^{1}H and ^{13}C NMR spectra of **30** (n = 8) in $CDCl_3$.

A.9. Rise time

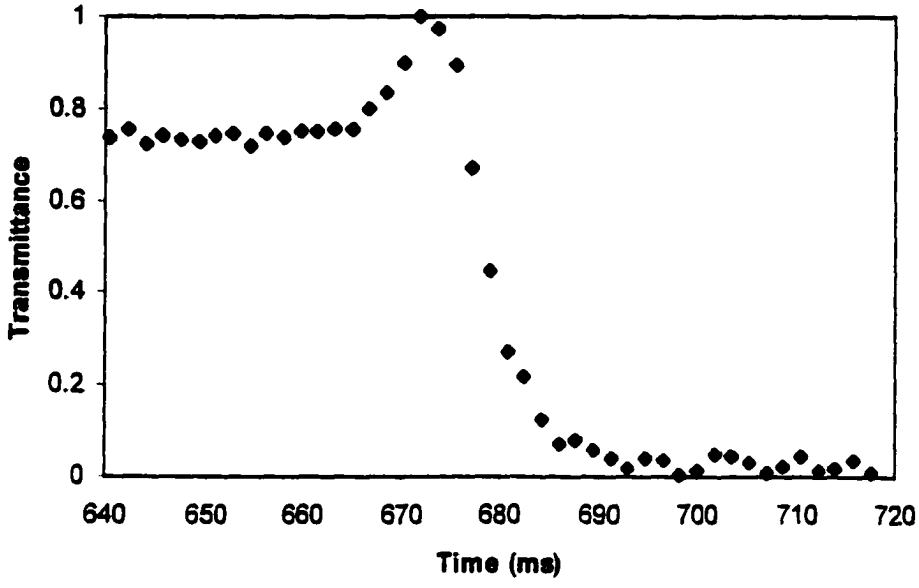

This is a plot of the rise time measurement for sample E7 and the time interval between points is 1.69 ms. Therefore, the rise time value (100-10%) is about $1.69 \times 8 = 13.52$ ms. This measurement was performed at 1060 nm and a driving voltage of 5.0 V was applied.

The measurement for other samples is based on the same principle.